Aus dem

Department für Diagnostische Labormedizin der Universität Tübingen

Institut für Medizinische Genetik und angewandte Genomik

The Role of Calpains in the Molecular Pathogenesis of Spinocerebellar Ataxia Type 17

Inaugural-Dissertation
zur Erlangung des Doktorgrades
der Medizin

der Medizinischen Fakultät
der Eberhard Karls Universität
zu Tübingen

vorgelegt von

Anger, Stefanie Cari

2023

Dekan:	Professor Dr. B. Pichler
1. Berichterstatter:	Professor Dr. O. Rieß
2. Berichterstatter:	Privatdozentin Dr. K. Brockmann
3. Berichterstatter:	Professorin Dr. D. Timmann-Braun
Tag der Disputation:	26.07.2023

DEDICATED TO THE PATIENTS SUFFERING FROM HEREDITARY DISEASES

Table of Contents

List of Figures

List of Tables

List of Abbreviations

(r)CAPN	(recombinant) calpain
A/A	antibiotic-antimycotic
aa	amino acid
AD	Alzheimer disease
ADCA	autosomal-dominant cerebellar ataxia
ADNIV	autosomal-dominant neovascular inflammatory vitreoretinopathy
AIF	apoptosis-inducing factor
ala	alanine
ALS	amyotrophic lateral sclerosis
APS	ammonium persulfate
bcl-2	B-cell lymphoma 2
bp	base pair
BSA	bovine serum albumin
BT	bis-tris
C2L	C2-like
CAPNS1	calpain small regulatory subunit
cb	cerebellum
CBP	CREB-binding protein
CBSW	calpain-type beta-sandwich domain
CH	China
CI-III	calpain inhibitor III
CL	large catalytic subunit
CMA	chaperone-mediated autophagy
CNS	central nervous system
CRB	calpain reaction buffer
CREB	cAMP response element-binding protein
ctx	cortex
CysPc	calpain-like cysteine protease
DAT	dopamine active transporter
ddH_2O	double distilled water
DE	Germany

DM	myotonic dystrophy
DMEM	Dulbecco’s modified eagle medium
DMSO	dimethyl sulfoxide
DPBS	Dulbecco’s phosphate-buffered saline
DRPLA	dentatorubral-pallidoluysian atrophy
DTT	dithiothreitol
EB	elution buffer
ECL	enzymatic chemiluminescence
EDTA	ethylenediaminetetraacetic acid
eg	endogenous
EGFP	enhanced green fluorescence protein
ER	endoplasmic reticulum
FCS	fetal calf serum
FR	filter retardation
FRAXA	fragile-X syndrome
FRAXE	fragile-XE syndrome
gln	glutamine
HAT	histone acetyltransferase
hCAST	human calpastatin
HD	Huntington disease
HDAC	histone deacetylase
HDL	Huntington disease-like
HEK cell	human embryonic kidney cell
HEPES	4-(2-hydroxyethyl)-1-piperazineethanesulfonic acid
HRP	horseradish peroxidase
hsp	heat shock protein
hTBP	human TBP
htt	huntingtin
inh	inhibition
iono	ionomycin
LB	lysogeny broth
LDS	lithium dodecyl sulfate
LGMD	limb-girdle muscular dystrophy

m	months
MANF	mesencephalic astrocyte-derived neurotrophic factor
MAP2	microtubule-associated protein 2
MES	2-(N-morpholino)ethanesulfonic acid
MS	multiple sclerosis
mTBP	murine TBP
mTOR	mammalian target of rapamycin
NC	nitrocellulose
N-CoR	nuclear receptor co-repressor 1
NEAA	non-essential amino acids
NF-Y	nuclear transcription factor Y
NLS	nuclear localization signal
NMDA(R)	N-methyl-D-aspartate
p/CAF	P300/CBP-associated factor
PC	protease core
PC12 cell	pheochromocytoma 12 cell
PD	Parkinson disease
PEF	penta-EF hand
PFA	paraformaldehyde
PIC	preinitiation complex
pol	polymerase
polyQ	polyglutamine
QBP1	polyQ-binding protein 1
RIPA	radioimmunoprecipitation assay
RT	room temperature
rTBP	rat TBP
SBMA	spinobulbar muscle atrophy
SCA	spinocerebellar ataxia
SDC	sodium deoxycholate
SDS	sodium dodecyl sulfate
Sp1	specificity protein 1
SPG	spastic paraplegia
str	striatum

Su(H)	suppressor of hairless protein
TA	tris-acetate
TAF	TBP-associated factor
TBS(T)	tris-buffered saline (with Tween 20)
TBP	TATA-box binding protein
TrkA	tropomyosin receptor kinase A
UPS	ubiquitin proteasome system
US	United States
UT	untransfected
v/v	volume/volume
w/v	weight/volume
WB	western blot
XBP1	X-box binding protein 1

1 Introduction

1.1 Overview of polyglutamine expansion diseases

Polyglutamine (polyQ) diseases are a heterogenous group of progressive neurodegenerative diseases. They are characterized by the expansion of CAG and CAA trinucleotide repeats in the exon of disease-specific, unrelated genes. This triplet expansion is translated into a glutamine stretch within the affected protein. PolyQ disorders comprise nine diseases, namely Huntington disease (HD), spinocerebellar ataxias (SCA) type 1, 2, 3, 6, 7, and 17, spinobulbar muscle atrophy (SBMA), and dentatorubral pallidoluysian atrophy (DRPLA). Except for SBMA, which is inherited in a X-chromosomal manner, all polyQ disorders are transmitted autosomal-dominantly (Orr and Zoghbi, 2007). Huntington disease is the most common polyQ disease with a prevalence of 2-3 per 100,000 people worldwide, assumingly followed by SCA3, SCA2 and 6, however, reliable data on the prevalence of SCA types are not yet available (Schols et al., 2004; Pringsheim et al., 2012). Furthermore, prevalence is highly dependent on geographic region due to founder effects (Manto, 2005; Durr, 2010). For instance, the prevalence of HD varies from 0.1-0.7 per 100,000 in Asian populations to 6-13.7 per 100,000 among Caucasians (Rawlins et al., 2016; Baig et al., 2016).

Phenotypically, these diseases manifest with progressive cerebellar, spinal, bulbar, cortical, subcortical and/ or global brain atrophy, resulting in a variety of neurological disturbances. While there is a wide spectrum of phenotypical appearance, some neurodegenerative patterns and symptoms are relatively specific for a disease. The group of spinocerebellar ataxias, also known as autosomal dominant cerebellar ataxias, particularly manifest with symptoms of spinal or cerebellar neuronal loss, such as ataxia, dysarthria, and tremor, but also cortical, pyramidal, and extrapyramidal symptoms, peripheral neuropathies, and psychiatric disorders (Manto, 2005; Schols et al., 2004). On average, symptomatic onset starts in the third decade and leads to death 10-20 years after symptom onset, mostly due to respiratory insufficiency or pneumonia (Orr and Zoghbi, 2007). The mutant gene of the particular disease, as well as its normal

and pathogenic CAG/CAA repeat lengths are depicted in Table 1 (Orr and Zoghbi, 2007).

Therapeutical approaches are still examined experimentally, and no causal treatment is available yet. Therapy is only supportive and symptom-oriented, including physiotherapy, logopaedics, orthosis, deep brain stimulation for tremor, pharmacological support for ataxia, and spasticity, but still, most patients become wheelchair-bound in the course of the disease.

Table 1. PolyQ diseases. The known polyQ diseases with affected gene and encoded protein, number of normal and pathogenic glutamine repeats are listed in the table below.

Disease	Affected Gene (encoded protein)	Normal repeat length	Expanded repeat length
DRPLA	DRPLA (atrophin-1)	7-34	49-88
HD	HD (huntingtin)	6-34	36-121
SBMA	AR (androgen receptor)	9-36	38-62
SCA1	ATXN1 (ataxin-1)	6-39	40-82
SCA2	ATXN2 (ataxin-2)	15-24	32-200
SCA3	ATXN3 (ataxin-3)	13-36	61-84
SCA6	CACNA1A ($CACNA1_A$)	4-20	20-29
SCA7	ATXN7 (ataxin-7)	4-35	37-306
SCA8	ATXN8 (untranslated)	16-34	>74
SCA17	TBP (TBP)	25-42	47-63

1.2 Spinocerebellar ataxia type 17 as a polyQ disease

Spinocerebellar ataxia type 17 (SCA17) is an autosomal-dominant cerebellar ataxia which was first described by Koide et al. (1999) in a Japanese patient. The cause of the disease was associated with an expanded CAG/CAA trinucleotide repeat in the TATA-box binding protein (TBP), a ubiquitously expressed transcription factor (Koide et al., 1999).

SCA17 is one of the very rare ADCAs, representing 1-3% of the spinocerebellar ataxias in Caucasian cohorts, in contrast to 0.3% in Japanese cohorts (Rolfs et al., 2003; Maruyama et al., 2002). Most of the reported cases are isolated incidents, and less than 100 families have been described until now. To date, most reports originate from Japan and Germany, China, Korea, Italy, and England (Zuhlke and Burk, 2007; Stevanin and Brice, 2008). However, TBP mutation is suspected to be more common than reported, as the mutation has been detected in patients diagnosed with sporadic ataxia, HD, AD and PD and is therefore often diagnostically neglected (Zuhlke and Burk, 2007).

TBP physiologically contains 25-40 glutamine repeats at the N-terminus (Gostout et al., 1993; Imbert et al., 1994; Schols et al., 2004). A polyQ length of 42-48 glutamines in TBP is associated with a reduced penetrance of SCA17 with variable symptoms and age at onset (Yang et al., 2016; Maltecca et al., 2003). Recently, the lower repeat length cut-off in SCA17 is considered indistinct as there are reported cases with 41-43 repeats that do not show ataxia but parkinsonism or cognitive deficits at an older age, hence, they are suggested to contribute to susceptibility in parkinsonism, dementia, and neurodegeneration (Choubtum et al., 2015). On the other hand, severe phenotypes with 41 repeats were reported including ataxia, one with age at onset in the mid-thirties (Herrema et al., 2014; Nanda et al., 2007). Also, choreatic disorders seem to be more likely in shorter repeat lengths, resembling rather an HD-like phenotype (Toyoshima and Takahashi, 2018). Consequently, the phenotypes are quite variable and can mislead to other neurodegenerative diseases or psychiatric disorders (Nolte et al., 2010; Alibardi et al., 2014; Choubtum et al., 2015; Kim et al., 2009; Park et

al., 2016; Doherty et al., 2014; Herrema et al., 2014; Nakamura et al., 2001; Nanda et al., 2007; Zuhlke and Burk, 2007).

Full penetrance for SCA17 occurs at repeat lengths of more than 48 CAG/CAAs showing an inverse correlation with the age at onset and age at death as portrayed in Figure 1 (Nakamura et al., 2001; Rolfs et al., 2003; Zuhlke and Burk, 2007; Fujigasaki et al., 2001; Koide et al., 1999; Maltecca et al., 2003; Oda et al., 2004). The average age at onset lies in the middle of the third decade, but shows a great variability from 3 to 74 years at onset (Stevanin and Brice, 2008). As known from many genetic diseases, the correlation between age at onset and the CAG/CAA repeat length in SCA17 differs between individuals due to environmental, genetic, and epigenetic factors (Bruni et al., 2004; Choubtum et al., 2015; Zuhlke and Burk, 2007).

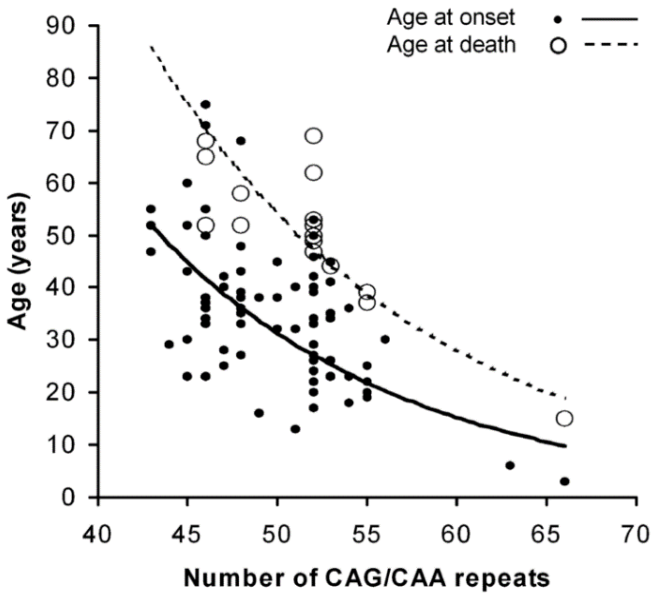

Figure 1. Correlation of age at onset and number of CAG/CAA repeats in SCA17 patients. Age at onset and age at death are inversely correlated to the number of CAG/CAA repeats but vary individually due to additional environmental and genetic modifying factors of SCA17 patients. Figure adapted from Stevanin and Brice, 2008).

1.3 Clinical and neuropathological manifestation of SCA17

PolyQ disorders differ in their clinical and neuropathological manifestations. While there are common symptoms, such as cerebellar deficits for spinocerebellar ataxias, including ataxia (90%), dysarthria, and tremor, or choreatic movement disorders for HD and DRPLA, other manifestations are typical for a certain type of polyQ disease (Orr and Zoghbi, 2007). The most important and characteristic symptoms and the pattern of neurodegeneration of the respective polyQ disease are listed in Table 2 . In the following, the clinical and the neuropathological appearance of SCA17 will be outlined.

Table 2. Characteristic symptoms and neuronal degeneration pattern of polyQ diseases. The most common symptomatic manifestations and affected brain regions due to neuronal degeneration are typical for the respective polyQ diseases (Gatchel and Zoghbi, 2005; Manto, 2005; Whaley et al., 2011).

Disease	Characteristic symptoms	Affected brain regions
DRPLA	Ataxia	Striatum
	Seizures	Cortex
	Dementia	
	Choreoathetosis	
HD	Chorea	Cerebellum
	Dystonia	Cortex
	Cognitive deficits	Basal ganglia
	Psychiatric problems	Subthalamic nucleus
SBMA	Motor weakness	Anterior horn neurons
	Dysphagia	Bulbar neurons
	Gynaecomastia	Dorsal root ganglia
	Decreased fertility	

SCA1	Ataxia Dysarthria Early swallowing signs Early respiratory signs Cognitive impairment Ophthalmoplegia Peripheral neuropathy	Purkinje cells (Cb) Dentate nucleus Brainstem
SCA2	Ataxia Ophthalmoplegia Decreased reflexes Peripheral neuropathy	Purkinje cells (Cb) Brain stem Frontotemporal lobes
SCA3	Ataxia Spasticity Fasciculations Ophthalmoplegia Parkinsonism Peripheral neuropathy	Cerebellar dentate neurons Basal ganglia Brain stem Spinal cord
SCA6	Ataxia Dysarthria Nystagmus Tremors	Purkinje cells Granule cell Inferior olive
SCA7	Ataxia Visual loss (pigmentary retinopathy) Cardiac failure (infantile form)	Purkinje cells Dentate nucleus Inferior olive
SCA17	Ataxia Dystonia Dementia Psychiatric problems Seizures	Cerebellum Brain stem Macula Visual cortex

1.3.1 Clinical appearance of SCA17

Besides ataxia as a shared feature, symptoms of SCA17, diverge from the ones most frequent in SCAs 1, 2, 3, and 6, that make up approximately 50% of all SCA cases (Boonkongchuen et al., 2014). The early onset of dementia and psychiatric manifestation, as well as extrapyramidal signs, such as chorea and dystonia, including torticollis, writer's cramp or blepharospasm, are only common in SCA17, while spasticity is observed in less than 50% of the patients (Rolfs et al., 2003; Zuhlke and Burk, 2007). Additionally, SCA17 shows more severe phenotypes than other polyQ disorders (Rolfs et al., 2003).

The symptoms of SCA17 are heterogenous and differ within affected families (Bauer et al., 2004). Symptoms at onset include ataxia of stance, gait, and limbs, dementia, psychiatric symptoms such as depression, psychosis, behavioural changes, cognitive impairment and insomnia, and extrapyramidal signs such as focal dystonia, chorea, and parkinsonism, especially bradykinesia, gait disturbance, and postural reflex disturbance (Stevanin and Brice, 2008; Nakamura et al., 2001). With further progression, many patients suffer from dysphagia, but also less common symptoms may occur such as seizures, spasticity, myoclonus, and muscle atrophy (De Michele et al., 2003; Hagenah et al., 2004; Zuhlke and Burk, 2007; Rolfs et al., 2003). In addition, disturbances of the autonomic system and mild sensorimotor axonal neuropathy were also observed (Maltecca et al., 2003; Zuhlke et al., 2001). The prevalence of symptoms is presented in Figure 2 (Stevanin and Brice, 2008).

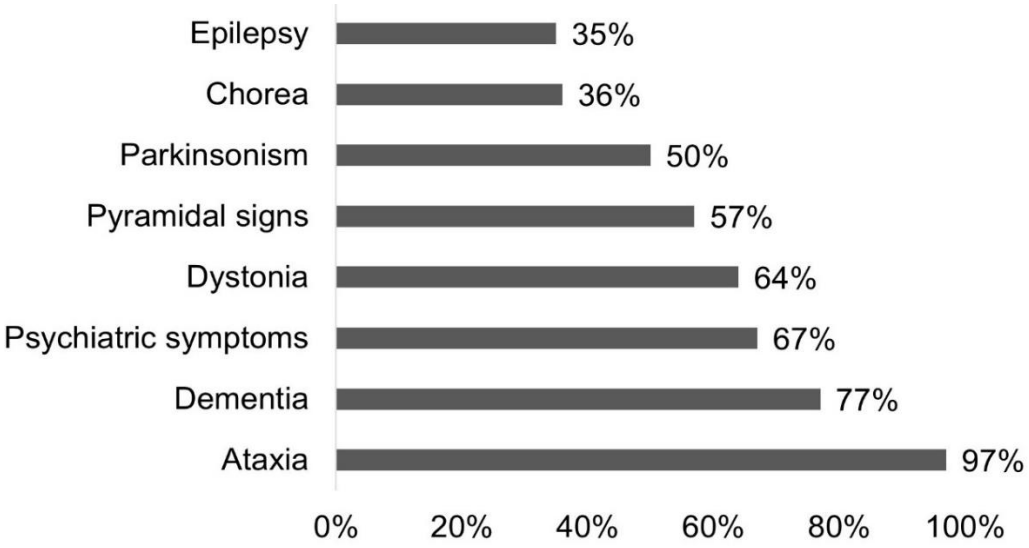

Figure 2. Frequency of symptoms appearing in SCA17. The most common manifestations of SCA17 comprise ataxia of gait, stance, and limbs (97%), dementia (77%), psychiatric symptoms (67%), and motor impairments of pyramidal and extrapyramidal kind (Stevanin and Brice, 2008).

Basal ganglia dysfunction, chorea, dystonia, dysphagia, and parkinsonism, that occur predominantly in cases with low and moderate repeat lengths, can resemble Huntington disease- or Parkinson disease-like phenotypes (Choubtum et al., 2015; Stevanin et al., 2003). Moreover, the early and frequent occurrence of dementia can mimic Alzheimer disease (AD) phenotypes (Stevanin and Brice, 2008). Based on these features, SCA17 was alternatively termed Huntington disease-like type 4 (HDL4), which highlights the close relationship between SCA17 and HD.

1.3.2 Neuropathological features of SCA17

Neuronal loss and gliosis were found most prominently in cerebellum, particularly affecting Purkinje cells (Nakamura et al., 2001; Rolfs et al., 2003). In addition, the motoric system was compromised by atrophy of the basal ganglia, the inferior olive, and the motor cortex, as a correlate of the various motoric impairments of SCA17 patients, while the spinal cord was only little or not affected (Bruni et al., 2004; Rolfs et al., 2003; Lasek et al., 2006; Gunther et al., 2004). Cortical atrophy in the frontal and temporal lobes, and neurodegeneration of visual areas in the occipital lobe were found to be particularly accentuated (Lasek et al., 2006;

Maltecca et al., 2003). Together with the impairment of the limbic system, the nucleus accumbens, thalamic nuclei, and hippocampus, the complexity of the aforementioned symptoms, especially of psychiatric and cognitive disturbances, correlate with this neuropathological pattern (Reetz et al., 2010; Nakamura et al., 2001; Lasek et al., 2006).

1.4 TATA-box binding protein (TBP)

The TATA-box binding protein (TBP) is a crucial factor for the transcription of most eukaryotic genes. Its name originates from the TATA box, a common DNA sequence localized around 30 base pairs (bp) upstream of transcription start in approximately 2-30% of eukaryotic promotors (Yella and Bansal, 2017). As the DNA-binding subunit, TBP, together with 14 other TBP-associated factors (TAFs), forms the transcription factor TFIID. TAFs, other cofactors, and chromatin marks, regulate the binding of TBP to DNA for TATA-containing and TATA-less promoters (Wong and Bateman, 1994; Patel et al., 2018; Thomas and Chiang, 2006). Besides its involvement in transcription by RNA polymerases I, II, and III, and consequently also in the expression snRNA, rRNA, and other RNA species, TBP is essential for the recruitment of other transcription factors TFIIA to H for the formation of the preinitiation complex with RNA polymerase II. The assembly is initiated by binding TFIID to the DNA and bending an 80° angle, thereby enabling RNA polymerase II to bind the complex and start with transcription downstream, hereby being a crucial transcription factor for the transcription of all protein-coding genes (Hernandez, 1993; Savinkova et al., 2009).

The structure of human TBP (isoform 1, UniProt identifier: P20226-1) is characterized by the non-conserved, highly variable amino-terminus consisting of 58 amino acids and the N-terminally localized polyQ domain with varying glutamine lengths of 25-40 repeats in a healthy person (Zuhlke and Burk, 2007). The COOH-terminus (C-terminus) contains the DNA binding region of 180 amino acids, which is highly conserved among species (Hoffman et al., 1990; Reid et al., 2003; Thomas and Chiang, 2006). The structure of TBP is schematised in Figure 3.

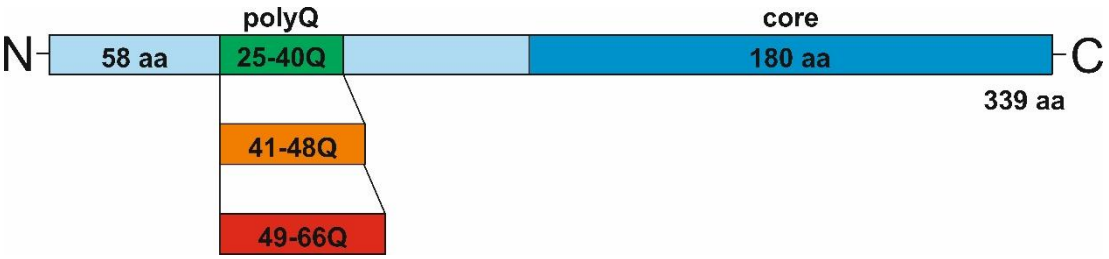

Figure 3. Schematic structure of the TATA-box binding protein (TBP). The N-terminus (N) of TBP consists of 58 amino acids (aa), followed by the polyQ sequence, which varies between 25 and 40 glutamine repeats for healthy individuals (green). Repeat lengths of 41 to 48 glutamines (orange) are associated with reduced penetrance for SCA17, whereas full penetrance occurs at more than 48 glutamines (red). The longer C-terminal part (C) contains 244 amino acids with the DNA binding core region of 180 aa (dark blue). Figure adapted from Zuhlke and Burk (2007).

1.5 Pathogenetic mechanisms

Investigations in several animal knockout models for polyQ proteins of HD, SCA1, and SBMA showed that the loss of the respective gene did not induce behavioural phenotypes, resembling respective characteristics of the polyQ diseases, or it was even lethal at embryonical stages, as for HD and SCA17 knockout models (Duyao et al., 1995; Zeitlin et al., 1995; Matilla et al., 1998; Martianov et al., 2002). While for HD, homozygous and heterozygous HD patients showed resembling phenotypes (Wexler et al., 1987), gene dosage effects were observed for SCA17 and SCA3 (Takiyama et al., 1995; Toyoshima et al., 2004). These findings indicate that the polyQ expansion is a mutation that can inactivate the protein's normal cellular functions or interactions as a loss-of-function, but can also induce a gain-of-function mechanism by provoking additional aberrant functional activities of the affected protein (Orr and Zoghbi, 2007).

Several theories have been developed over time to explain the phenomena and to understand the pathomechanisms underlying polyQ expansion diseases. In the following, three of those principles of polyQ disease mechanisms will be explained and put in context of how they could contribute to the pathogenesis of SCA17.

1.5.1 Transcriptional dysregulation

One central hypothesis how polyQ-expanded proteins may cause toxicity in neuronal cells is their potential impact on transcriptional activity, which is considered an early event in pathogenesis and was found in pre-symptomatic disease states of HD (Luthi-Carter et al., 2000). Markedly, in a polyQ repeat length-dependent manner altered interactions with various proteins were shown in different polyQ diseases, e.g. with CBP (CREB-binding protein), p/CAF (p300/CBP-associated factor), mSin3a, Sp1, and its coactivator TAFII130, N-CoR (nuclear receptor co-repressor), and p53 (Shao and Diamond, 2007; Shimohata et al., 2000; Steffan et al., 2000; Boutell et al., 1999; Dunah et al., 2002). Said proteins, which are involved in transcriptional processes, often possess glutamine-rich domains, and are thought to interact with polyQ disease proteins via polyQ-polyQ-interactions. These aberrant interactions may subsequently compromise transcription, especially affecting genes which encode for proteins involved in signalling pathways, neuronal transmission, and retinoid pathways (Lieberman et al., 2019; Lee et al., 2020; Dunah et al., 2002; Luthi-Carter et al., 2000; Hoshino et al., 2004).

On the one hand, transcriptional downregulation can result from enhanced interaction of mutant TBP with and sequestration of several transcriptional regulators. On the other hand, transcriptional impairment may result from TBP's loss of function, which is characterized by reduced interactions with transcription factors and reduced DNA-binding affinity (Reid et al., 2003; Friedman et al., 2008; Yang et al., 2016). In the following, some of the altered interactions of polyQ-expanded TBP are presented in Figure 4.

PolyQ-expanded TBP was shown to feature an increased interaction with its transcriptional partner TFIIB, which subsequently reduced the expression of the heat shock protein HSPB1 (Friedman et al., 2007). Also, affinity for nuclear factor-Y (NF-Y), that is involved in transcription of genes encoding for heat shock proteins, is increased upon expression of polyQ-expanded TBP (Huang et al., 2011). Mutant TBP also showed enhanced association with specificity protein 1 (Sp1), resulting in reduced expression of the nerve growth factor tropomyosin

receptor kinase A (TrkA) (Shah et al., 2009). Resembling effects were found for the interaction with the transcription factor Suppressor of Hairless (Su(H)), which is involved in Notch signalling (Ren et al., 2011). However, decreased gene expression due to reduced interactions with mutant TBP in terms of a loss-of-function mechanism were found for X-box binding protein 1 (XBP-1), which consequently lowered the expression of mesencephalic astrocyte-derived neurotrophic factor (MANF), that is a part of ER stress response (Yang et al., 2014). Loss of function was also implicated by reduced expression of several muscle-specific genes due to dysfunction of the muscle-specific transcription factor MyoD in the presence of expanded TBP of SCA17 mice, causing muscular degeneration (Huang et al., 2015; Yang et al., 2014).

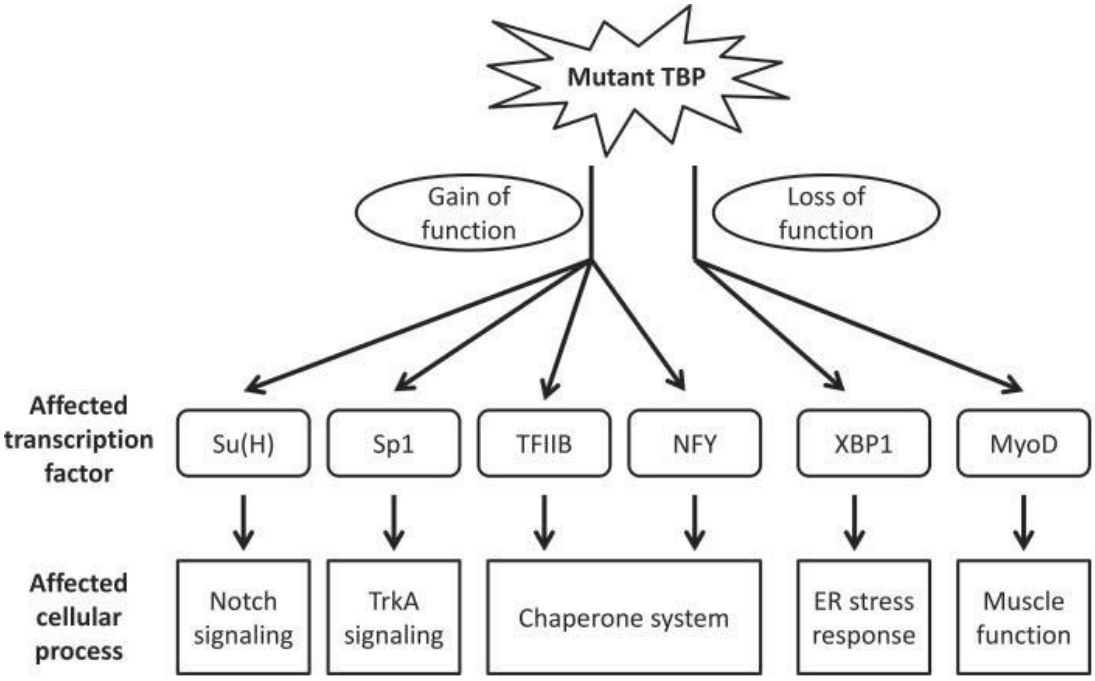

Figure 4. Transcriptional disruptions in SCA17. Overview of transcriptional alterations caused by interaction of mutant TBP with transcription factors and resulting effects on cellular pathways. TBP interactions can be either enhanced (gain of function) or decreased (loss of function), affecting diverse cellular processes (Yang et al., 2016).

Another aspect of disruption of gene expression was found to be related to mutant CAG-containing RNA (mCAG-RNA) (Wojciechowska and Krzyzosiak, 2011; Mykowska et al., 2011). Nuclear accumulations are caused by repeat length-dependent recruitment of RNA-binding proteins to the hairpin structure of mCAG-RNA. Hereby, splicing factors are sequestrated into these nuclear foci, causing

splicing changes. RNA foci were found in patient's fibroblast of HD, SCA1, 3, 7, and DRPLA (Bogomazova et al., 2019). Another RNA-dependent alteration in polyQ diseases is repeat-associated non-ATG (RAN-)translation, which can be triggered by the hairpin mCAG-RNA, leading to abnormal ATG-independent bidirectional translation of the coding mRNA (Cleary and Ranum, 2013). In HD disease brains, respective homopolymers were detected, which originate from RAN-translation, although their pathological relevance is disputed (Bañez-Coronel et al., 2015; Yang et al., 2020). Further CAG expansion-dependent perturbations on the mRNA level include increased translation of mutant RNA when compared to wild-type RNA, nucleolar stress by association of mCAG-RNA with nucleolin, which is involved in rRNA processing and ribosome assembly, as well as disturbances of nucleocytoplasmic transport and nuclear envelope integrity (Lieberman et al., 2019; Bogomazova et al., 2019).

1.5.2 Aggregation and impairment of protein degradation

The occurrence of insoluble, fibrillary aggregates is a pathological hallmark that connects the polyQ diseases to other, non-polyglutamine neurodegenerative diseases, such as AD, Parkinson disease (PD), or amyotrophic lateral sclerosis (ALS). These polyQ protein-containing inclusions appeared before symptom onset in HD and SCA1 (Gutekunst et al., 1999; Lunkes et al., 1998) and were found in all polyQ diseases (Takeuchi and Nagai, 2017; Gatchel and Zoghbi, 2005).

Aggregates impair cellular functions by aberrant interactions of the disease protein with cellular components (Shao and Diamond, 2007; Schaefer et al., 2012; Gatchel and Zoghbi, 2005). Consequently, transcription factors, parts of the protein degradation system, especially chaperones and ubiquitin, as well as proteasomal components but also mitochondria were shown to be recruited into inclusions in HD, SCA1, SCA3, SCA7, and SBMA (Weber et al., 2014; Haacke et al., 2007; Ishihara et al., 2003; Yvert et al., 2000; Nucifora et al., 2001; Shimohata et al., 2000; Gatchel and Zoghbi, 2005). This sequestration of important cellular components leads to their depletion and eventually to functional

impairment (Lieberman et al., 2019; Kazantsev et al., 2002; Weber et al., 2014). Moreover, truncated parts of polyQ proteins were detected in neuronal inclusions of affected brains with an inverse correlation between length of the fragment and its potential to aggregate and to cause apoptotic stress (Davies et al., 1997; Igarashi et al., 1998; Hackam et al., 1998; Lunkes et al., 1998; Martindale et al., 1998). In SCA3, also the full-length disease protein ataxin-3 was recruited into inclusions by the interaction with its fragmented forms (Haacke et al., 2006; Paulson et al., 1997).

Considering SCA17, intranuclear inclusions were found in cerebellum and basal ganglia of SCA17 patients that contained truncated TBP and ubiquitin (Friedman et al., 2008; Nakamura et al., 2001; Rolfs et al., 2003; Kim et al., 2002; Fujigasaki et al., 2001). In accordance with the reported findings in other polyQ diseases, truncated mutant TBP was shown to form more intranuclear, polyQ length-dependent inclusions than the respective full-length species in mouse and cell models, while endogenous fragments lacking the polyQ repeat did not form stable inclusions (Friedman et al., 2008). Overexpression of wild-type TBP to reverse depletion of full-length TBP likewise showed inclusion formation (Hsu et al., 2014). Nevertheless, data for SCA17 is still scarce, and therefore it can only be assumed that mechanisms resemble those of other polyQ diseases.

Over time, the toxicity of aggregates was challenged intensely as findings showed that suppression of inclusion formation increased cell death while inclusion formation improved survival and reduced levels of mutant protein in neurons by sequestering the toxic soluble species as a last cellular response upon degradation failure (Saudou et al., 1998; Klement et al., 1998; Slow et al., 2005; Hodgson et al., 1999; Arrasate and Finkbeiner, 2012; Taylor et al., 2003). Consequently, inclusions were thought to have a protective characteristic. However, whether protective or toxic, they depict an end state of cells when overloaded with misfolded diseases proteins (Haacke et al., 2006).

1.5.3 Proteolytic cleavage

Several studies on polyQ diseases demonstrated the occurrence of fragments of the disease-causing proteins and led to the concept of the “toxic fragment hypothesis” (Wellington and Hayden, 1997; Orr and Zoghbi, 2007; Ikeda et al., 1996; Mangiarini et al., 1996; Igarashi et al., 1998; Ellerby et al., 1999). Although the pathogenic relevance of truncated disease proteins is not fully understood, cell models of HD, SCA3, and DRPLA expressing these truncated forms exhibited increased toxicity and cell death (Hackam et al., 1998; Ikeda et al., 1996; Szebenyi et al., 2003). They were found in brain tissue or cell models of all polyQ diseases, as described in 1.5.2, thus also represent an important component of neuronal inclusions (Weber et al., 2014; Orr and Zoghbi, 2007). Studies with SCA3, SCA6, SCA7, and HD mouse models demonstrated that the expression of fragment protein was sufficient to induce severe and early-onset disease phenotypes, indicating a negative correlation between fragment length and their neuronal toxicity (Mangiarini et al., 1996; Cemal et al., 2002; Ikeda et al., 1996; Yvert et al., 2000; Garden et al., 2002).

The hypothesis of toxicity of protein fragments is schematized in Figure 5 and underlines the crucial role of disease-protein fragmentation in the axis of transcriptional disruption, fragmentation, and aggregation, all being common findings in the pathology of polyQ diseases. The source of truncated species of polyQ proteins can be proteolytic cleavage or mis-splicing (Sathasivam et al., 2013; Weber et al., 2014). These processes can release polyQ-containing stretches or other portions of the disease protein, divergently exposing them to the cellular environment and thereby inducing detrimental effects (Ikeda et al., 1996; Schaffar et al., 2004). When fragments are small enough, the pathological threshold for a conformational change is reached and amplified by the presence of a polyQ domain. In that way, fragments undergo beta sheet-based reorganization (Scherzinger et al., 1997; Lunkes et al., 1999). Thus, the truncated protein is more susceptible towards self-association due to a higher tendency to misfolding and aggregation with a propensity that increases inversely proportional to the fragment length (Wanker, 2000; Scherzinger et al., 1997;

Lunkes et al., 1999; Perutz et al., 1994). Moreover, fragments of polyQ proteins were shown to differentially interact with other, often polyQ-containing, proteins such as transcription factors (Perutz et al., 1994; Wanker, 2000; Lunkes et al., 1998). Truncation may also reduce binding sites for physiological interaction partners, subsequently hindering the protein from cellular processes and regulatory activities (Lieberman et al., 2019). Consequently, a pathological fragmentation of disease proteins may lead to impaired cellular functions via their abnormal interactions with other cellular factors and through the formation of the typical neuronal inclusions (Haacke et al., 2006; Paulson et al., 1997).

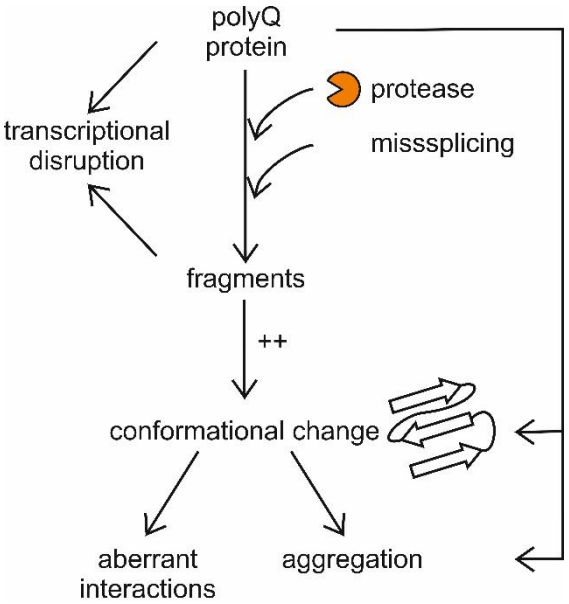

Figure 5. Cellular effects of disease protein truncation. Proteolytic cleavage and altered splicing patterns are thought to release truncated forms of disease proteins into the cellular context. This makes this protein species prone (++) for conformational changes, for aberrant interactions, and for self-aggregation.

However, the cytotoxicity of fragments appears to be not applicable for all polyQ diseases, as it was proven invalid for SCA1 and SCA2 (Ng et al., 2007; Klement et al., 1998; Huynh et al., 2000). Research on SCA2 even suggested that neither fragments, nor inclusions contribute to pathology of the disease (Huynh et al., 2000; Ng et al., 2007).

One pathway of fragment formation was mentioned in the context of RNA-dependent splicing alterations in 1.5.1. Transcripts of different length that are translated into a highly toxic fragment of htt result from aberrant splicing due to the separation of splicing factors by mCAG-RNA and deceleration of RNA-polymerase by the repeat sequence, thereby making polyA signals more available for polyadenylation (Bogomazova et al., 2019). Another way of fragment genesis is the proteolytic cleavage. Several proteolytic systems have been suspected to be associated with polyQ diseases, specifically caspases, calpains, MMPs, and endopeptidases (Weber et al., 2014). A lot of research has been conducted on the common pathway of caspase-dependent cleavage in diseases such as HD, SCA3, and SCA7, and several caspase isoforms were shown to be involved in proteolytic processing of the respective disease proteins (Weber et al., 2014). Despite observing TBP fragments in the disease context, early investigations on SCA17 could not show an involvement of this group of enzymes in the presumably proteolytic processing of TBP, suggesting that other proteases such as calpains might be responsible (Wellington et al., 1998).

1.5.3.1 Calpains

Calpains (CAPNs) form a group of calcium-activated cysteine proteases. Until now, 15 calpain isoforms have been identified in humans. They can be divided into classical calpains, that contain a cysteine protease sequence (CysPc), a calpain-type beta-sandwich domain (CBSW), previously called C2 domain-like domain (C2L), a penta EF-hand (PEF) motif, and into non-classical calpains, that do not contain CBSW and/or PEF domains (Ono and Sorimachi, 2012; Sorimachi et al., 2011). The classical calpains comprise CAPN1, -2, -3, -8, -9, -11, -12, -13, and -14, the non-classical types include CAPN5, -6, -7, -10, -15, and -16.

The best characterized calpains are the ubiquitously expressed CAPN1 and -2, which are also called “conventional calpains”. They consist of a large catalytic subunit (CL) of 80 kDa and a regulatory small subunit (CAPNS) of 28 kDa, that is necessary for stability of the large subunit (Camins et al., 2006; Ono and Sorimachi, 2012). The CL comprises four domains: First, the N-terminal anchor

helix region (domain I) that regulates calpain activity. It is autolyzed by different calcium levels, substrates, and situations (Sorimachi et al., 2011). Second, the protease domain CysPc (domain II) that inherits calcium-dependent protease activity (Ono and Sorimachi, 2012; Sorimachi et al., 2011). Third and fourth, the calcium-binding domains III and IV that include PEF (PEF(L)) domains (Curcio et al., 2016). CAPNS also consists of a PEF domain (PEF(S)), also called domain VI, and a N-terminal glycine-rich domain (GR) (domain V), that is mostly autolyzed during activation. PEF(S) and PEF(L) form the heterodimer with both subunits (Ono and Sorimachi, 2012; Sorimachi et al., 2011).

CAPN1 and -2 mainly differ in the calcium level needed for their activation *in vitro*. Calpain-1 requires micromolar ranges (3-50 µM) of calcium, giving it the name µ-calpain, whereas calpain-2 requires calcium levels 10-fold higher, nearly in the millimolar range (0,4-0,8 mM), and is therefore called m-calpain (Camins et al., 2006; Cheng et al., 2018). Both show 60% sequence homology and are, so far, almost impossible to distinguish in their substrates, although sporadically, some isoform-specific targets are identified. For instance, Briz et al. were the first to identify the calpain-2-specific substrate, PTEN (Carragher, 2006; Sorimachi et al., 2011; Briz et al., 2013). As the calcium concentrations needed for calpain activation *in vitro* are unavailable *in vivo,* it raises the question how *in vivo* activation proceeds (Ono and Sorimachi, 2012). Some findings hint to an explanation of high local concentrations rather than intracellular levels and to other activation mechanisms: Firstly, phospholipids localized in the cellular membrane were able to lower calcium levels that are required for calpain activation and calpains were translocated from cytoplasm to the membrane when calcium levels increase (Cheng et al., 2018; Ono and Sorimachi, 2012). Secondly, a locally impaired calcium buffering reaching required concentrations was suggested by the finding that calpains are specifically localized at NMDA receptors, where calcium transport takes place (Briz and Baudry, 2017). And lastly, also non-calcium-dependent pathways of calpain activation via phosphorylation were found (Zadran et al., 2009).

There is a broad range of cellular functions in which calpains were shown to be involved. Calpains have been linked to general cellular processes such as cell

signalling (Noguchi et al., 1997), subcellular, cytoskeletal organization (Pontremoli and Melloni, 1988), motility (Wells et al., 2005; Glading et al., 2002), apoptosis and necrosis (Cheng et al., 2018), synaptic plasticity, neuroprotection and neuronal differentiation (Briz and Baudry, 2017), and membrane repair (Mellgren and Huang, 2007). Therefore, substrates known to be proteolyzed by calpains include cytoskeletal cytosolic proteins, e.g. actin-binding proteins such as *α*-spectrin, actinin, tubulin, microtubule-associated protein 2 (MAP2), tau, and neurofilaments, growth factors, NMDA receptors, mitochondrial proteins, nuclear proteins such as transcription factors, e.g. E2F-1 and c-jun, and signal transduction proteins, including members of the apoptotic pathways such as Bcl-2, AIF and caspases (Carafoli and Molinari, 1998; Camins et al., 2006)). In contrary to other main cellular proteolytic systems, speaking of the autophagy-lysosome-system and caspases, that degrade cellular components unspecifically, calpains rather function as a proteolytic processing system that modifies the activity, function, structure, or localization of specific substrates (Sorimachi et al., 2011).

A crucial element of the so-called calpain system in the living cell is calpastatin (CAST), a highly specific, endogenous inhibitor of the conventional calpains (Maki et al., 1987). CAST comprises four inhibitory units, each of which inhibits one calpain molecule (Hanna et al., 2007). Although calpastatin itself lacks calcium-binding sites, it is activated by calcium increase as it associates in aggregates in an inactive state and is redistributed when calcium levels rise, even though the calcium concentrations needed for calpastatin-mediated inhibition are significantly lower than those needed for effective proteolysis by calpains (Curcio et al., 2016; Goll et al., 1992; Wendt et al., 2004). Overexpression of CAST did not have negative effects on life span, behaviour, development, or fertility, indicating that CAST acts as an inhibitor of calpains only under pathological conditions (Takano et al., 2005).

In contrast to neurodegenerative diseases, which are linked to alterations of calpain activity as addressed in 1.5.3.2, there is a phenotypically heterogenous group of diseases, termed calpainopathies, that are caused by mutations in calpain genes. A mutation in CAPN3 that is mainly expressed in skeletal muscle

and responsible for sarcomere remodelling causes limb-girdle muscular dystrophy type 2A (LGMD2A), the most common type of LGMD (Hosseini et al., 2018). Spastic paraplegia 76 (SPG76) is linked to a loss-of-function mutation in the gene of CAPN1 (Gan-Or et al., 2016). Gene mutations leading to hyperactivation of CAPN5 are causative for autosomal-dominant neovascular inflammatory vitreoretinopathy (ADNIV) (Mahajan et al., 2012; Tang et al., 2020). Single nucleotide polymorphisms in genes encoding for CAPN8 and CAPN9 are implicated in gastric injury and CAPN10 polymorphisms are related to type 2 diabetes mellitus (Hosseini et al., 2018).

1.5.3.2 The role of calpains in neurodegenerative diseases

Calpains were shown to be over-activated in many neurodegenerative diseases and to cleave disease-causing proteins. The group of disorders or pathological conditions showing raised calpain activity comprises HD (Clemens et al., 2015; Weber et al., 2018), SCA3 (Haacke et al., 2007; Hubener et al., 2013), AD (Higuchi et al., 2012; Mahaman et al., 2019), ALS (Wootz et al., 2006), PD (Mouatt-Prigent et al., 1996; Diepenbroek et al., 2014), multiple sclerosis (MS) (Shields et al., 1999), brain ischemia, and traumatic brain injury (Bartus et al., 1994; Hosseini et al., 2018). Calpains also show an involvement in non-neurological diseases such as muscular dystrophy, cataract, arthritis, cancer, diabetes, cardiomyopathy, or endothelial dysfunction (Ono and Sorimachi, 2012; Hosseini et al., 2018). Furthermore, inhibition of calpain activity could reduce toxicity and phenotypical appearance in various studies (Weber et al., 2019). Although calpains might be overactivated as a concomitant of cell death, it is assumed for diseases, like HD, SCA1, SCA3, and AD that calpain activation occurs before symptom onset without connection to an apoptotic or necrotic processes, but is correlated to a concurrent disruption of cellular calcium balance as an early event in pathogenesis (Haacke et al., 2007; Kurbatskaya et al., 2016; Lin et al., 2000; Clemens et al., 2015). Investigations in a rat model of HD revealed mitochondrial dysfunction in calcium buffering by binding of polyQ-expanded htt to the mitochondrial membrane and transcriptional disruption of mitochondrial genes (Clemens et al., 2015). In addition, polyQ-expanded htt

was shown to further sensitize NMDA receptors and the inositol triphosphate receptor IP3R, a calcium channel in the smooth endoplasmic reticulum, resulting in enhanced calcium influx and release from ER stores (Gafni et al., 2004; Lieberman et al., 2019). Moreover, expression of calcium-sensing and -binding proteins are downregulated in HD, SCA1, AD, ALS, and PD (Haacke et al., 2006; Muddapu et al., 2020). Regarding SCA17, expression levels of calcium-regulating proteins such as calbindin, a calcium-binding protein, and IP3R, were shown to be altered (Chang et al., 2011; Weber et al., 2022). In summary, these findings suggest calcium dyshomeostasis and thus aberrant calpain activation as a unifying neurodegenerative mechanism. However, as respective evidence on calpain activation in SCA17 is still missing, further analyses are necessary.

1.6 What makes SCA17 interesting?

Although SCA17 is so far thought to represent only 0.5-1% of all ADCA cases, it constitutes a valuable model disease for other polyQ disorders and for elucidating the function of the transcription factor TBP itself (Brusco et al., 2004; Craig et al., 2005). Especially the widely discussed pathomechanisms of transcriptional disruption highlights the importance of investigations on wild-type and polyQ-expanded TBP. This is further stressed by the fact that wild-type TBP was found to be sequestered in protein aggregates formed in HD, SCA1, SCA3 and DRPLA (Hsu et al., 2014; Perez et al., 1998; van Roon-Mom et al., 2002; Yamada et al., 2001). The phenotype of SCA17 comprises characteristics known from HD and spinocerebellar ataxias, particularly SCA3. Understanding SCA17 draws a connective link between these diseases and may broaden our knowledge of polyQ disorders. Last, moderate expansions of TBPs polyQ stretch have been associated with a wide range of impairments in neuronal pathways. Being one of the very few monogenetic causes known for psychiatric disorders, SCA17 can symptomatically manifest solely as a psychiatric phenotype with dementia and therefore represents a suitable model for idiopathic diseases of this kind (Rolfs et al., 2003). Furthermore, it is discussed as a susceptibility gene and differential diagnosis for PD as manifestation can be limited to parkinsonism (Choubtum et al., 2015; Kim et al., 2009; Wu et al., 2004).

1.7 Aim of the thesis

Multiple research approaches and the comparison to other polyQ diseases were aiming at elucidating the underlying disease mechanisms of SCA17 to find potential therapeutic targets. A yet underinvestigated field within SCA17 is proteolytic cleavage and the occurrence of protein fragments of polyQ-expanded TBP, which can be found in affected neuronal cells. These fragments were described as toxic, as they tend to misfold, aggregate, and dysregulate TBPs transcriptional activity (Friedman et al., 2008). Several proteolytic systems have been described as the source of polyQ disease proteins fragments (Weber et al., 2014). However, none of them has yet been shown to cleave polyQ-expanded TBP.

Therefore, this study aims at the unknown origin of TBP's fragmentation and focuses on proteolysis by the class of calcium-dependent cysteine proteases called calpains, which have previously been associated with disease conditions such as HD, SCA3, AD, ALS, PD, multiple sclerosis, brain ischemia, and neurodegeneration in general (Weber et al., 2019; Hosseini et al., 2018).

First, by performing western blot analysis, it should be clarified if TBP cleavage products can be found in SCA17 cells and our SCA17 animal model, the TBP64Q rat (Kelp et al., 2013).

Second, using calpain activation assays *in vitro* with exogenous calpains and *in cellulo* with pharmacologic means, it will be assessed if these fragments derive from calpain-mediated cleavage.

Third, by analysing levels of the endogenous inhibitor calpastatin and the well-described calpain substrate *αII*-spectrin (Briz and Baudry, 2017), it needs to be analysed if calpains are overactivated in our SCA17 models at baseline.

And last, this study must evaluate the targetability of the calpain system as a therapeutic approach for SCA17, which was approached by overexpressing calpastatin and applying pharmacologic inhibitors of calpains and assessed by measuring the effects on TBP fragmentation and aggregation.

2 Material

2.1 Equipment

Table 3. List of used equipment.

Equipment	Type	Supplier
cell counting chamber	Neubauer improved counting chamber bright line depth: 0.1 mm plain: 0.0025 mm^2	Glaswarenfabrik Karl Hecht GmbH & Co. KG, Sondheim, DE
centrifuges	centrifuge Eppendorf 5415 R (cooling centrifuge)	Eppendorf AG, Hamburg, DE
	centrifuge Eppendorf 5417 C	
	centrifuge Eppendorf 5418	
	centrifuge Eppendorf 5810 R	
clean benches	HERAsafe HS 12	Heraeus Holding GmbH, Hanau, DE
	HERAsafe HS 18	
	HERAsafe HS 18	
CO_2 incubator	CB219	Binder GmbH, Tuttlingen, DE
disperser	Ultra-Turrax disperser	VWR International, Radnor, US
tank blotter	TE22 mighty small transfer tank	Hoefer Inc., Holliston, US
slot blot system	Minifold II slot blot system GZ-28567-30	Cole-Parmer GmbH, Wertheim, DE
gel system (SDS-PAGE)	mini gel tank	Life Technologies (Thermo Fisher Scientific), Carlsbad, US

	mini-protean	Bio-Rad Laboratories GmbH, Munich, DE
heating block	HLC HBT 130	HLC Haep Labor Consult, Bovenden, DE
	HLC HTM 130	
	Thermomixer compact	Eppendorf AG, Hamburg, DE
	ThermoStat plus	
incubator shaker	Multitron HT	Infors GmbH, Einsbach, DE
microplate reader	Synergy HT	BioTek Instruments Inc., Winooski, US
microscopes	ECLIPSE TS100	Nikon, Tokio, JPN
	EVOS XL core imaging system	Invitrogen (Thermo Fisher Scientific), Darmstadt, DE
mixing devices	Polymax 1040	Heidolph Instruments GmbH & Co. KG, Schwabach, DE
	RM 5	Ingenieurbüro CAT, M. Zipperer GmbH, Ballrechten-Dottingen, DE
	RM 5 type 348 (rolling shaker)	Glaswarenfabrik Karl Hecht GmbH & Co. KG, Sondheim, DE
pH meter	S20 SevenEasy pH	Mettler-Toledo GmbH, Gießen, DE
photometer	BioPhotometer with Eppendorf µcuvette G1.0	Eppendorf AG, Hamburg, DE
power supplies	BluePower 500	Serva Electrophoresis GmbH, Heidelberg, DE
	Consort E443	Consort bvba, Turnhour, BE

	electrophoresis power supply EPS301	GE Healthcare Life Science, Amersham, UK
scales	Precisa 404 A	Precisa Gravimetrics AG, Dietikon, CH
	Precisa XB 620M	
	Precisa XT 6200C-FR	
ultrasonicator	Boosterhorn SH213 G	Bandelin electronic GmbH & Co. KG, Berlin, DE
	Sonopuls HD2200	
	Sonotrode MS 73	
	UW 2200	
vacuum pump	ECOM-P 1453	Eppendorf AG, Hamburg, DE
	XX552050 Millipore membrane vacuum pump	Merck Millipore, Billerica, US
vortex	REAX Control	Heidolph Instruments GmbH & Co. KG, Schwabach, DE
	Vibro-Fix VF2	IKA Werke GmbH & Co. KG, Staufen, DE
	Vortex Genie 2	Bender & Hobein AG, Zurich, CH
	Vortex Mixer 7-2020	neoLab Migge Laborbedarf-Vertriebs GmbH, Heidelberg, DE
water bath	GFL 1008	Gesellschaft für Labortechnik GmbH, Burgwedel, DE
	GFL 1083	
western blot imaging system	Odyssey Fc dual-mode imaging system	LI-COR Bioscience, Lincoln, US

2.2 Expendable materials

Table 4. List of expendable material.

Material	Type	Supplier
pre-cast gels	NuPAGE 4-12% bis-tris precast gels	Life Technologies (Thermo Fisher Scientific), Carlsbad, US
	NuPAGE 7% tris-acetate precast gels	
cell culture flasks	CELLSTAR 25 and 75 cm^2	Greiner Bio One GmbH, Frickenhausen, DE
cell culture microplates	CELLSTAR 96 wells	Greiner Bio One GmbH, Frickenhausen, DE
cell culture multi-well plates	Falcon polystyrene 6, 12 and 24 wells	Corning Inc., New York, US
chromatography and FR paper	Whatman 17CHR, 0.92 mm and 3 mm	Carl Roth, Karlsruhe, DE
nitrocellulose membranes	Amersham Protran 0.45µm NC	GE Healthcare Life Science, Amersham, UK
	Amersham Protran Premium 0.2µm NC	

2.3 Chemicals

Table 5. Table of applied chemicals.

Chemical	Supplier
acrylamide/N,N´-methylenbisacrylamide (29:1), 30%	Bio-Rad Laboratories GmbH, Munich, DE
ampicillin sodium salt 100 mg/ml	Carl Roth, Karlsruhe, DE
dithiothreitol (DTT)	VWR International, Radnor, US
ethylendiaminetetraceticacid (EDTA)	Carl Roth, Karlsruhe, DE
Odyssey blocking buffer	Li-COR Bioscience, Lincoln, US
phosphatase inhibitor PhosSTOP EASYpack	Sigma Aldrich, St. Louis, US
Pierce bovine serum albumin (BSA) (2 mg/ml)	Thermo Fisher Scientific, Waltham, US
protease inhibitor, cOmplete mini (EDTA-free)	Sigma Aldrich, St. Louis, US
Slimfast	Allpharm Vertriebs-GmbH, Messel, DE
tetramethylethylendiamin (TEMED)	AppliChem GmbH, Darmstadt, DE
Triton X-100	Carl Roth, Karlsruhe, DE
trypsin-EDTA 0.25% (1x)	Life Technologies (Thermo Fisher Scientific), Carlsbad, US

2.4 Kits and reagents

Table 6. Listing of reagents and kits.

Kit/reagent	Specification	Supplier
calpain inhibitor III	208722	Calbiochem (Merck Millipore), Billerica, US
calpain-1	208712	Calbiochem (Merck Millipore), Billerica, US
calpain-2	208718	Calbiochem (Merck Millipore), Billerica, US

calpain-2	TP305642	OriGene Technologies, Inc., Rockville, US
calpain-2	TP720945	OriGene Technologies, Inc., Rockville, US
Coomassie Brilliant Blue G-250 Dye		Thermo Fisher Scientific, Waltham, US
5xBio-Rad protein assay dye reagent concentrate		BioRad Laboratories, Inc., Hercules, US
Quick Start Bradford protein assay		BioRad Laboratories, Inc., Hercules, US
WesternBright ECL/ Sirius chemiluminescent detection kit		Advansta Inc., San Jose, US

2.5 Molecular weight protein standards

Table 7. Register of molecular weight standards.

Molecular weight protein standard	Supplier
HiMark pre-stained protein standard	Life Technologies (Thermo Fisher Scientific), Carlsbad, US
SeeBlue plus2 pre-stained protein standard	Life Technologies (Thermo Fisher Scientific), Carlsbad, US

2.6 Buffer and solutions

Table 8. List of buffers and solutions. If not stated differently, all solutions are aqueous and prepared with ddH_2O.

Buffer/Solution	Composition
10% APS	10% (w/v) ammonium persulfate
10% SDS solution	10% (w/v) sodium dodecyl sulfate
2% NaN_3	2% (w/v) sodium azide
3.5x gel buffer pH 6.5 – 6.8	1.25 M bis-tris
4% PFA	4% paraformaldehyde (w/v) in DPBS (1x)

blocking buffer	5% (w/v) Slim fast in TBS (1x)
calpain reaction buffer pH 7.6	20 mM HEPES/KOH 10 mM KCl 1.5 mM $MgCl_2$ 1 mM DTT 0.1% (v/v) Triton X-100
EB buffer pH 8.5	10 mM tris base
LDS loading buffer (4x) pH 8.5	40% (v/v) glycerol 1 M tris base 8% LDS 2 mM EDTA 0.075% (v/v) Coomassie brilliant blue G250 0.025% (v/v) phenol red
MES SDS running buffer (20x) pH 7.7	1 M MES 1 M tris base 69.3 mM SDS 20.5 mM EDTA
NuPAGE running buffer (20x) pH 8.25	1 M tricine 1 M tris base 70 mM SDS
NuPAGE transfer buffer (20x) pH 7.2	500 mM bicine 500 mM bis-tris 20.5 mM EDTA
RIPA buffer	150 mM NaCl 50 mM tris-HCl 1% (v/v) Triton X-100 0.5% SDC 0.1% SDS cOmplete mini, PhosSTOP

stripping buffer (1x) pH 2.0	25 mM glycine 1% (w/v) SDS 1% (v/v) Tween-20
TBE buffer (10x)	0.89 mM tris-HCl 0.89 mM boric acid 2 mM EDTA
TBS buffer (10x) pH 7.5	1.5 M NaCl 100 mM tris-HCl
TBST buffer (10x) pH 7.5	1.5 M NaCl 100 mM tris-HCl 1% (v/v) Tween-20

2.7 Animals

Table 9. List of the used animals. The age is indicated in months (m).

Animal No.	Date of birth	Genotype	Line	Sacrificed on	Age (m)
AK.R.P (8.4) 268	7/13/2014	WT	PRP-TBP-Q64 (8.4)	6/9/2015	10
AK.R.P (8.4) 272	7/13/2014	WT	PRP-TBP-Q64 (8.4)	6/9/2015	10
AK.R.P (8.4) 275	7/13/2014	WT	PRP-TBP-Q64 (8.4)	6/9/2015	10
AK.R.P (8.4) 284	8/8/2014	WT	PRP-TBP-Q64 (8.4)	6/9/2015	10
AK.R.P (8.4) 288	8/8/2014	WT	PRP-TBP-Q64 (8.4)	6/9/2015	10

AK.R.P (8.4) 290	8/15/2014	WT	PRP-TBP-Q64 (8.4)	6/9/2015	9
AK.R.P (8.4) 291	8/15/2014	WT	PRP-TBP-Q64 (8.4)	6/9/2015	9
AK.R.P (8.4) 001	8/20/2014	TBPQ64	PRP-TBP-Q64 (8.4)	6/9/2015	9
AK.R.P (8.4) 276	7/13/2014	TBPQ64	PRP-TBP-Q64 (8.4)	6/9/2015	10
AK.R.P (8.4) 286	8/8/2014	TBPQ64	PRP-TBP-Q64 (8.4)	6/9/2015	10
AK.R.P (8.4) 289	8/8/2014	TBPQ64	PRP-TBP-Q64 (8.4)	6/9/2015	10
AK.R.P (8.4) 127.12	2/2/2015	TBPQ64	PRP-TBP-Q64 (8.4)	6/9/2015	9
AK.R.P (8.4) 127.15	2/2/2015	TBPQ64	PRP-TBP-Q64 (8.4)	6/9/2015	9
AK.R.P (8.4) 127.16	2/2/2015	TBPQ64	PRP-TBP-Q64 (8.4)	6/9/2015	9

2.8 Cell culture material and media

Table 10. List of material used specifically for cell culture methods.

Substance	Specification	Supplier
A/A (100x)	10.000 U/ml penicillin, 10.000 µg/ml streptomycin, 25 µg/ml Fungizone	Life Technologies (Thermo Fisher Scientific), Carlsbad, US
4% PFA	4% in DPBS	-
Attractene	Attractene transfection reagent	Qiagen, Venlo, NL
DMEM GlutaMAX	DMEM + L-alanyl-L-glutamine, high glucose (4.5 g/l), pyruvate Catalogue no.: 31966021	Life Technologies (Thermo Fisher Scientific), Carlsbad, US
DMSO	-	Sigma Aldrich, St. Louis, US
DPBS (1x)	-	Life Technologies (Thermo Fisher Scientific), Carlsbad, US
FCS	-	Life Technologies (Thermo Fisher Scientific), Carlsbad, US
G418-BC	30.000 U/ml Geneticin in ddH_2O	Biochrom AG, Berlin, DE
horse serum	-	Thermo Fisher Scientific, Waltham, US
ionomycin	ionomycin, free acid, *Streptomyces conglobatus* 407950	Calbiochem® (Merck Millipore), Billerica, US

NEAA (100x)	-	Life Technologies (Thermo Fisher Scientific), Carlsbad, US
Opti-MEM(1x)	-	Life Technologies (Thermo Fisher Scientific), Carlsbad, US
poly-L-lysine	0.01% (w/v) poly-L-lysine (70-150 kDa)	Sigma Aldrich, St. Louis, US
trypsin-EDTA (1x)	0.25% trypsin, 1 mM EDTA	Life Technologies (Thermo Fisher Scientific), Carlsbad, US

2.9 Cell lines

Table 11. List of used cell lines.

Cell line	Type	Medium
HEK 293T	human embryonal kidney 293 cells ATCC: CRL-3216	DMEM (1x) GlutaMAX + 10% FCS + 1% NEAAs + 1% A/A
PC12	rat embryonic neural crest cells, stably transfected with murine TBP-13Q and TBP105-Q with EGFP-tag, emission at 507nm, provided by Xiao-Jiang Li & Shihua Li, Jinan, University Guangzhou, China	DMEM (1x) + 10% horse serum + 5% foetal calf serum + 1% G-418 + 1% A/A

2.10 Bacteria culture and media

Table 12. List of material used specifically for cell culture methods.

Substance	Specification	Supplier
ampicillin	Ampicillin sodium salt 100 mg/ml	Carl Roth, Karlsruhe, DE
LB medium	1% (W/v) NaCl 1% (w/v) tryptone 0.5% (w/v) yeast extract	-
QIAprep Spin Miniprep Kit (250)	-	Qiagen, Venlo, NL

2.11 Plasmids

Table 13. Overview of applied vectors and expression constructs with characteristics. All plasmids were expressed in E. coli DH5α.

Plasmid	Specification	Protein	Characteristics	Supplier
pBS II SK (+) mPrP	empty size: 2961 bp promotor: PrP (mammalian expression) selection: amp^R	human TBP-38Q human TBP-64Q	5'-myc-tag	(Kelp et al., 2013)
pCMS-EGFP	empty size: 5500 bp promotor: CMV (mammalian expression) selection: amp^R	murine TBP-13Q murine TBP-105Q	coexpression of EGFP	(Friedman et al., 2007)
pRK5	empty size: 4754 bp	human CAST control (mock)		(Weber et al., 2018)

	promotor: CMV (mammalian expression) selection: amp^R	human CAST	mock vector: inactivation of the CMV promotor by excision using the restriction enzymes SpeI and XbaI

2.12 Antibodies

Table 14. List of primary antibodies. All antibody solutions were supplemented with 0.02% NaN_3.

Target	Host	Catalog No.	Dilution	Supplier
β-actin	mouse	A5441 clone AC - 15	1:5.000 in TBST + 5% BSA	Sigma Aldrich, St. Louis, US
calpain-1	rabbit	ab39170	1:500 in TBST	Abcam, Cambridge, UK
calpain-1	rabbit	PA5-14547	1:500 in TBST	Invitrogen (Thermo Fisher Scientific) Darmstadt, DE
calpain-2	rabbit	ab39165	1:500 in TBST	Abcam, Cambridge, UK
calpastatin	rabbit	4146	1:1000 in TBST + 5% BSA	Cell Signaling Technology®, Danvers, US
c-myc 9E10	mouse	sc-40	1:200 in TBST	Santa Cruz Biotechnology, Inc., Dallas, US
polyQ 1C2	mouse	MAB1574	1:1.000 in TBST	Merck Millipore, Billerica, US

spectrin αII-chain	mouse	MAB1622	1:1000 in TBST + 5% BSA	Merck Millipore, Billerica, US
TBP 58C9	mouse	T1827	1:500 in TBST	Sigma Aldrich, St. Louis, US
TBP 8515	rabbit	8515	1:1000 in TBST + 5% BSA	Cell Signaling Technology®, Danvers, US
TBP D5G7Y	rabbit	12578	1:500 in TBST + 5% BSA	Cell Signaling Technology®, Danvers, US
TBP N-12	rabbit	sc-204	1:250 in TBST	Santa Cruz Biotechnology, Inc., Dallas, US
α-tubulin	mouse	CP06	1:6.000 in TBST	Merck Millipore, Billerica, US
vinculin	rabbit	13901	1:1000 in TBST + 5% BSA	Cell Signaling Technology®, Danvers, US

Table 15. List of secondary antibodies.

Antibody	Host	Catalog No.	Dilution	Supplier
Goat anti-rabbit IgG H&L (HRP)	goat	ab97071	1:5000 in TBST	Abcam, Cambridge, UK
IRDye 680LT goat anti-mouse	goat	926-68020	1:10.000 in TBST	Li-COR Bioscience, Lincoln, US
IRDye 800CW goat anti-mouse	goat	923-32210	1:10.000 in TBST	Li-COR Bioscience, Lincoln, US
IRDye 800CW goat anti-rabbit	goat	923-68071	1:10.000 in TBST	Li-COR Bioscience, Lincoln, US
Rat anti-mouse IgG (HRP)	rat	ab131368	1:5000 in TBST	Abcam, Cambridge, UK

2.13 Software

Table 16. List of applied software programs and their supplier.

Software	Supplier
CorelDRAW Graphics Suite X5	Corel GmbH, München, DE
Gen5 data analysis software	BioTek Instruments Inc., Winooski, US
GPS-CCD	The Cuckoo Workgroup, Hubei, CH
GraphPad Prism 5	GraphPad Software Inc., San Diego, US
Image Studio Software Version 2.1	LI-COR Bioscience, Lincoln, US
Microsoft Excel	Microsoft Corporation, Redmond, US

3 Methods

3.1 Cell culture

3.1.1 Cultivation of HEK 293T cells

For culturing, HEK 293T cells were maintained in glutamine containing 1x Dulbecco's modified eagle medium (DMEM GlutaMAX) supplemented with 10% foetal calf serum (FCS), 1% non-essential amino acids (NEAAs), and 1% antibiotic-antimycotic (A/A) using 75°cm² cell culture flasks. The cells were kept at standard culturing conditions with 5% CO_2 at 37 °C and 100% humidity. Splitting was performed every 2-7 days, depending on their appearance in light microscopy and medium pH-value. For splitting, the old medium was aspirated, and the flask was washed with 1x Dulbecco's phosphate-buffered saline (DPBS). Cells were then detached from the bottom of the flask by incubation with 1 ml trypsin for 2 min at 37 °C. After incubations, cells were separated by shear forces by pipetting up and down after adding 7 ml medium. 1 ml of cell suspension was then filled with 9 ml of new medium, while 7 ml were either discarded or used for subculturing or other experiments.

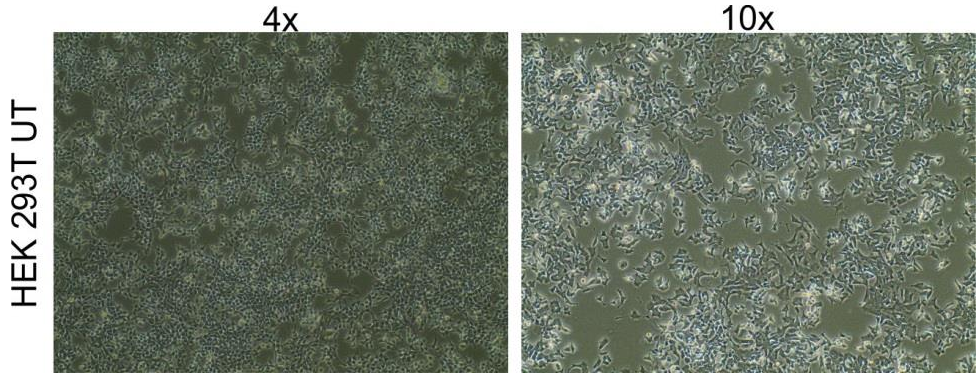

Figure 6. Light microscopy of untransfected HEK 293T cell culture. Untransfected HEK 293T cells were microscoped using a 4x and 10x objective lens of a EVOS XL Core microscope (Invitrogen, Darmstadt, DE).

3.1.2 Cultivation of PC12 cells

PC12 cells stably expressing murine (m-) TBP-13Q and mTBP-105Q plasmids were grown in 1x DMEM, supplemented with 10% horse serum, 5% FCS,1% G-418, and 1% A/A. Growing conditions and splitting correspond to those applied for culturing of HEK 293T cells (see 3.1.1).

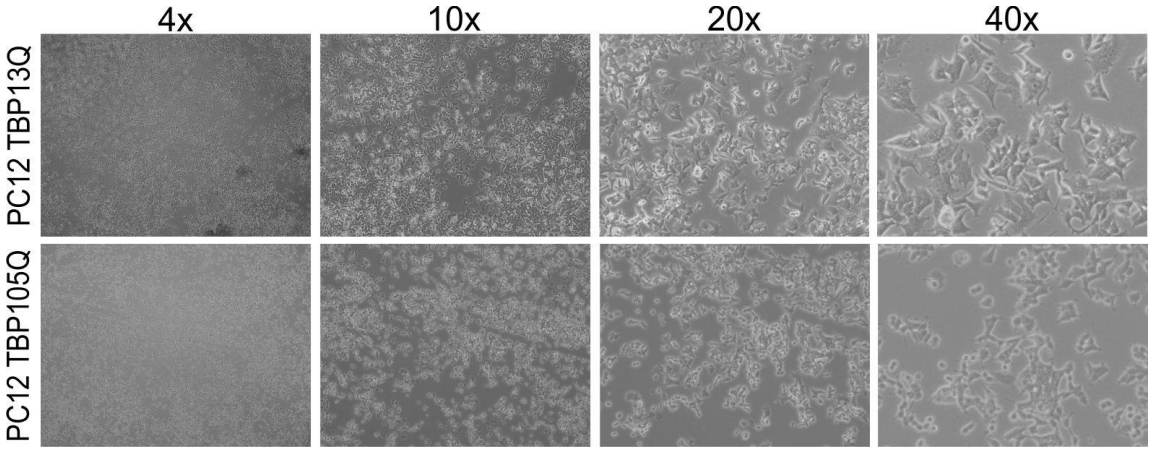

Figure 7. Imaging of PC12 cell culture under light microscopy. PC12 cells expressing mTBP-13Q (upper row) and mTBP-105Q (lower row) were microscoped with the EVOS XL Core microscope (Invitrogen, Darmstadt, DE) using 4x, 10x, 20x and 40x objectives.

3.1.3 Cell counting

Cells were counted using the Neubauer Improved Counting Chamber (Karl Hecht GmbH & Co. KG, Sondheim, DE) filled with 10 µl of cell suspension. Using light microscopy, cells within four 1x1 mm squares were counted and the mean number was calculated for one square. This value, representing the cell number of 0.1 mm^3 volume, was multiplied with the factor 10^4 to obtain the cell count for 1 ml cell suspension.

3.1.4 Seeding

For further seeding, cell suspensions were obtained as described in 3.1.1, diluted up to 20 ml with 1x DPBS. The cell number of the suspension was then determined as described in 3.1.3 and centrifuged at 250 rpm for 5 min to retrieve a cell pellet. The pellet was resuspended in cell culture medium to a stock

concentration of 10^7 cells/ml and then further diluted and seeded in desired amount for subsequent experiments.

3.1.5 Expression constructs

For overexpression of TBP with 38 or 64 glutamines, pBSSKII+ mPrP vectors carrying cDNA for myc-tagged full-length human TBP (hTBP) were applied (Kelp et al., 2013). Expression constructs for murine TBP, were based on TBP cDNA coding for TBP with 13 or 105 glutamines integrated into pCMS-EGFP vectors (Friedman et al., 2007). A pRK5 vector carrying the cDNA for full-length hCAST was used for overexpression of calpastatin. A mock vector with a removed promotor region was used as control for transfections with hCAST (Weber et al., 2018).

3.1.6 Plasmid preparation

To isolate plasmids for the aforementioned constructs hTBP-38Q (Stock 146), hTBP-64Q (Stock 147), hCAST, and CAST mock, a scrape of a cryostock of respectively transformed *E. coli* bacteria, were transferred to 10 ml LB medium (1% (w/v) NaCl, 1% (w/v) tryptone, 0.5% (w/v) yeast extract) supplemented with 100 µg/ml ampicillin using a pipette tip and incubated overnight at 37 °C and 225 rpm in a shaking incubator. The plasmid preparation for DNA isolation was performed using the QIAprep® Spin Miniprep Kit following the manufacturer's protocol by alkaline lysis of the cells and binding of the DNA to a silica membrane (Qiagen, Venlo, NL). Plasmids were eluted in 50 µl elution buffer EB (10 mM tris-Cl pH 8.5). All centrifugation steps were performed at 17,900 x g. Afterwards, the concentration of double-strand plasmid DNA was measured photometrically using 1.5 µl of the eluate via a BioPhotometer and a µCuvette G1.0 (both Eppendorf AG, Hamburg, DE). Hereby, the optic density for DNA was measured at 260°nm. Moreover, the purity of the DNA isolation was determined by calculating the ratio of extinctions at 260 nm and 280 nm wavelength ($OD_{260/280}$) considering a value of 1.8 as optimal.

3.1.7 Transfections

Cells were seeded 24 h prior to transfection. For standard approaches, HEK 293T cells were seeded in 6-well plates with 500,000 cells in 2 ml medium per well. For transfections, the non-liposomal transfection reagent Attractene (QIAGEN, Venlo, NL) was used following the manufacturer's protocol.

In brief, purified plasmid DNA was diluted in 100 µl serum-free medium and supplemented with Attractene in the ratio 1:3.75 with 1.2 µg DNA and 4.5 µl transfection reagent per well of a 6-well plate. The transfection mix was then vortexed, centrifuged and incubated for 15 min at room temperature (RT), added to the cells, and incubated for the desired time.

3.1.8 Cell-based calpain activation assays with ionomycin

To analyse the effects of calpain activation and calpain inhibition on TBP fragmentation and the calpain system in an intact cellular environment, cell-based calpain activation assays were performed in living HEK 293T and PC12 cells. For activation of endogenous calpains, the calcium ionophore ionomycin was used, which allows calcium ions to pass into the cell by binding the ion and diffusing through the cell membrane, releasing the calcium ion again on the intracellular side. The increase of intracellular calcium activates the calcium-dependent calpain system. The alterations caused by calpain activation were analysed in control samples treated with the vehicle DMSO in cells treated with ionomycin/calcium supplemented with DMSO, and with the inhibitor controls, which were treated with both calpain inhibitors and ionomycin/calcium to observe the efficiency of calpain inhibition under activating conditions.

Prior to the treatment, 500,000 HEK 293T cells were seeded, transfected the next day, and cultured for an additional 48 h. For PC12 cells, 1,000,000 cells were seeded and cultured for 48 h. For both transfected HEK 293T cells and PC12 cells, medium was then replaced with 1 ml OptiMEM for the treatment.

Calpain inhibition was performed by preincubating HEK 293T cells for 1 h with the 25 µM calpain inhibitor III (CI-III: 208722, Calbiochem, Billerica, US),

prediluted in Opti-MEM prior to ionomycin/calcium addition. The DMSO controls and the ionomycin/calcium treatment samples were incubated with similar concentration of DMSO to exclude effects by the vehicle. Subsequently, 1 µM ionomycin and 5 mM calcium were diluted in Opti-MEM and 50 µl per well added and incubated at 37 °C at different time points for up to 2 h. The time points were established as described in 4.4.

3.1.9 Calpain inhibition in PC12 cells

The efficacy of longer calpain inhibition was investigated in PC12 cells expressing mTBP-13Q and mTBP-105Q for 24 h and 48 h of inhibitor treatment. Before seeding, the 6-well cell culture plates were coated with poly-L-lysine to avoid cell detachment during treatments. Therefore, poly-L-lysine was distributed on the wells by rocking gently. The solution was removed after 5 min, rinsed with sterile water, then dried for at least 2 h at 37 °C. 1 million cells were seeded per well and grown for 48 h. As described for cell based calpain activation assays in 3.1.8, 25 µM CI-III diluted in 100 µl Opti-MEM were applied for the 24 and 48 h of treatment at 37 °C.

3.1.10 Harvesting of the cells

After transfection for baseline analysis or after cell-based treatments, the cells were harvested and collected as a cell pellet. Before harvesting, confluence and integrity of the cell layer was monitored by microscopy to avoid cell loss during aspiration of medium.

Subsequently, medium was removed, the cells were washed once with 1x DPBS and detached from the bottom of the well by addition of 1 ml 1x DPBS per well and resuspension. Cell suspension was transferred to 1.5 ml reaction tubes and then centrifuged for 2.5 min at 400 x g. After aspiration of the supernatant, cell pellets were kept on ice until further processing or moved to -80 °C for longer storage.

3.2 Protein methods

3.2.1 Protein isolation of brain tissue

Rat brain samples were obtained from male hTBP-64Q animals, generated at our institute (Kelp et al., 2013), together with the respective male wild-type littermates. At the age of 9 or 10 months, rats were sacrificed by CO_2 inhalation and brains dissected on ice in the brain areas cerebellum, cortex, and striatum. The samples were snap-frozen in liquid nitrogen and stored at -80 °C. For preparation of protein extracts, tissue samples were lysed in calpain reaction buffer CRB (20 mM HEPES/KOH pH 7.6, 10 mM KCl, 1.5 mM $MgCl_2$, 1 mM DTT, 0.1% (v/v) Triton X-100) in a ratio 1:10 (w/v) (for detailed list of tissue weights see Table 17) and homogenized for 30 s at level 4 using a Ultra-Turrax disperser (VWR International, Radnor, US). Thereby generated homogenates were incubated on ice for 25 min with vortexing every 5 min. For generation of lysates, the full cell homogenate was centrifuged for 15 min at 16,200 x g and 4 °C. Every sample was processed into a homogenate and a lysate. To store the gained material at -80 °C, 86% glycerol was added as a cryoprotectant to a final concentration of 10% (v/v).

Table 17. List of sample weight (in g) of specific brain areas of the dissected rat brains.

Animal No.	Dissections (in g) from brain area		
	Cb left	Str left	Ctx left
AK.R.P (8.4) 268	0.1905	0.0843	0.3666
AK.R.P (8.4) 272	0.1834	0.0547	0.4062
AK.R.P (8.4) 275	0.1853	0.0655	0.4124
AK.R.P (8.4) 284	0.1780	0.0746	0.5391
AK.R.P (8.4) 288	0.1428	0.0642	0.4219
AK.R.P (8.4) 290	0.1832	0.0657	0.4009
AK.R.P (8.4) 291	0.1739	0.0641	0.4670
AK.R.P (8.4) 001	0.1679	0.0541	0.4207
AK.R.P (8.4) 276	0.1997	0.0652	0.4020
AK.R.P (8.4) 286	0.1709	0.0683	0.3752
AK.R.P (8.4) 289	0.1746	0.0474	0.3800
AK.R.P (8.4) 127.12	0.2065	0.0500	0.3910
AK.R.P (8.4) 127.15	0.1445	0.0696	0.4242
AK.R.P (8.4) 127.16	0.1708	0.0748	0.4007

3.2.2 Protein isolation from cultured cells

Cell pellets generated by harvesting respective cell culture experiments were lysed in either calpain reaction buffer, if used for *in vitro* calpain activation assays, or in RIPA buffer supplemented with cOmplete™ mini protease inhibitor cocktail to protect from proteolysis and phosphatase inhibitor phosSTOP™ to protect from dephosphorylation after *in cellulo* reactions (150 mM NaCl, 50 mM tris-HCl, 1% (v/v) Triton X-100, 0.5% SDC, 0.1% SDS, cOmplete mini, PhosSTOP). Samples were then incubated on ice for 25 min, vortexing every 5 min. For lysate preparation, samples were centrifuged for 10 min at 16,200 x g and 4 °C and the supernatant was transferred into a fresh tube for further use. In case of full cell sample homogenate preparation, samples were treated with ultrasound for 10 s at 10% power and pulse cycles of 50% (Bandelin electronic GmbH & Co. KG,

Berlin). For cryoprotection, all samples were supplemented with 10% glycerol (see 3.2.1).

3.2.3 Measurement of protein concentration

Protein concentrations of lysates and homogenates were measured using the Bradford assay. This method determines the protein concentration of a solution colorimetrically based on the protein-binding dye Coomassie brilliant blue G250 and featuring a high precision for low protein concentrations, while it is unsuitable for concentrations higher than approximately 20 µg/µl. Therefore, adequate sample dilution is crucial for a proper measurement. The dye Coomassie brilliant blue G250 forms complexes with cationic and neutral side chains of proteins, changing its absorbance maximum from a wavelength of 470 nm in the unbound state to 595 nm in its complexed form, which can be measured photometrically.

For the determination of protein concentration, a standard curve based on a solution with known protein concentration was applied. For this purpose, bovine serum albumin (BSA) at a concentration of 1 µg/µl was diluted in 800 µl ddH_2O in the following amounts:

Table 18. BSA standard amounts for calibration of the Bradford assay.

Amount of BSA (1 µg/µl) in µl							
0	1.25	2.5	5	7.5	10	12.5	15

For sample preparation, 2 µl of lysates or homogenates were likewise diluted in 800 µl ddH_2O. Both diluted BSA standards setups and samples were then supplemented with 200 µl 5x Bio-Rad Protein Assay Dye Reagent (Bio-Rad Laboratories GmbH, Munich, DE) and, after mixing, incubated for 5 min at RT. Thereof, 100 µl of each setup was loaded in triplicates on a 96 well microplate and measured at 595 nm wavelength using a microplate reader Synergy HT together with the Gen5 Data Analysis Software (both BioTek Instruments Inc., Winooski, US). Protein concentrations were calculated based on the BSA standard curve using Microsoft Excel (Microsoft Corporation, Redmond, US).

3.2.4 *In vitro* calpain cleavage assay

In vitro calpain cleavage assays (IVCCA) were based on the set-up described by Hübener *et al.* (2013). Assays were performed to trigger calpain-mediated cleavage in protein extracts of rat cerebellum tissue and HEK 293T cells *in vitro* for the investigation of alterations in TBP fragmentation. This was achieved either by addition of calpain-1 (CAPN1: 208712, Calbiochem, Billerica, US) and recombinant calpain-2 (rCAPN2: 208718, Calbiochem, Billerica, US) or by exogenous addition of $CaCl_2$ to activate endogenous calpains. For that, protein homogenates were generated by lysing tissues and cells in CRB.

3.2.4.1 Addition of exogenous calpains

The treatment conditions for exogenous addition of CAPNs (exoCAPNs) were the following:

Table 19. Treatment conditions for *in vitro* calpain cleavage assays with exoCAPN. CI-III was only applied for inhibitor samples.

Treatment condition	
$CaCl_2$ concentration	2 mM
protein amount	25 µg
CI-III concentration	0.5 mM
set-up volume	20 µl

Table 20. Concentration of the stock solutions used for *in vitro* calpain cleavage assays.

Stock solution	
$CaCl_2$ (in CRB)	20 mM
CI-III	25 mM
CAPN1 (exoCAPN1)	100 ng/µl
rCAPN2 (exoCAPN2)	110 ng/µl

The activation of proteolysis by calpains was investigated in a time-dependent manner. For controls, reaction was terminated at time point 0 min by adding 4x

LDS buffer in a ratio 1:3 to the control sample (40% (v/v) glycerol, 1 M tris base, 8% LDS, 2 mM EDTA, 0.075% (v/v) of Coomassie brilliant blue G250, 0.025% (v/v) of phenol red, pH 8.5) and mixed with DTT to 0.1 M final concentration for reduction of disulfides. For the time-dependent cleavage, protein samples were supplemented with calcium, CRB, and exoCAPN1 or exoCAPN2.

To establish a comparable reactivity of the two calpain isoforms, the effect of different amounts of exoCAPN1 and -2 (50, 100, 150, 200 ng) were compared for untransfected HEK cells as described in 4.3.1.

This assay also aimed to investigate if the specific inhibition of calpains under calpain activating conditions *in vitro* was able to reduce the formation of fragments, excluding other or additional proteolytic processes being responsible for the observed effects. Therefore, an inhibitor control sample was generated by preincubating the mix of sample, CRB, and rCAPN with 0.5 mM CI-III for 5 min on ice. After preincubation, 2 mM calcium were added to the sample and incubated for 30 min at RT according to the longest time of calpain activation without inhibition, thereby demonstrating if a sufficient inhibition over this time is reached.

3.2.4.2 Sole addition of calcium

Activation of calpains *in vitro* was also performed without the addition of recombinant calpains, but only by incubation with calcium to activate endogenous, still enzymatically functional calpains. The experimental setup was as described in 3.2.4.1, but without the use of exoCAPN and with incubation at 37 °C for longer times. Termination of the reaction was conducted at 30 min, 60 min, 90 min, and 120 min.

3.2.5 SDS-polyacrylamide gel electrophoresis (SDS-PAGE)

Sodium dodecyl sulfate (SDS)-polyacrylamide gel electrophoresis (PAGE) is a method for separating proteins according to their molecular mass in an electric field (Laemmli, 1970). SDS, as a detergent, binds proteins and covers their

intrinsic charge, consequently converting them to SDS-bound complexes with an evenly distributed negative charge. The binding of SDS denatures the protein into its linear form, which is further facilitated by subjecting the protein to heat denaturation. This allows the SDS-covered protein to move towards the anode by application of an electric current.

The polyacrylamide gel consists of acrylamide as the gel basis and N,N'-methylenebisacrylamide in a ratio 29:1 (v/v) to crosslink the gel, which is conducted by radical polymerisation. Depending on the acrylamide concentration and the ratio of acrylamide to bisacrylamide, the gel consists of pores of a few nanometres, through which the linear proteins pass. As the negative charge of the SDS-protein complex is proportional to the molecular weight and smaller proteins can move through the pores more easily in the direction of the anode, the passage through the gel is a measure for the protein length. For bigger proteins, gels with a lower percentage of acrylamide are used, whereas low molecular weight proteins need a higher percentage gel for being separated.

Addition of tetramethylethylenediamine (TEMED) as catalyst and of the radical initiator ammonium persulfate (APS) to the mixture of acrylamide and bisacrylamide to start the gel polymerisation. Moreover, depending on the desired gel and the running buffer system, a specific gel buffer is used for the gel mix. In this study, bis-tris buffer (357 mM bis-tris in ddH_2O pH 6.65)-based gels were used, which consisted of an upper 5% stacking gel for protein sample collection within the gel and lower 12% separating gel (see detailed recipes in Table 21 and Table 22).

Table 21. Composition of 1 bis-tris stacking gel (5%).

5% Bis-tris stacking gel (for 3.5 ml/ 1 gel)	
30% acrylamide/bisacrylamide (29:1)	0.58 ml
ddH_2O	1.92 ml
3.5x buffer	1.00 ml
TEMED	6.7 µl
10% APS	35.0 µl

Table 22. Composition of 1 bis-tris separating gel (12%).

12% Bis-tris separating gel (for 5 ml/ 1 gel)	
30% acrylamide/bisacrylamide (29:1)	2.00 ml
ddH_2O	1.58 ml
3.5x buffer	1.42 ml
TEMED	7 µl
10% APS	25 µl

Polyacrylamide gels were prepared and run using the Mini-Protean® system (Bio-Rad Laboratories GmbH, Munich, DE). First, the separating gel mix was poured between two glass plates of 10.1 x 7.3 cm with 1 mm spacers. To protect the gel mix from oxygen and to reach a smooth and air-free meniscus, it was covered with 300 µl isopropanol. After 15 min polymerization, the isopropanol was removed using a filter paper and the stacking gel was poured on top of the separating gel together with a sample comb to create pockets for loading the sample. After further 15 min of stacking gel polymerization, the prepared gel was transferred into the gel electrophoresis chambers of the Mini-Protean® system and comb was removed. Each chamber was filled with 800 ml 1x MES SDS running buffer (50 mM MES, 50 mM tris base pH 7.7, 3.465 mM SDS, 1.025 mM EDTA).

Except for samples from cell-based calpain activation assays and CAST overexpression from which lysates were loaded, full cell homogenates were used for gel electrophoretic analysis. For the sample preparation, 20 µg to 30 µg of diluted proteins were mixed with 4x LDS sample buffer in a ratio 3:1 and supplemented with 0.1 M DTT. The samples were heat denatured at 70 °C for 5 min, shortly centrifuged, and stored on ice until loading. Respective volumes of the prepared sample were filled in each gel pocket. As molecular weight protein standard, 2.5 µl and 1.5 µl of SeeBlue® Plus2 Pre-Stained Protein Standard (Life Technologies, Thermo Fisher Scientific, Carlsbad, US) were loaded in empty pockets flanking the samples. Afterwards, the electrophoresis was conducted at 80 V during the sample migration through the stacking gel, and then increased to 120 V for the separating gel. After approximately 90 min total running time,

proteins were subsequently blotted on a nitrocellulose membrane, as described in 3.2.6.

Alternative to home-made gels, precast NuPAGE® 4-12% bis-tris gels and NuPAGE® 7% tris-Acetate precast gels (both Life Technologies, Carlsbad, US) were used similarly, except for some differences for Tris-Acetate gels. For the latter, HighMark™ Pre-Stained Protein Standard (Life Technologies, Carlsbad, US) was used as a molecular weight protein standard and gels were run with 1x NuPAGE® running buffer (50 mM tricine, 50 mM tris base, pH 8.25, 3.5 mM SDS) at constant 150 V. Precast bis-tris gels with an acrylamide gradient of 4% to 12% were used to reach a better separation of a wide spectrum of molecular masses.

3.2.6 Gel blotting

After SDS-PAGE (see 3.2.5), molecular weight-separated proteins were transferred from their gels to a nitrocellulose membrane (Amersham Protran Premium 0.2 µm NC, GE Healthcare Life Science, Amersham, UK) via western blotting. For this, gels were removed from the glass plates, covered with the membrane, and placed between filter papers pre-soaked in transfer buffer, which protect the gel against drying and pulling forces. Subsequently, this blotting sandwich was placed in a cassette and transferred into to a TE22 Mighty Small Transfer Tank (Hoefer Inc., Holliston) with 1.2 l 1x NuPAGE® transfer buffer (25 mM bicine, 25 mM bis-tris pH 7.2, 1.025 mM EDTA), supplemented with 15% methanol, and was electroblotted at 4 °C for 1.5 h at 80 V and 250 mA. The electric field was applied vertically towards gel and membrane, positioning the latter towards the side of the anode, to allow negatively charged proteins to run from the gel into the membrane. The protein binding to the nitrocellulose membrane is facilitated by the pores of the nitrocellulose membrane, predominantly due to ionic, hydrophobic, and polar interactions. The afore described blotting set-up is depicted in Figure 8.

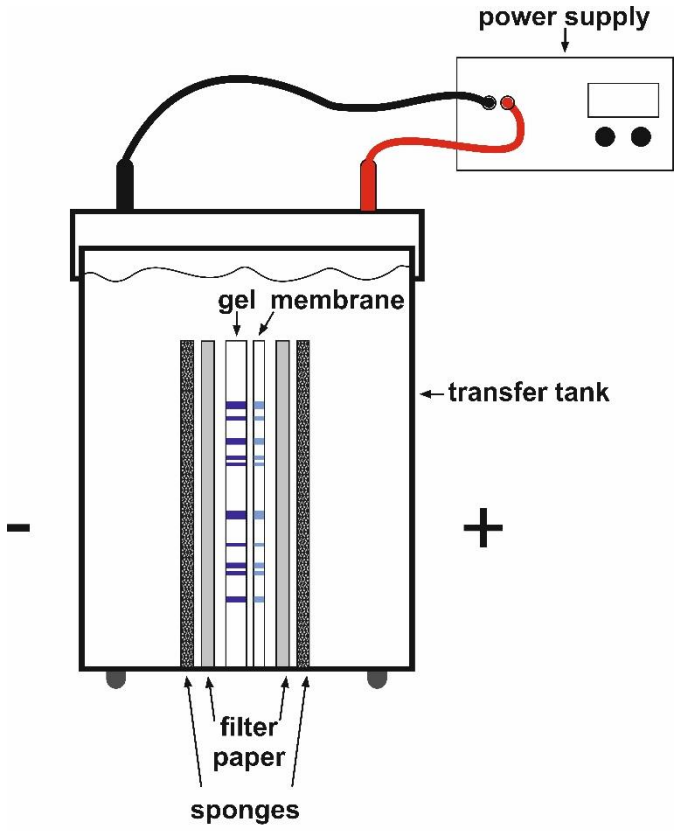

Figure 8. Setup of a gel blotting system. The nitrocellulose membrane is located between the anode (+) and the gel containing the separated proteins. Membrane and gel are bordered by filter papers and sponges on both sides and transferred into a transfer buffer solution. The applied electric current pulls the negative proteins towards the anode through the membrane, where they are trapped.

3.2.7 Filter retardation assay

For analysing intracellular inclusions of disease proteins, SDS-insoluble aggregates in cell homogenates were detected by filter retardation assays. As for western blotting, the proteins are bound on a nitrocellulose membrane, but with a bigger pore size of 0.45 µm. Samples were diluted in SDS-containing buffer, allowing the flowthrough of smaller soluble proteins. The assays were performed as described previously (Weber et al., 2017). The samples were lysed for obtaining full cell homogenates and their concentrations were determined by Bradford assay (see 3.2.1 and 3.2.3). 25 µg of protein were diluted in a total volume of 100 µl 1x DPBS supplemented with 2% (w/v) SDS and 50 mM DTT and boiled at 95 °C for 5 min. Samples were cooled down at RT to avoid SDS precipitation. The filter retardation apparatus was prepared as follows: The

nitrocellulose membrane (Amersham Protran 0.45 µm NC, GE Healthcare Life Science, Amersham, UK) was placed on two 3MM Whatman filter papers (Carl Roth, Karlsruhe, DE) within a Minifold II slot-blot manifold (Cole-Parmer GmbH, Wertheim, DE). A vacuum pump was connected via a liquid collection container to the manifold and a vacuum at 100-200 mmHg was applied. First, the membrane was equilibrated by pipetting 100 µl of 1x DPBS supplemented with 0.1% (w/v) SDS into the slots. Thereafter, 100 µl per samples were pipetted and sucked through the membrane. Slots were washed twice with 100 µl 1x DPBS. Subsequently, the membrane was removed from the apparatus, placed in a container, and washed for 2x 5 min with 1x TBS (150 mM NaCl, 10 mM tris-HCl, pH 7.5). Then, the membrane was blocked and immunodetection of trapped protein aggregates was performed as described in 3.2.8.

3.2.8 Immunodetection

Proteins transferred onto nitrocellulose membranes are visualized with indirect immunodetection. Epitopes of the proteins are bound by a primary antibody, which itself is recognized by a secondary antibody, which can either be fluorescence-tagged or conjugated with horseradish peroxidase (HRP). The fluorescence antibodies are detected directly at corresponding wave lengths, whereas HRP conjugated antibodies need to be supplemented with a chemiluminescent reagent. Here, the reagent is luminol, which is converted into its oxidised form via catalysation by HRP in the presence of hydrogen peroxide, thereby producing enzymatic chemiluminescence (ECL).

After gel-blotting, nitrocellulose membranes were transferred into a 50 ml tube and blocked with 5% SlimFast (Allpharm, Messel) diluted in 1x TBS (150 mM NaCl, 10 mM tris-HCl, pH 7.5) for 1 h on a roller shaker for blocking non-occupied binding sites on the membrane with unspecific proteins. Afterwards, membranes were washed 3x 5 min with 1x TBST (150 mM NaCl, 10 mM tris-HCl, 0.1% (v/v) Tween-20, pH 7.5) to remove milk powder and SDS, which allows the proteins to renature and to partly regain their secondary or tertiary structure. Subsequently, 5 ml of the primary antibody, diluted in 1x TBST (for specific antibodies and

dilutions see Table 14) and supplemented with 0.02% (v/v) of the preservative NaN_3, were added to the membrane and incubated overnight at 4 °C on a roller shaker.

Membranes were then washed with 1x TBST three times for 5 min to remove unspecifically bound antibodies. The secondary antibody, either fluorescence or HRP-tagged, was diluted as listed in Table 15 and incubated on the membranes for 1 h at RT. Again, membranes were washed with 1x TBST for 15 min, then put on a detection tray. For fluorescence detection, membranes were directly covered with a transparent foil and detected at the respective wavelengths using an Odyssey Fc dual-mode imaging system (LI-COR Bioscience, Lincoln, US) for 3-5 min. For ECL detection, membranes were incubated for 1 min with a 1:1 (v/v) mix of the two components of the WesternBright™ ECL/ Sirius Chemiluminescent Detection Kit (Advansta Inc., San Jose, US) before proceeding similarly with the fluorescence detections but using the chemiluminescence channel instead.

For redetection of the membranes with other antibodies, membranes were washed twice for 5 min with TBST, then twice stripped off the antibodies using a mild stripping buffer for 5 min (25 mM glycine, 1% (w/v) SDS pH 2.0, 1% (v/v) Tween-20), washed three times for 5 min with TBST, re-blocked for 1 h, and then it was further proceeded with immunodetection as previously described.

3.2.9 Quantitative analysis of immunodetections

The applied Image Studio Software Version 2.1 (LI-COR Bioscience, Lincoln, US) offers the possibility for a semiquantitative analysis of the protein levels by measurement of the density of immunodetected band signals. To increase the reliability, it is important to subtract the background and to relate measurements with the detection of house-keeping proteins used as loading controls, here vinculin, β-actin, or α-tubulin, to rule out falsifications by loading variabilities.

3.3 *In silico* cleavage site prediction

In silico prediction of calpain cleavage sites is mainly based on the comparison of the target protein sequence with databases of known calpain substrates and

their cleavage sites. The comparison with these data can predict domains that are likely to be proteolyzed by calpains. Here, the software GPS-CCD (Liu et al., 2011), which predicts cleavage sites with an 89.98% accuracy, a sensitivity of 60.87%, and a specificity of 90.07%, was applied to perform a calpain cleavage site prediction on human TBP (isoform 1, UniProt identifier: P20226-1) using a cut-off value of 0.654 (Weber, 2017).

3.4 Statistical analysis

Statistical analysis was performed with GraphPad Prism Software (GraphPad Software Inc., San Diego).

Data was analysed using unpaired Student's *t*-tests and one-way analysis of variance (one-way ANOVA) where necessary. Post-hoc tests were performed with Bonferroni test, while for multiple comparisons, Dunnett's method was applied. Results are presented as means ± SEM. P-values of $p \leq 0.05$ were considered statistically significant (*), $p \leq 0.01$ as very significant (**), $p \leq 0.001$ as highly significant (***).

4 Results

Spinocerebellar ataxia type 17 is a progressive neurodegenerative disorder with inevitable fatal outcome (Koide et al., 1999). Pathogenetically, it belongs to the group of polyQ disorders, which are characterized by a CAG/CAA repeat expansion in the mutant protein, encoding for an elongated polyQ stretch. The mutation within the SCA17 disease protein TBP shows a reduced penetrance for the disease at a polyQ length of 41-48 repeats, whereas a full penetrance with a manifestation as spinocerebellar ataxia is reached from 49 glutamines onwards (Nakamura et al., 2001; Kim et al., 2009; Alibardi et al., 2014). Fragmentation of the disease proteins by proteases has been implicated as a common pathomechanism of the polyQ disorders (Ikeda et al., 1996; Weber et al., 2014). Resulting fragments are prone to aggregate and interact and are therefore responsible for associated functional disruptions and formation of protein inclusions in affected neurons. So far, truncated, N-terminal TBP has been found in intranuclear inclusions of mice and HEK cell models of SCA17 (Friedman et al., 2008). Most importantly, caspases and calpains have been in the focus of research as they were shown to be responsible for proteolysis of other polyQ-expanded disease proteins, thereby initiating the pathological process in most polyQ diseases (Weber et al., 2014; Wellington et al., 1998). As caspases were excluded to participate in TBP fragmentation, the aim of this study was to identify the role of calpains in the pathogenesis of SCA17 by investigating the association of fragment and aggregate occurrence, calpain activity, and polyQ mutation.

4.1 Analysis of TBP expression in rat brain areas

For analysis of TBP fragment patterns *in vivo* and for comparing potential differences between the wild-type and the mutant genotype in rat brain tissue, the brain area of our hTBP-64Q rats with the highest expression of mutant TBP had to be selected. Following investigations of the applied rat model by Kelp et al. (2013), the highest expression levels is expected in the cerebellum, followed by cortex and olfactory bulb with medium expression levels, whereas brain stem, hypothalamus, and striatum had low mutant TBP levels.

To confirm this, we immunoblotted homogenates of cerebellum, striatum, and cortex of wild-type rats and human TBP (hTBP) 64Q-expressing transgenic SCA17 rats. All samples showed an expression of endogenous TBP at approximately 40 kDa as detected with the C-terminally binding antibody anti-TBP 58C9. Full-length hTBP-64Q was appearing as two bands at around 49 kDa, with highest levels in cerebellum, whereas cortex and striatum samples showed low to no expression of mutant TBP64Q (Figure 9a). Hence, with rat cerebellum being the centre of interest for our analysis, further analyses were performed using this tissue. Using the N-terminal anti-TBP N-12 antibody, endogenous and expanded full-length TBP were detected likewise. Figure 9b presents the expression pattern comparison of three wild-type and three TBP64Q rat cerebellum samples. Rat cerebellum of hTBP-64Q animals (M = 5.375, n = 3) compared to wild-type rats (M = 1, n = 3) showed significantly increased total TBP levels, $t(4) = 6.502$, $^{**}p = .0029$ (unpaired t-test) due to the overexpression (Figure 9c), which must be taken into account when comparing different genotypes in further analysis. Interestingly, levels of endogenous TBP in hTBP-64Q rat cerebellum (M = 0.6442, n = 3) compared to wild-type rat cerebellum (M = 1, n = 3) were significantly lower, $t(4) = 3.954$, $^{**}p = .0168$ (unpaired t-test) (Figure 9d). These results have been published by Weber et al. (2022).

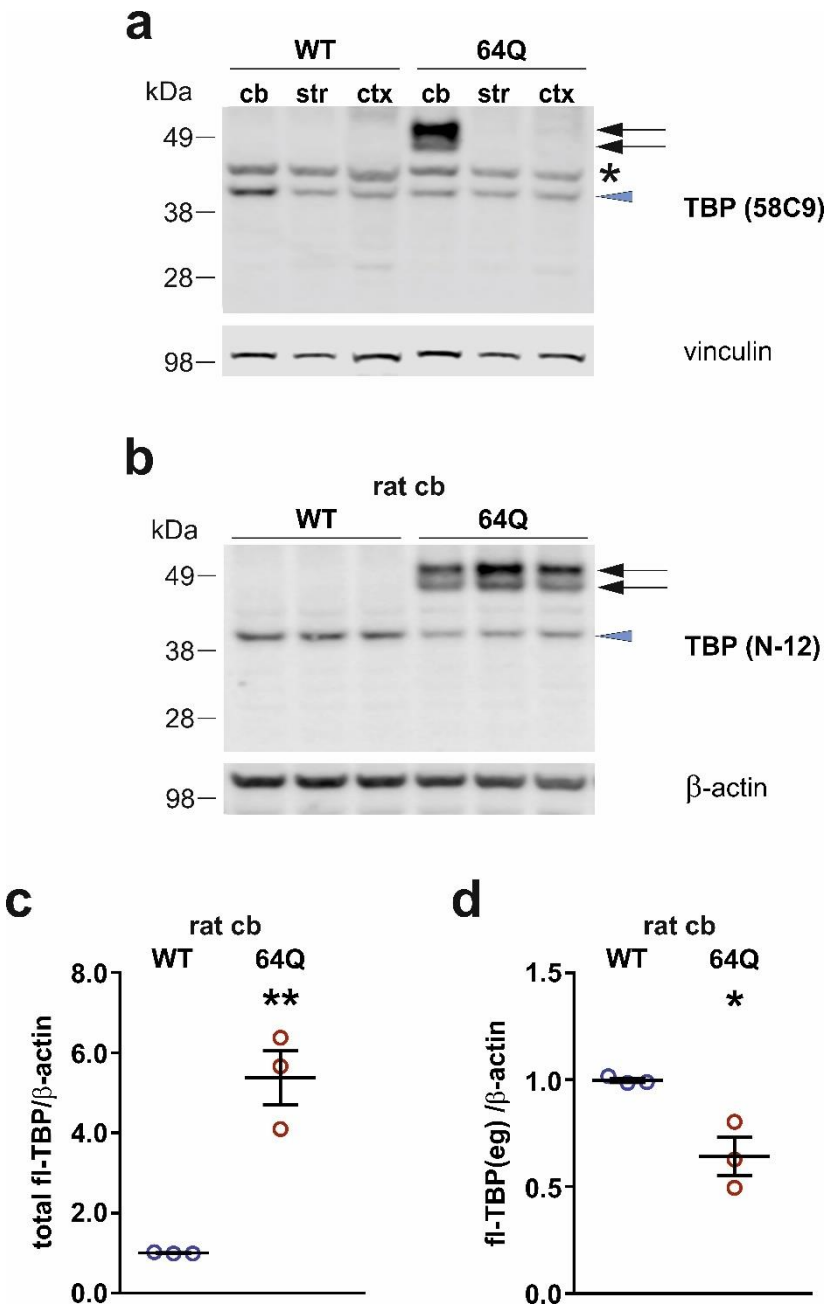

Figure 9. TBP expression levels in brain areas of the SCA17 rat model. a) Expression levels of endogenous TBP and hTBP-64Q were detected in cerebellum (cb), striatum (str), and cortex (ctx) of wild-type (WT) and hTBP-64Q rats(64Q) via immunoblotting with antibody anti-TBP 58C9 (a and b). The highest levels of mutant TBP were found in cerebellum due to the Prp promotor-mediated overexpression, also resulting in significantly higher total full-length TBP (total fl-TBP) in SCA17 rats (c). d) Endogenous TBP (fl-TBP(eg)) levels were reduced significantly in hTBP-64Q cerebellum. Full-length hTBP-64Q: black arrows. Endogenous TBP: light blue arrowhead. Unspecific band: asterisk. Vinculin and β-actin served as loading controls. $n = 3$. Bars represent mean ± SEM. *$p \leq .05$; **$p \leq .01$; unpaired *t*-test. Figure adapted from Weber et al. (2022).

4.2 Testing of antibodies for immunodetection

So far, two antibodies with respective epitopes at the opposite ends of TBP, anti-TBP 58C9 and N-12, were tested in our laboratory and were able to detect endogenous rat and expanded hTBP in rat tissue. To identify additional suitable and combinable antibodies for detection of full-length and fragmented TBP, different TBP-specific antibodies with various epitopes as well as c-myc tag-specific and polyQ-specific antibodies were tested on homogenates of rat cerebellum and of untransfected, myc-hTBP-38Q, or myc-hTBP-64Q-expressing HEK 293T cells. A schematic of TBP and the target epitopes of the applied antibodies are depicted in Figure 10.

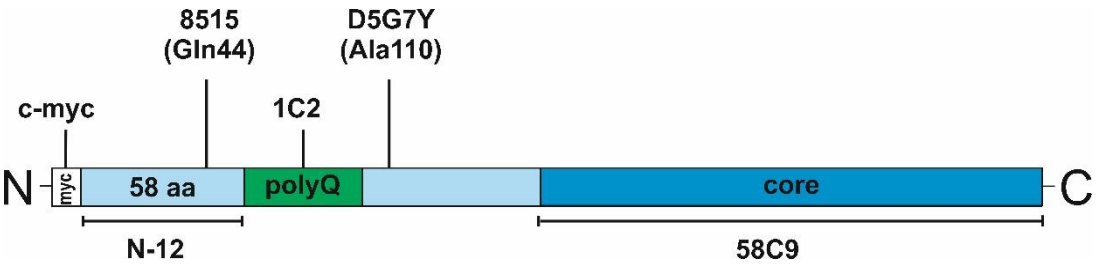

Figure 10. Epitopes of the applied anti-TBP antibodies within the TBP sequence. The schematic shows the epitopes of the tested antibodies within TBP. Anti-c-myc detects the c-myc-tag (c-myc) of transgenic TBP, anti-TBP N-12 recognizes an unmapped epitope at the N-terminus (N) of TBP. Anti-TBP 8515 is known to bind amino acid (aa) glutamine at position 44 (Gln44), anti-polyQ 1C2 detects the polyQ stretch. For the antibodies binding C-terminally (C) of the polyQ region, only the epitope of anti-TBP D5G7Y is known, which is localized around alanine at position 110 (Ala110), whereas anti-TBP 58C9 is directed against an unmapped epitope within the DNA binding core region at the C-terminus of TBP.

Immunodetections with tested antibodies are shown in Figure 11 (Weber et al., 2022). As expected, anti-TBP D5G7Y (Figure 11c), anti-polyQ 1C2 (Figure 11d) and anti-c-myc (Figure 11f) could not detect full-length endogenous rat TBP due to lack of the respective epitopes: The epitope of anti-polyQ 1C2 is a polyQ repeat of at least 37 glutamines. Anti-TBP D5G7Y detects only human TBP due to a missing sequence homology of rat TBP. Last, rat TBP does not possess a c-myc tag, unlike the modified human TBP transgenes.

The endogenous rat TBP, which contains 318 amino acids (aa), including 15 glutamines in average, is smaller than the human isoform with 339 aa, which is

for instance expressed in HEK 293T cells. This difference of a few kDa can be seen the immunodetections when comparing the endogenous TBP in rat and HEK 293T homogenates. The overexpressed myc-hTBP-38Q was detected as an additional band a few kDa above the endogenous TBP. Aside from the full-length protein, some anti-TBP antibodies could visualize smaller bands, indicating the presence of TBP fragments at baseline *in vivo* and *in vitro*. Anti-TBP 58C9 (Figure 11e) was able to detect two potential fragment bands, at around 28 kDa and 30 kDa. Anti-TBP D5G7Y and anti-TBP 8515 (Figure 11b) detected only one weak fragment band approximately at the size of the 30°kDa band of the anti-TBP 58C9 detection. Neither of the antibodies N-terminally binding antibodies, namely anti-TBP N-12 (Figure 11a), anti-polyQ 1C2 (Figure 11), and anti-c-myc (Figure 11e) showed N-terminal fragment bands. In these immunodetections, β-actin and α-tubulin served as loading controls. As α-tubulin is a sensitive substrate of calpains itself, it was abandoned as loading control for further experiments.

As detections of both full-length and fragmented TBP were best for the C-terminally binding anti-TBP 58C9, most of the subsequent detections were performed with this antibody. In addition, the anti-TBP 58C9 antibody was combined with the N-terminally binding anti-TBP N-12 antibody to assess presence of or effects on the N-terminal portion of TBP.

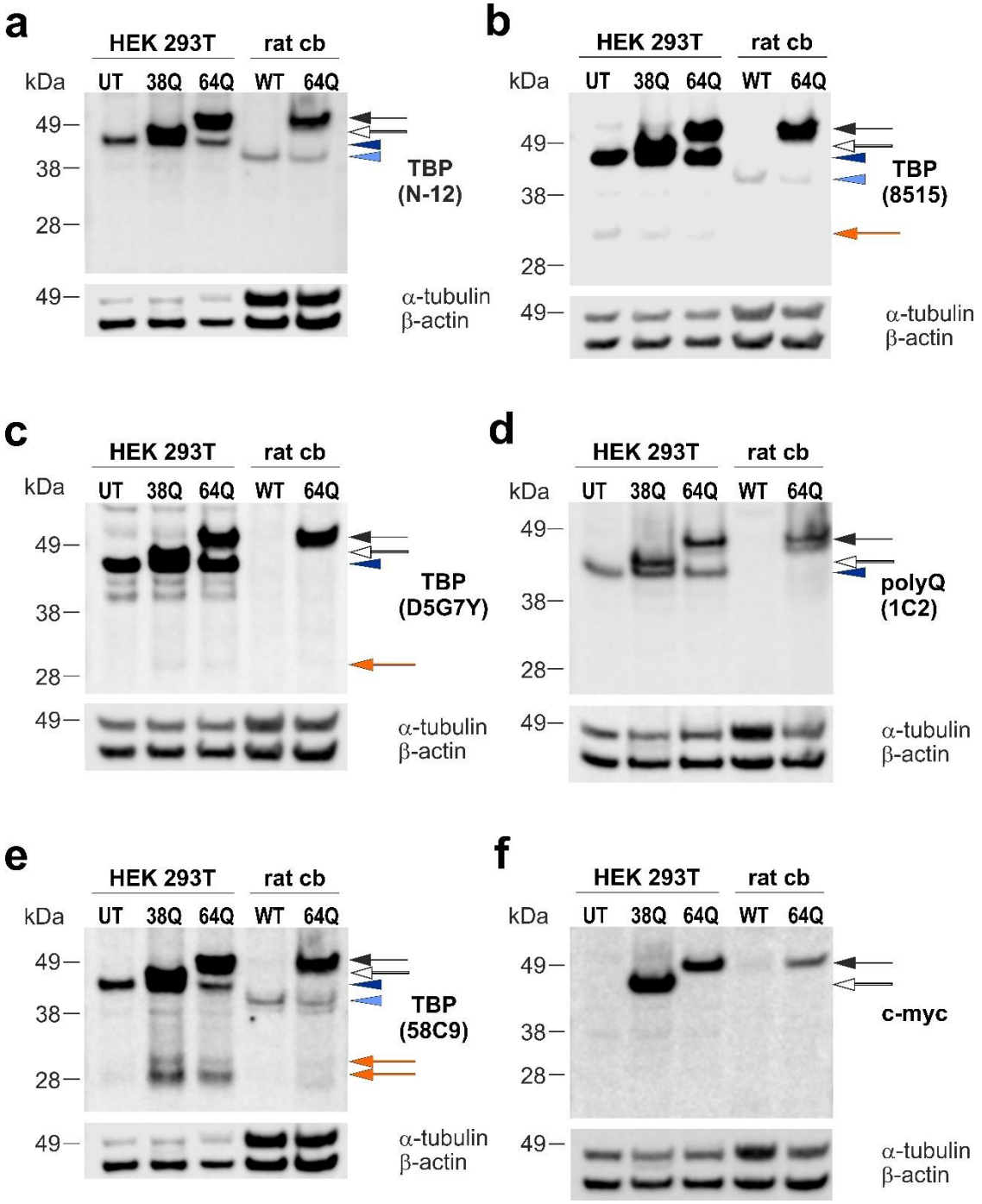

Figure 11. Testing of antibodies for immunodetection of TBP. HEK 293T cells without transfection (UT), transfected with myc-tagged hTBP-38Q (38Q), and myc-tagged hTBP-64Q (64Q) as well as rat cerebellum (rat cb) samples of wild-type (WT) and hTBP-64Q (64Q) rats were analysed by immunodetection for their baseline TBP expression using different antibodies. Full-length endogenous TBP of rat and HEK cells was detected differently by the specific antibodies. Two smaller bands, which might represent fragments of TBP, could be detected by the anti-TBP 58C9 (e), and the upper of both bands by the anti-TBP 8515 (b) and D5G7Y (c) antibodies in HEK 293T cells, whereas N-terminally binding antibodies did not detect any fragments (a, d, f). Full-length hTBP-64Q: black arrows. Full-length hTBP-38Q: white arrow. Endogenous hTBP: dark blue arrowhead. Endogenous rat TBP: light blue arrowhead. TBP fragments: orange arrows. β-actin and α-tubulin were used as loading controls. Figure adapted from Weber et al. (2022).

4.3 Fragmentation of TBP by calpains using *in vitro* calpain cleavage assay

To investigate if the truncation of TBP as seen in rat cerebellum and cell culture samples results from calpain cleavage rather than random proteolytic degradation by other proteases or other processes, as a first assessment, an *in silico* cleavage site prediction was performed by Jonasz J. Weber to predict possible cleavage sites of human TBP (isoform 1, UniProt identifier: P20226-1) and published by Weber et al. (2022). C-terminally of the polyQ domain, multiple possible cleavage sites could be calculated, while cleavage sites at the N-terminus were scarcely detected above the cut-off value. Amino acids between alanine at position 96 (A96) and glutamine 117 (Q117) obtain the highest score of calpain cleavage likelihood (CCL) that is quantified as the CCL score (Figure 12).

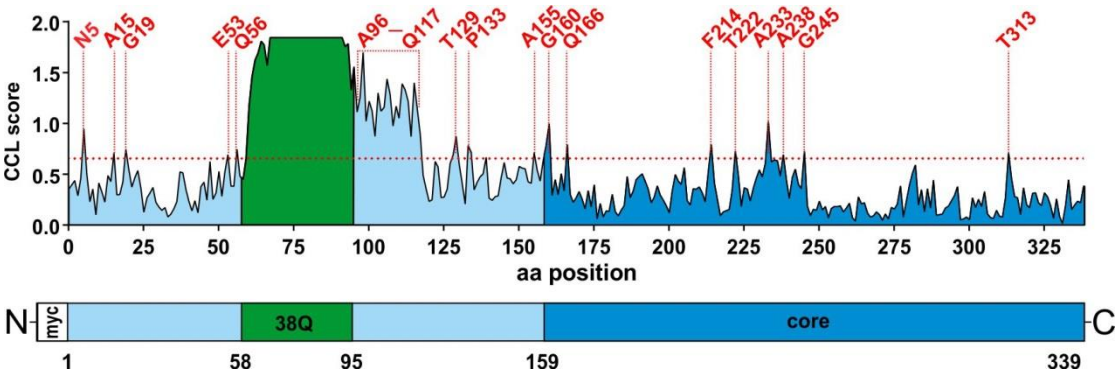

Figure 12. *In silico* cleavage site prediction for TBP. The prediction of amino acid (aa) positions within human wild-type TBP (isoform 1, UniProt identifier: P20226-1) that are likely to be a cleavage site of calpains was performed with the GPS-CCD software (Liu et al., 2011). Positions with a high calpain cleavage likelihood (CCL) score above the pre-set maximum cut-off value of 0.654 (red dotted horizontal line) and are indicated with vertical red dotted lines and labelled with their respective amino acid and position. N: asparagine, G: glycine, E: glutamate, T: threonine, P: proline, F: phenylalanine. Figure adapted from Weber et al. (2022).

As *in silico* cleavage site assays are only a theoretical assumption based on known cleavage motifs characterized in other calpain substrate proteins as performed using the GPS-CCD tool (Liu et al., 2011), TBP had to be confirmed as a calpain substrate using an *in vitro* calpain cleavage assay (IVCCA) based on the addition of exogenous calpains. For this, rat cerebellum homogenates

were incubated with purified calpain-1 and calpain-2 to compare the fragmentation pattern to baseline detections. As a control of calpains as the main proteolytic actor, calpain inhibition was applied simultaneously to exogenous calpain addition. Those IVCCAs were previously described for calpain cleavage analysis of ataxin-3 (Hubener et al., 2013). By application of the two best characterized calpain isoforms in the IVCCAs, the commensurability of their function in TBP cleavage could also be tested.

4.3.1 Establishment of calpain amounts

To determine the optimal amounts of exogenous calpains for achieving comparable activities in the TBP fragmentation assessments, different quantities of exogenous calpain-1 (exoCAPN1) and calpain-2 (exoCAPN2) were tested on HEK 293T cell homogenates. For that, 25 µg of protein sample from a homogenate of untransfected HEK 293T cells was supplemented with 2 mM calcium, calpain reaction buffer (CRB) and 50 ng, 100 ng, 150 ng and 200 ng of exoCAPN1 or -2. A sample without calpain addition was used as negative control. The other samples were incubated with the different calpain amount for 15 min and reactions were stopped by adding 4x LDS sample buffer and 1 mM DTT. Afterwards, reactions were analysed via western blotting using the anti-TBP 58C9 antibody (Figure 13).

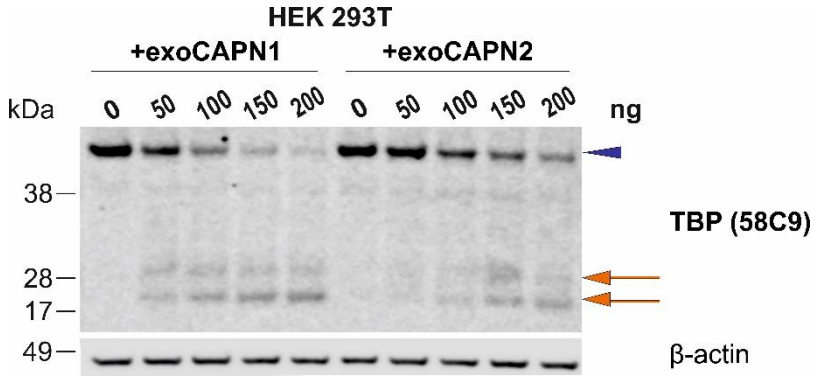

Figure 13. Western blot detection of TBP incubated with various amounts of CAPN1 and CAPN2. Addition of various amounts of exogenous calpain-1 (exoCAPN1) and calpain-2 (exoCAPN2) in an *in vitro* calpain cleavage assay (IVCCA) of untransfected HEK 293T cells shows a decrease of full-length endogenous TBP band in immunoblots. In parallel, two TBP fragments are formed. Endogenous hTBP: dark blue arrowhead. TBP fragments: orange arrows. β-actin was used as a loading control. Figure adapted from Weber et al. (2022).

The full-length TBP signal was analysed quantitatively by normalizing the CAPN2 control value to the respective CAPN1 control. Results are shown in Table 23 to determine the calpain amounts that are the most comparable regarding activity and cleavage intensity. Based on this determination, twice as much exoCAPN2 was needed for comparable activity, subsequently, 100 ng exoCAPN1 and 200 ng exoCAPN2 were applied in the IVCCAs.

Table 23. Quantification of the immunodetection signal of full-length TBP after addition of different amounts of purified CAPN1 or CAPN2. Proportion of full-length TBP band intensity in western blots of untransfected HEK 293T cells after addition of 0, 50, 100, 150, 200 ng of exogenous CAPN1 (exoCAPN1) and -2 (exoCAPN2) amounts were quantified and normalized to the signal without addition of calpains.

ng	0	50	100	150	200
exoCAPN1	100 %	44.97 %	23.49 %	10.01 %	6.7 %
exoCAPN2	100 %	85.23 %	44.97 %	34.23 %	22.82 %

4.3.2 Induction of TBP fragmentation by exogenous CAPN1 and CAPN2

The established calpain amounts of 100 ng for CAPN1 and 200 ng for CAPN2 were used for the subsequent IVCCA*s* in a time-dependent manner with termination of the reaction after 5, 10, 15, and 30 min. Calpain inhibition was conducted as a negative and specificity control by preincubation with 0.5 mM calpain inhibitor III (CI-III) for 5 min before starting the reaction with both exogenous calpains. Afterwards, samples were analysed via western blotting.

In rat cerebellum homogenates, full-length TBP was cleaved time-dependently by addition of purified CAPN1 and -2 leading to an almost complete degradation of polyQ-expanded hTBP-64Q, while endogenous TBP of both wild-type rats and hTBP-64Q rats was not fully degraded (Figure 14). Although this incomplete degradation might suggest a higher susceptibility of expanded TBP towards proteolytic cleavage, wild-type rats lack the overexpression of a respective TBP transgene, therefore it is hard to analyse differences between wild-type and polyQ-expanded TBP regarding its cleavage propensity towards calpains.

Simultaneously, the two fragment bands, as seen in the previous baseline analysis for TBP antibody establishment (see 4.2), accumulated during incubation with both calpain isoforms and could be visualized by anti-TBP 58C9 detection. It shows a dominating and rather cumulative lower fragment band, while the upper band appears to diminish at the time point of 30 min.

While the rather centrally binding antibody anti-TBP D5G7Y was able to visualize the upper of the two fragment bands detected by the anti-TBP 58C9 antibody (Figure 14a), in contrast, the antibody anti-TBP N-12 did not detect any generated TBP fragments (Figure 14b). These results indicate that the two fragments detected by antibodies anti-TBP 58C9 and D5G7Y, which bind C-terminally of the polyQ stretch of TBP, comprise C-terminal portions of TBP and that, further, a calpain cleavage site lies between the epitopes of both antibodies. As no antibody binding a N-terminal epitope antibody clearly showed a fragment band, and as no size shift of bands could be seen amongst the detected fragment bands, when comparing samples of wild-type and transgenic rats, it concludes to two C-terminal, polyQ independent. The induced fragmentation patterns by both CAPN1 and CAPN2 were similar, indicating conserved cleavage sites in TBP. However, detections for exoCAPN1 and -2 addition were not conducted with the same antibodies, therefore they are not fully comparable.

Calpain inhibition by CI-III preincubation effectively, but not completely, prevented cleavage of full-length TBP despite addition of purified CAPN1 or CAPN2, as indicated by nevertheless increased fragment levels when compared to time point 0 min (Figure 14b). Still, there is notable preservation of full-length TBP, which indicates a calpain-specific degradation (Weber et al., 2022).

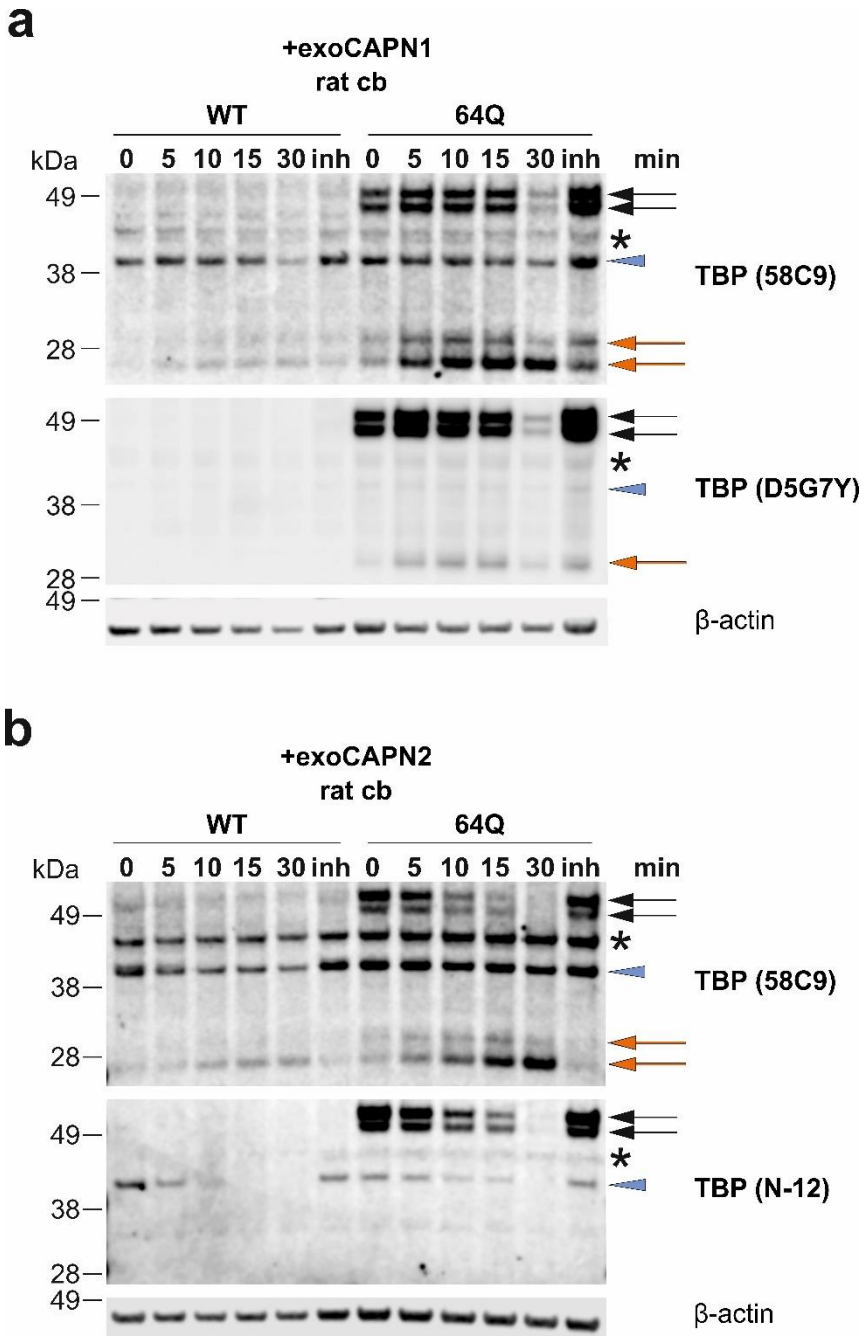

Figure 14 Immunodetection of *in vitro* calpain cleavage assays of TBP expressed in rat cerebellum using exogenous CAPN1 or CAPN2. Rat cerebellum homogenates of wild-type (WT) and hTBP-64Q rats were incubated with purified exogenous CAPN1 (exoCAPN1) (a) and CAPN2 (exoCAPN2) (b) for 0, 5, 10, 15 and 30 min and, as a negative control, incubated with 0.5 mM calpain inhibitor III (inh) for 30 min. Full-length TBP was degraded in a time-dependent manner with simultaneous occurrence of fragments. Calpain inhibition partly counteracted fragmentation despite presence of exogenous calpains. Application of antibody anti-TBP 58C9 detected two fragment bands similar for both calpain isoforms. The antibody anti-TBP D5G7Y (a) detected one fragment band above 28 kDa, while anti-TBP N-12 could not visualize any truncated forms of TBP (b). Full-length hTBP-64Q: black arrows. Endogenous TBP: light blue arrowhead. Unspecific band: asterisk. TBP fragments: orange arrows. β-actin served as a loading control. Figure adapted from Weber et al. (2022).

To confirm the observations in rat cerebellum homogenates in a cell culture-based model, the *in vitro* calpain cleavage assays were reproduced using homogenates of HEK 293T cells transfected with myc-hTBP-38Q and myc-hTBP-64Q. The IVCCAs were performed as described for rat samples and likewise analysed via western blotting.

Compared to IVCCAs of rat tissue samples, calpain-mediated cleavage of both full-length hTBP-38Q and -64Q was more prominent than for rat samples, occurring in a time-dependent and gradual manner for both calpain isoforms (Figure 15). Simultaneous accumulation of the fragment bands was seen for both the addition of exogenous CAPN1 (Figure 15a) and exogenous CAPN2 (Figure 15b), again with a dominating lower fragment band and a partly vanishing, potentially further degraded upper one. The effects of preincubation with CI-III were even more clear for IVCCAs using cell culture samples, as it could effectively prevent fragment formation under calpain addition. Overlaying immunodetections of the antibodies anti-TBP 58C9 and anti-TBP D5G7Y confirmed the hypothesis that the anti-TBP D5G7Y antibody binds the upper fragment band, which constitutes a longer C-terminal fragment featuring epitopes of both antibodies (Figure 15a). These results have been published by Weber et al. (2022).

These *in vitro*-based results confirm the direct involvement of CAPN1 and CAPN2 in the generation of the fragments observed at baseline and show that proteolytic cleavage of wild-type and expanded TBP is comparable in both human cell lines and in the rat model.

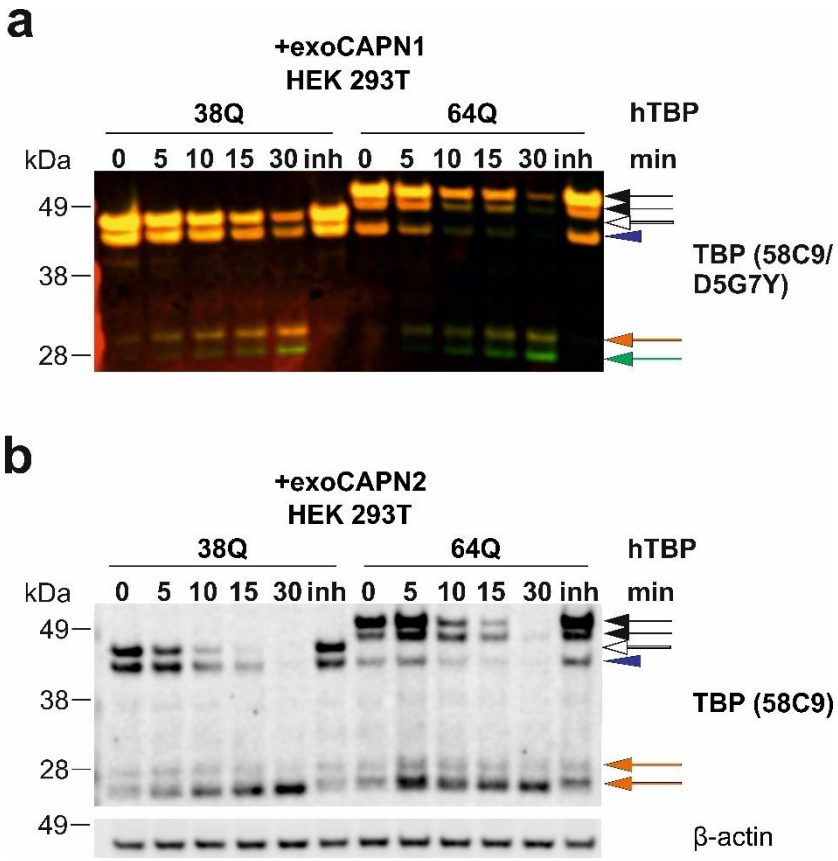

Figure 15. Immunodetection of *in vitro* calpain cleavage assays of TBP expressed in HEK 293T cells using exogenous CAPN1 or CAPN2. IVCCAs with HEK 293T cell homogenates, expressing myc-hTBP-38Q (38Q) and polyQ-expanded myc-hTBP-64Q (64Q) were performed as described for rat cerebellum samples. Accordingly, gradual degradation of full-length TBP into fragments by exoCAPN1 (a) and exoCAPN2 (b) can be seen (orange and green arrows). Levels of full-length and truncated protein upon calpain inhibition with calpain inhibitor III (inh) are comparable to the control levels (0). a) Overlay of anti-TBP 58C9 and anti-TBP D5G7Y detections show that a C-terminal fragment band above 28 kDa can be detected with both antibodies, as overlaying detections are coloured in orange, while detection solely by anti-TBP 58C9 is presented as a green band. Full-length myc-hTBP-64Q: black arrows. Full-length myc-hTBP-38Q: white arrow. Endogenous hTBP: dark blue arrowhead. TBP fragments: orange and green arrows. β-actin served as a loading control. Figure adapted fromWeber et al. (2022).

4.3.3 Induction of calpain cleavage by addition of calcium

Calpain-mediated proteolysis cannot only be performed by addition of exogenous calpains, but also by activation of endogenous calpains solely through supplementation of calcium. For this, homogenates of HEK 293T cells transfected with myc-hTBP-38Q and myc-hTBP-64Q were incubated with 2 mM $CaCl_2$ for 30, 60, 90, and 120 min at 37 °C and samples were analysed by western blotting. Incubation times were prolonged and reaction temperature

increased in consequence of the much lower amounts of endogenous calpains in the samples compared to the amount of the added exogenous proteases. Figure 16 shows the respective immunoblots using the anti-TBP 58C9 antibody. The time-dependent occurrence of TBP fragments resembled the effects observed in IVCCAs with exogenous CAPN addition, although not being as distinct and strong. Moreover, the reduction of full-length protein was barely visible. Also, preincubation with CI-III could effectively prevent fragment formation under activating conditions as shown in the previous assays. These experiments confirm that the observed TBP fragmentation can also be triggered by activating the endogenous calpains. Further, the detected TBP fragmentation patterns between assays using exogenous calpains or activating the endogenous proteases seem to be comparable.

Still, the reactivity of the endogenous proteases is apparently not as strong as what was reached by an overload of exogenous calpains. This discrepancy might be compensated by higher protein concentrations in the setups or an even longer incubation time.

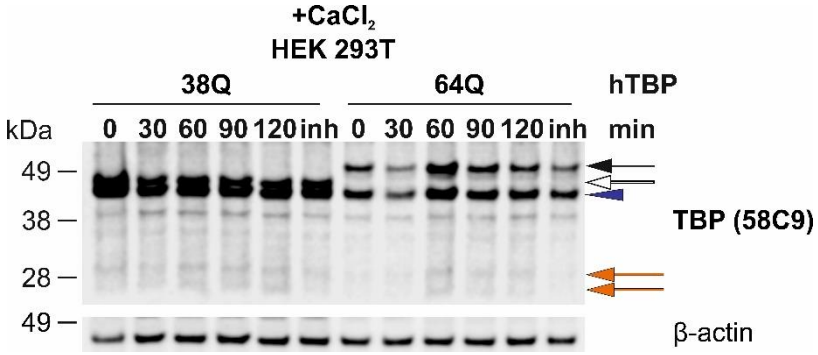

Figure 16. Immunodetection of *in vitro* calpain cleavage assays of TBP expressed in HEK 293T cells upon sole addition of calcium. Activation of endogenous calpains was induced by incubation of homogenates of HEK 293T cells transfected with hTBP-38Q and hTBP-64Q with 2 mM $CaCl_2$ for 30, 60, 90, and 120 min. Cleavage of full-length TBP is not clearly visible, while there was emergence of fragments, although being less strong than after exogenous calpain addition. Calpain inhibition (inh) with 0.5 mM CI-III prevented fragment formation. Full-length myc-hTBP64Q: black arrow. Full-length myc-hTBP-38Q: white arrow. Endogenous hTBP: dark blue arrowhead. TBP fragments: orange arrows. β-actin served as a loading control.

4.4 *Cell-based* calpain activation by ionomycin treatment

To transfer the observations from *in vitro* conditions to an intact cellular system and thereby investigate how endogenously expressed and activated calpains proteolyze TBP time-dependently in living cells, cell-based calpain cleavage assays were performed. For endogenous calpain activation the calcium ionophore ionomycin was used, which allows calcium to pass the cellular membrane, raising the intracellular calcium levels and inducing calpain activation.

HEK 293T cells transfected with myc-hTBP-38Q or -64Q were incubated with 1 µM ionomycin and 5 mM $CaCl_2$ for 30, 60, 90 and 120 min. DMSO cells served as vehicle-treated controls, as well as cells which were preincubated with 25 µM CI-III for 60 min prior to ionomycin treatment for confirming the specificity of the calpain activation and cleavage. After cell harvest and protein extraction, samples were analysed by western blotting. As markers of calpain activity, the endogenous calpain inhibitor calpastatin (CAST), the known calpain substrate α-spectrin and CAPN1 itself were used. Responsive to calpain activation, CAST levels decrease (Rao et al., 2008), spectrin is cleaved into fragments of around 145 and 150 kDa, and calpain is autolysed (Ono and Sorimachi, 2012). Immunodetections of the respective markers indicate a successfully increased calpain activation as a response to the ionomycin treatment by showing the reduction of calpastatin levels, an enhanced *α*-spectrin cleavage and CAPN1 autolysis (Figure 17a) (Weber et al., 2022). In association with calpain activation, the formation of TBP fragments occurred over time and was comparable to the observations in the previous *in vitro* cleavage assays (Figure 17b). It is therefore conclusive that, also in an intact cellular environment, calcium-activated calpain cleavage plays a crucial role in TBP proteolysis and generates a specific set of C-terminal cleavage products, as detected with the antibody anti-TBP 58C9 (Weber et al., 2022). Still and as expected, endogenous calpains appeared to be less reactive than exogenous added CAPNs. The *cell-based* cleavage assay did not, like the calcium activation in *in vitro* assays, lower full-length TBP as prominently. However, calpain inhibition by CI-III successfully prevented calpain activation, as shown by all respective markers as well as TBP fragment and full-

length levels. This effect even overcompensated the baseline activation, as all markers were less cleavage than the vehicle-treated control.

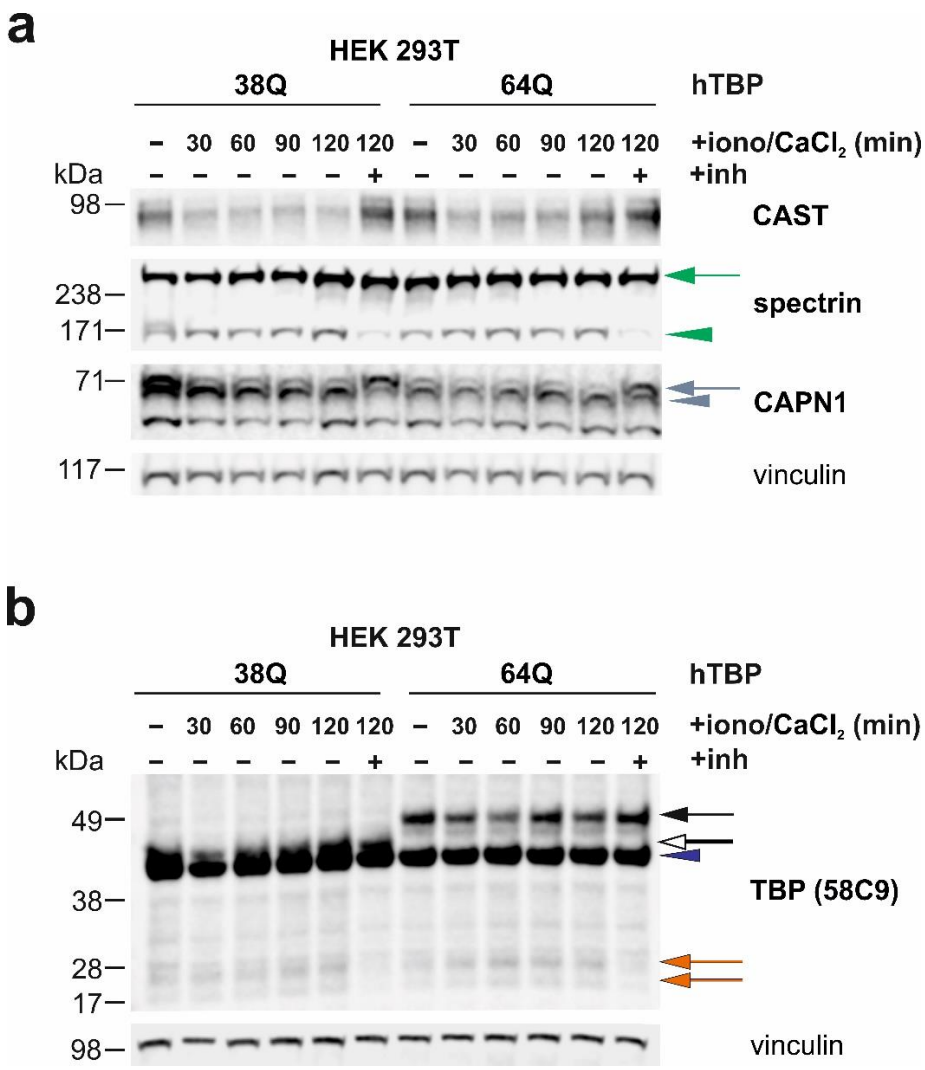

Figure 17. Calpain activity markers and TBP degradation in a time-dependent cell-based calpain activation by ionomycin addition. Endogenous calpains in myc-hTBP-38Q (38Q) and -64Q (64Q)-transfected HEK 293T cells were activated by incubation with 1 µM of the calcium ionophore ionomycin and 5 mM $CaCl_2$ (iono/$CaCl_2$) for 30, 60, 90 and 120 min. As controls, cells were pre-treated with 25 µM CI-III treatment(inh) for 1 h prior to iono/$CaCl_2$ administration or treated only with DMSO as a vehicle control. a) Calpastatin (CAST), *α*-spectrin and CAPN1 indicate successful calpain activation by iono/$CaCl_2$ treatment and inhibition by CI-III. b) TBP fragmentation was induced by iono/$CaCl_2$ treatment-dependent calpain activation over time. Calpain inhibition by CI-III prevented TBP fragment formation, reaching lower levels of fragmentation than the baseline cleavage seen in the vehicle control. Full-length spectrin: green arrow. Truncated spectrin: green arrowhead. Full-length CAPN1: grey arrow. Autolysed CAPN1: grey arrowhead. Full-length myc-hTBP-64Q: black arrow. Full-length myc-hTBP-38Q: white arrow. Endogenous hTBP: dark blue arrowhead. TBP fragments: orange arrows. Vinculin served as a loading control. Figure adapted from Weber et al. (2022).

To perform a quantitative analysis of the cleavage induction with ionomycin, the time point of 90 min was chosen as it showed a representative and robust treatment effect. These experiments were performed with myc-hTBP-38Q or -64Q-transfected HEK 293T cells and stably murine TBP (mTBP)-13Q- or -105Q-expressing PC12 cells.

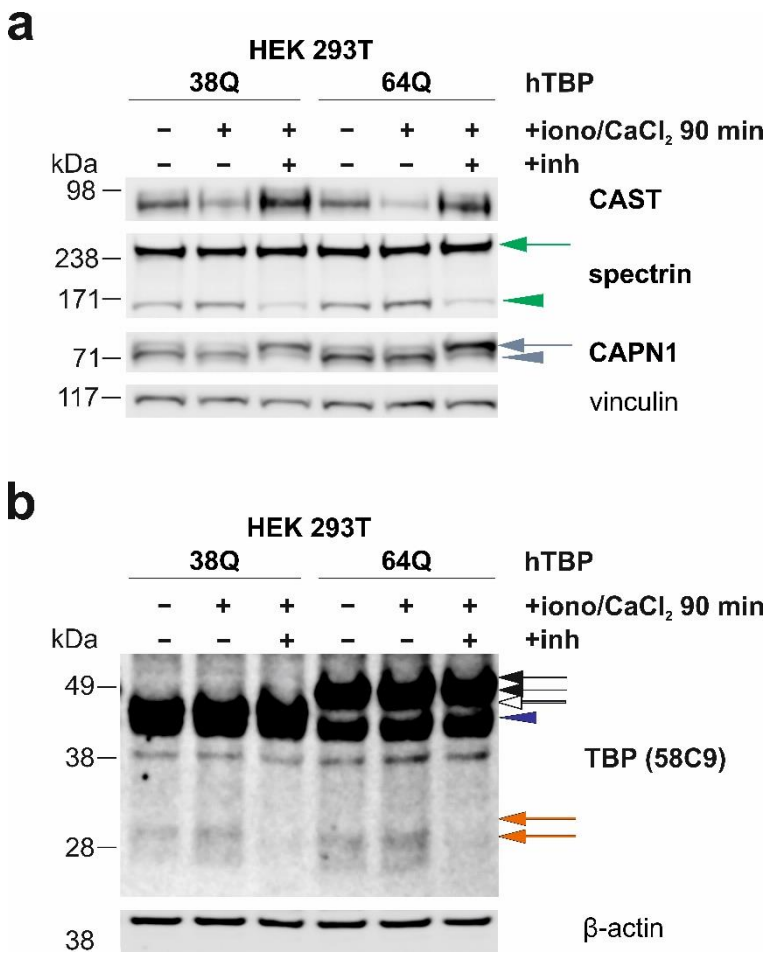

Figure 18. Immunoblot of HEK 293T cells depicting calpain activity and TBP proteolysis in cell-based calpain activation assay. Cell-based assays were conducted as described before with iono/$CaCl_2$ treatment for 90 min using myc-hTBP-38Q or -64Q-expressing HEK 293T cells. Qualitative analysis by immunoblotting confirmed the successful calpain activation (a) and induction of TBP fragmentation (b) by iono/$CaCl_2$ treatment and the countering effect of CI-III pre-incubation (inh). Figure adapted from Weber et al. (2022). Full-length spectrin: green arrow. Truncated spectrin: green arrowhead. Full-length CAPN1: grey arrow. Autolysed CAPN1: grey arrowhead. Full-length hTBP-64Q: black arrow. Full-length hTBP-38Q: white arrow. Endogenous hTBP: dark blue arrowhead. TBP fragments: orange arrows. Vinculin and β-actin served as loading controls.

For transfected HEK 293T cells, western blot analysis of calpain activation markers (Figure 18a) and TBP cleavage (Figure 18b) showed effects comparable to the previous time-dependent assays with ionomycin (Weber et al., 2022). Based on this data, densitometric measurement was, different from Weber et al. (2022), statistically analysed using one-way ANOVA with Dunnett's and Bonferroni post-test. Regarding the TBP fragment levels (Figure 19), treatment with ionomycin/calcium and CI-III in hTBP-38Q cells had highly significant effects, $F(2, 15) = 33.07$, $^{****}p < .0001$, $n = 18$ (one-way ANOVA). Dunnett's test for multiple comparisons confirmed highly significantly increased TBP fragment levels after addition of ionomycin by approximately 50% ($M = 1.6501$, $SD = 0.3691$, $^{***}p < .0005$, $n = 6$) compared to the standardized hTBP-38Q control. Inhibitor treatment of hTBP-38Q cells ($M = 0.5522$, $SD = 0.1720$, $^{**}p = .0091$, $n = 6$) reduced fragment levels by half compared to the normalized control. Under conditions of calpain activation by ionomycin and calcium, calpain inhibition restored to fragment levels to 30% (****p < .0001, Bonferroni post-hoc test). Highly significant results could also be shown for hTBP-64Q expressing cells, $F(2, 15) = 37.785$, $^{****}p < .0001$, $n = 18$ (one-way ANOVA). A very significant increase in TBP fragment levels of approximately 40% was reached by ionomycin treatment *(*$M = 1.4521$, $SD = 0.2866$, $^{**}p = 0.0034$, $n = 6$), while inhibitor treatment reached a reduction of TBP fragments by more than 50% compared to control ($M = 0.4166$, $SD = 0.2151$, $^{***}p = 0.0004$, $n = 6$), as revealed by Dunnett's test. Comparison of the two treatments by Bonferroni post-hoc test showed restoration of fragment levels to 30% by calpain inhibition compared to ionomycin treatment (****p < .0001).

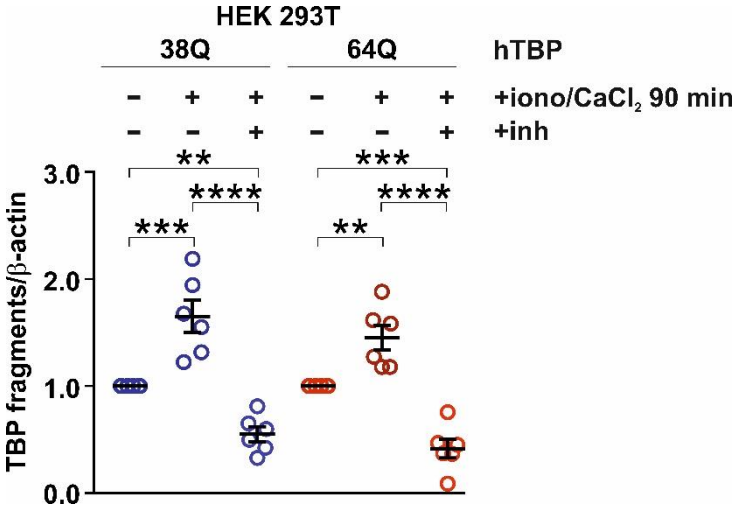

Figure 19. Quantitative investigation of TBP proteolysis in cell-based calpain activation assay in HEK 293T cells. Statistical analysis of TBP fragmentation before and after iono/$CaCl_2$ treatment show significant enhancement of TBP fragmentation by approximately 40-50% for both genotypes after iono/$CaCl_2$ addition and an effective reduction of fragments to 30% through calpain inhibition by CI-III (inh) compared to ionomycin treatment and by 50% compared to the vehicle control. *n* = 6. Bars represent mean ± SEM. **p ≤ .01; ***p ≤ .001; ****p ≤ .0001; one-way ANOVA. Figure adapted from Weber et al. (2022).

To confirm the results obtained from treatment of HEK 293T cells, the investigations were extended to PC12 cells, a neuron-like cell model deriving from a pheochromocytoma of the rat adrenal medulla and genetically altered to stably express murine TBP (mTBP) with a longer polyQ expansion of 105Q or a wild-type mTBP featuring 13Q.

Western blot analysis showed that the induction of calpain activity by ionomycin treatment and inhibition of activity by CI-III measured with CAST, spectrin, and CAPN1 in PC12 cells was comparable to HEK 293T cells (Figure 20a). Also, strong TBP degradation into the known fragment bands was comparable to the previous results, with an extensive reduction of full-length protein and appearance of fragments, presenting slightly stronger for mTBP-105Q (Figure 20b). However, full-length mTBP-13Q cleavage was hard to assess as it is overlayed by the endogenous rat TBP (isoform 1, UniProt identifier: Q66HB1-1), representing the endogenous species in PC12 cells. Endogenous rat TBP with a length of 318 aa and a normal glutamine region of 15Q is only a few amino acids longer than the murine variant, which comprises 316 aa with 13 glutamines (mTBP; isoform 1, UniProt identifier: P29037-1). Inhibition also worked effectively

for fragmentation prevention, keeping full-length and fragment levels approximately at control levels. Also, for PC12 cells, anti-TBP N-12 immunodetection did not reveal any fragments. These findings also additionally approved the PC12 cell line as a suitable cell model for further investigations. Interestingly, both TBP detections showed an unspecific protein band of different size, which could not be classified. Anti-TBP 58C9 detected a band at around 43 kDa, while anti-TBP N-12 detected a band at with a length of approximately 47 kDa. Both appeared in mTBP-13Q- and mTBP-105Q-expressing cells and reacted towards calpain induction by iono/$CaCl_2$ addition. These results have been published by Weber et al. (2022).

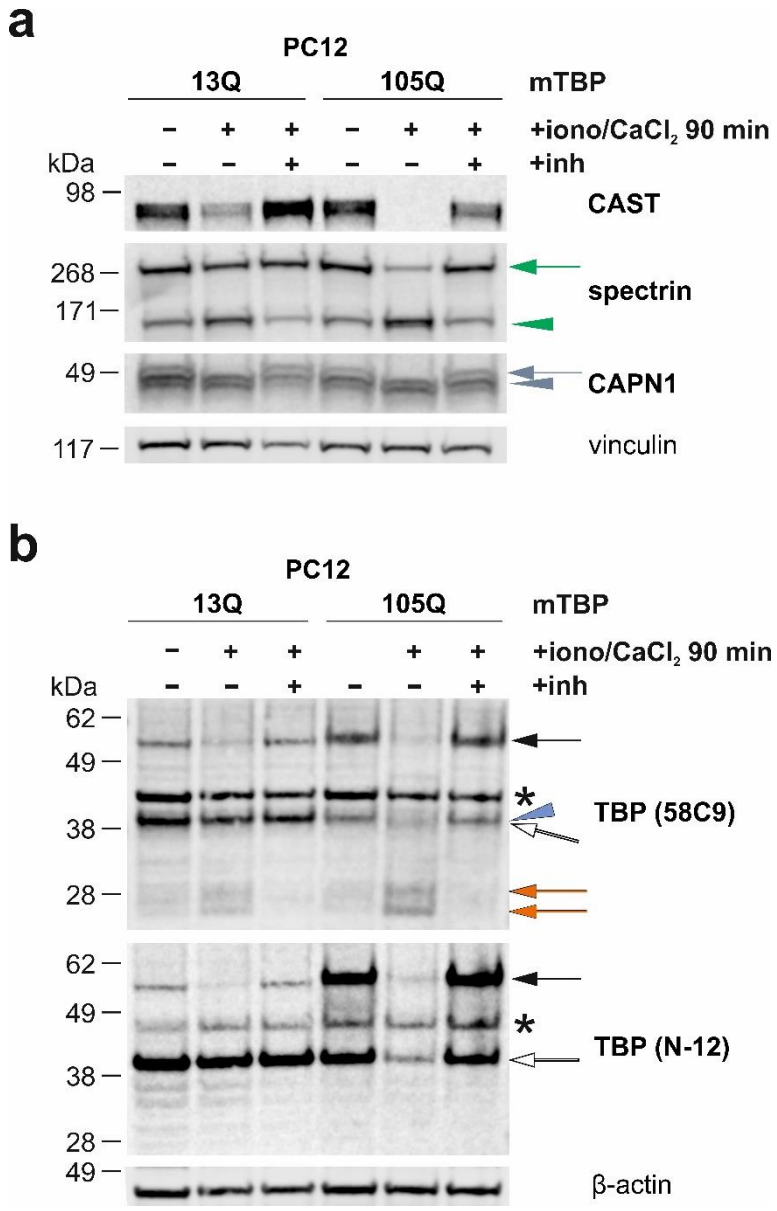

Figure 20. Immunodetection of ionomycin-induced cell-based cleavage assays in the PC12 cell line. PC12 cells stably expressing murine mTBP-13Q (13Q) and mTBP-105Q (105Q) were incubated with iono/$CaCl_2$ for 90 min. As inhibitor control, cells were preincubated for 1 h with CI-III (inh) prior to the 90 min iono/$CaCl_2$ administration. As vehicle control, cells were treated only with DMSO. a) Calpastatin (CAST), *α*-spectrin, and CAPN1 autolysis indicate an effective calpain activation by iono/$CaCl_2$ treatment and the successful inhibition by CI-III. Those results are comparable to HEK 293T cells. b) TBP fragmentation, immunodetected by anti-TBP 58C9 but not by anti-TBP N-12, shows a strong effect on TBP fragmentation into two fragment bands, again in line with the previous findings in HEK 293T cells and rat samples, but suggesting a stronger effect on mTBP-105Q-expressing PC12 cells than on transfected HEK 293T cells. Full-length spectrin: green arrow. Truncated spectrin: green arrowhead. Full-length CAPN1: grey arrow. Autolysed CAPN1: grey arrowhead. Full-length mTBP-105Q: black arrow. Endogenous rat TBP. Light blue arrowhead. Full-length mTBP-13Q: white arrow. Unspecific band: asterisk. TBP fragments: orange arrows. β-actin and vinculin served as a loading control. Figure adapted from Weber et al. (2022).

4.5 Overactivation of the calpain system in SCA17 rat and cell culture

Calpain activity has been shown to be increased in multiple neurodegenerative conditions (Weber et al., 2019). To test this in our cell and animal models of SCA17, markers of calpain activity and cleavage of TBP at baseline were investigated by western blotting.

In PC12 cells expressing mTBP-105Q, the parameters of calpain activity, namely CAST levels, spectrin cleavage, and CAPN1 autolysis, indicate an increase in calpain activity in comparison to the mTBP-13Q-expressing control cells (Figure 21a). Analysis of CAST levels (Figure 21b) in mTBP-105Q PC12 cells (M = 0.6692, n = 13, SD = 0.1747) compared to mTBP-13Q PC12 cells (M = 1, n = 13, SD = 0) revealed around 50% lower levels of CAST, $t(24) = 5.746$, ****$p < .0001$ (unpaired t-test). Spectrin cleavage (Figure 21c) in mTBP-105Q PC12 cells (M = 1.522, n = 13, SD = 0.5832) compared to mTBP-13Q PC12 cells (M = 1, n = 13, SD = 0) showed increased cleavage by 50%, $t(24) = 3.293$, **$p = .0031$ (unpaired t-test). These results have been published by Weber et al. (2022).

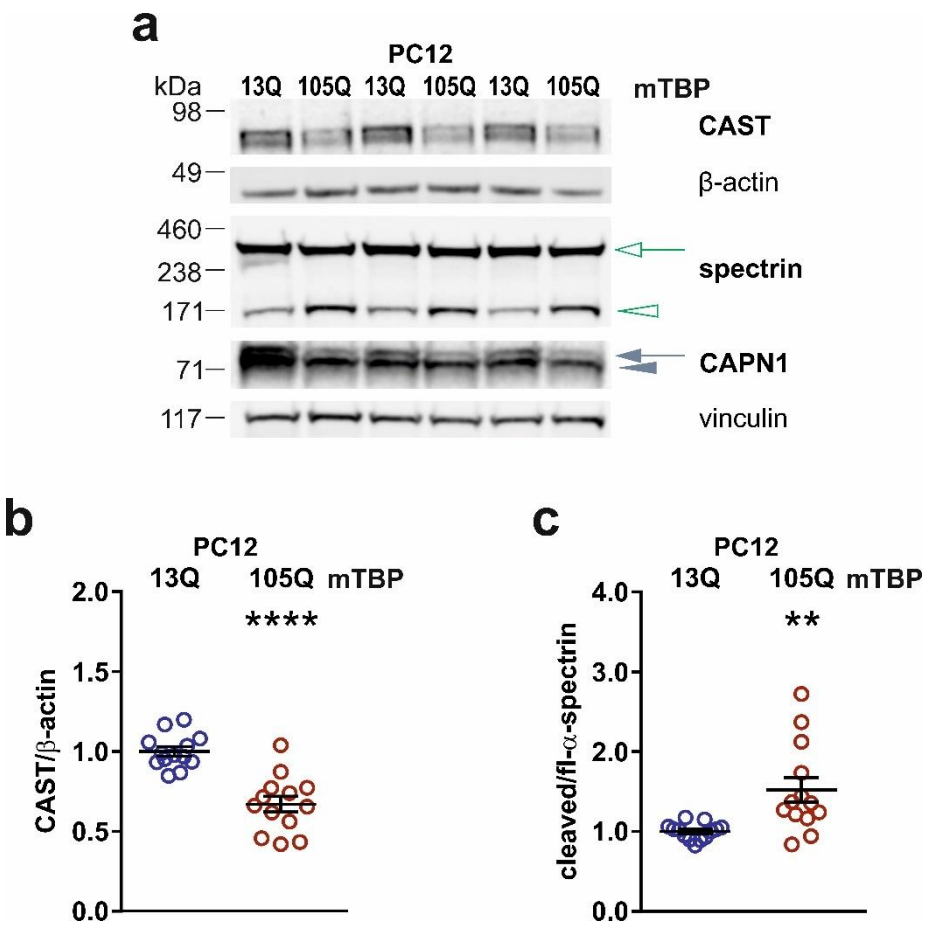

Figure 21. Analysis of calpain activation markers in PC12 cells at baseline. PC12 cells expressing mTBP-13Q and mTBP-105Q were cultured for 48 h, homogenized, and subjected to western blot to analyse calpain activation marker at baseline. a) CAST, spectrin cleavage and CAPN1 autocleavage indicate enhanced calpain activity for mTBP-105Q cells in comparison to mTBP-13Q cells. Densitometry and statistical analysis revealed significant calpain overactivation for TBP-105Q cells by highly significant reduction of calpastatin (b) and increased spectrin cleavage (c). Full-length spectrin: green arrow. Cleaved spectrin: green arrowhead. Full-length CAPN1: grey arrow. Autolysed CAPN1: grey arrowhead. Vinculin served as a loading control. *n* = 13. Bars represent mean ± SEM. **p ≤ .01;**** p ≤ .0001; unpaired *t*-test. Figure adapted from Weber et al. (2022).

Subsequently, western blot analysis and immunodetection of the calpain activity markers (Figure 22) was performed for the SCA17 rat cerebellum samples of 9 months old animals to investigate the observed effects in an *in vivo* model. Consistent with the observations in the PC12 cells, the analysis showed significantly higher baseline calpain activity, as indicated by CAST level reduction by approximately 50%, $t(4) = 6.101$, $^{**}p = .0037$ (unpaired *t*-test) in SCA17 rat cerebellum ($M = 0.4721$, $n = 3$) in comparison to wild-type animals ($M = 1$, $n = 3$) (Figure 22b). Likewise, spectrin cleavage in SCA17 rat cerebellum ($M = 1.450$,

n = 3) compared to wild-type rats (*M* = 1, *n* = 3) reached around 50% higher levels, t(4) = 6.159, ***p* = .0035 (unpaired *t*-test) (Figure 22c).

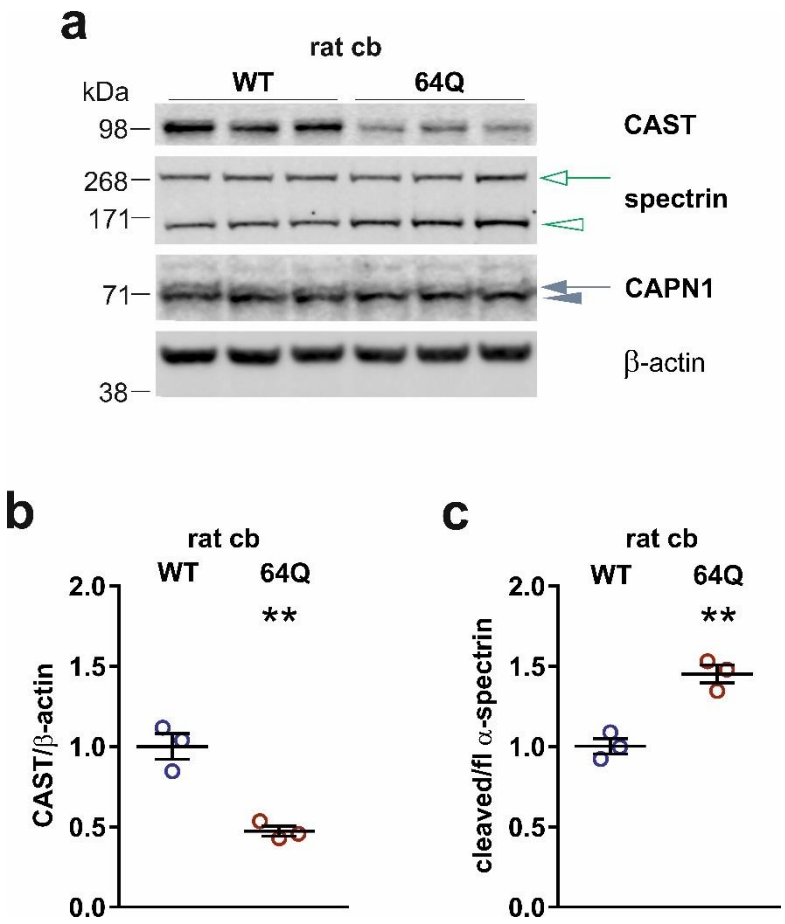

Figure 22. Analysis of calpain activation markers in wild-type and SCA17 rat cerebellum at baseline. Immunodetection (a) and quantitative analysis of calpain activation markers in cerebellum homogenates of 9 months old rats shows significant calpain overactivation in SCA17 rats expressing hTBP-64Q (64Q) as indicated by reduction of CAST levels (b) and enhanced spectrin cleavage (c) when compared to wild-type animals (WT). Full-length spectrin: green arrow. Cleaved spectrin: green arrowhead. Full-length CAPN1: grey arrow. Autolysed CAPN1: grey arrowhead. β-actin served as a loading control. *n* = 3. Bars represent mean ± SEM. **p ≤ .01; unpaired *t*-test. Figure adapted from Weber et al. (2022).

Regarding TBP fragmentation (Figure 23a, b), in SCA17 rat cerebellum (*M* = 2.847, *n* = 3) compared to wild-type rat cerebellum (*M* = 1, *n* = 3), it was increased almost 3-fold, *t*(4) = 11.88, ****p* = .0003 (unpaired *t*-test). As the increased levels are also due to the overexpression of the TBP transgene, fragment levels were normalized to total full-length TBP levels (Figure 23c). Taking this into account, the overactivation of the calpain system in hTBP-64Q

rat cerebellum (*M* = 1.206, *n* = 3) compared to wild-type rats (*M* = 1, *n* = 3) can be still associated with significantly increased TBP truncation of around 20%, *t*(4) = 5.740, ***p* = .0046 (unpaired *t*-test). These results of baseline calpain activity markers and TBP fragmentation in rat cerebellum have been published by Weber et al. (2022), where the observations were emphasized by a higher sample amount.

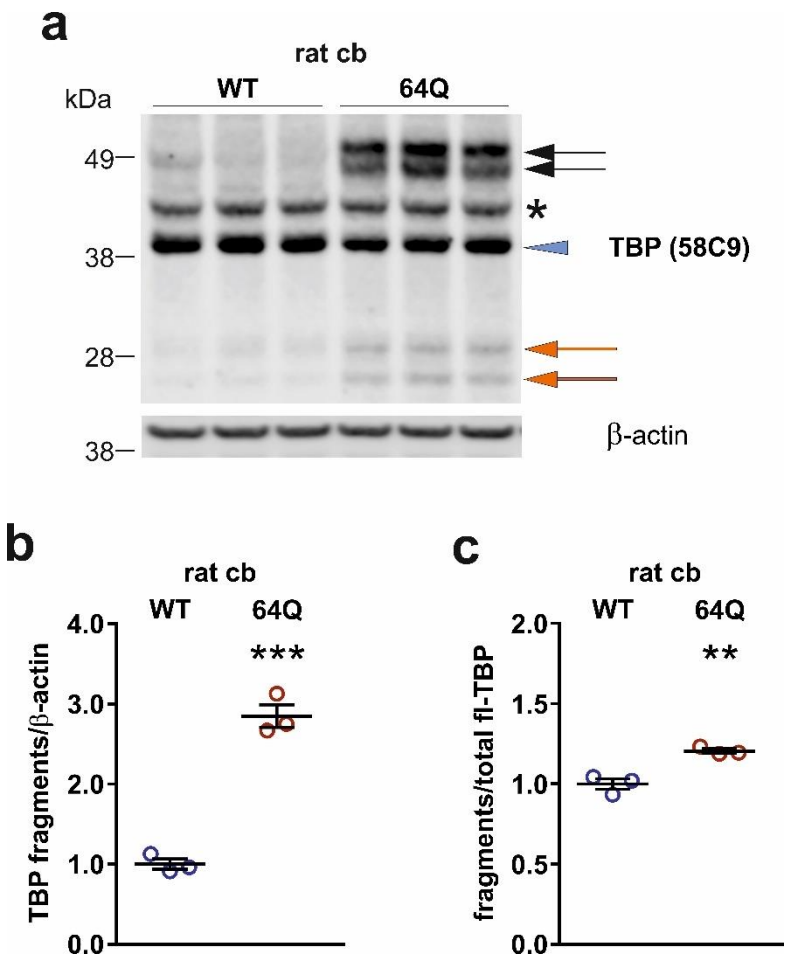

Figure 23. Analysis of TBP fragmentation in wild-type and SCA17 rat cerebellum at baseline. a, b) Cerebellum of SCA17 rats shows nearly three-fold increased absolute TBP fragment levels (64Q) compared to wild-type animals (WT). c) When normalized to the total full-length protein, it remains significantly increased by 20%. Full-length hTBP-64Q: black arrows. Endogenous rat TBP: light blue arrowhead. Unspecific band: asterisk. TBP fragments: orange arrows. β-actin served as a loading control. *n* = 3. Bars represent mean ± SEM. **p ≤ .01; ***p ≤ .001; unpaired *t*-test. Figure adapted from Weber et al. (2022).

To determine whether the calpain overactivation is due to overexpression of the polyQ-expanded transgene, brain areas of hTBP-64Q rats with a low to no

expression of hTBP-64Q were analysed for their calpain activation by western blotting. For this, striatum and cortex samples were investigated which did not show a hTBP-64Q expression in the previous analysis (see 4.1).

Regarding the striatum (Figure 24a-c), detection of CAST revealed no significantly different levels in SCA17 rat striatum (M = 0.8824, n = 3) and wild-type rat striatum (M = 1.0, n = 3), $t(4) = 0.5172$, p = .6323 (unpaired t-test). For spectrin cleavage also, no difference was found, when SCA17 rat striatum (M = 1.051, n = 3) was compared to wild-type animals (M = 1.028, n = 3), $t(4) = 0.7057$, p = .5193 (unpaired t-test). In the cortex (Figure 24d-f) no significant difference could be detected between SCA17 rats (M = 1.093, n = 3) compared to wild-type rats (M = 1, n = 3) for CAST levels, $t(4) = 0.6033$, p = .5789 (unpaired t-test). With regard to spectrin cleavage, no significantly different cleavage products were found for SCA17 rats (M = 1.020, n = 3) and wild-type rats (M = 1, n = 3), t(4) = 0.5003, p = .6431 (unpaired t-test). These results have been published by Weber et al. (2022).

In sum, baseline overactivation of calpains in relation to the expression of a polyQ-expanded TBP could be validated both in the PC12 cell model and *in vivo* in SCA17 rats.

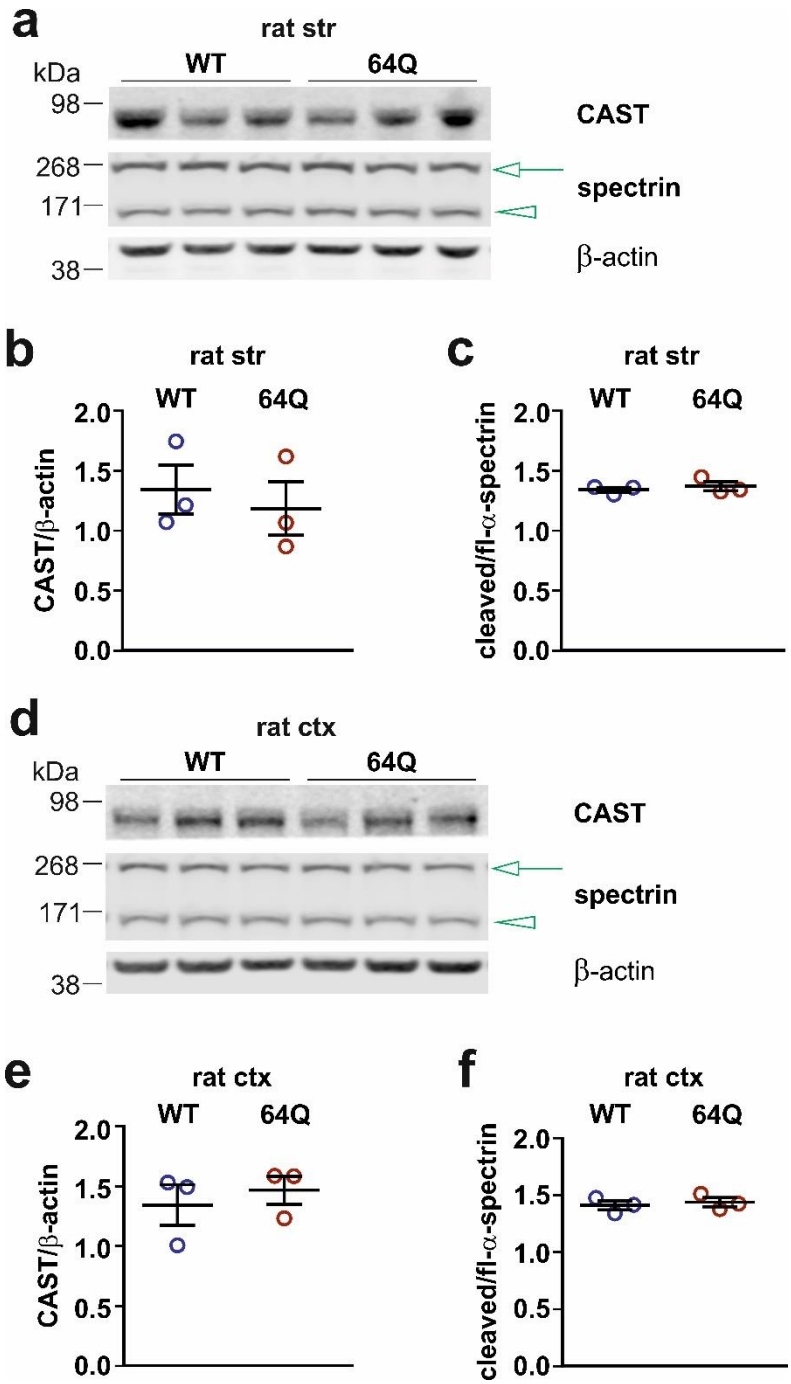

Figure 24. Analysis of calpain activation markers in striatum and cortex of wild-type and SCA17 rats. Immunodetection and quantification of calpastatin levels (CAST) and spectrin cleavage in striatum (str, a) and cortex (ctx, b) did not indicate a significant difference between wild-type (WT) and SCA17 rats (hTBP-64Q). Full-length spectrin: green arrow. Cleaved spectrin: green arrowhead. β-actin served as a loading control. *n* = 3. Bars represent mean ± SEM. Unpaired *t*-test. Figure adapted from Weber et al. (2022).

4.6 Effects of long-term cell-based calpain inhibition with calpain inhibitor and CAST overexpression

Pharmacological calpain inhibition and CAST overexpression were both demonstrated to reduce calpain overactivation, fragment formation, and disease protein aggregation, ameliorating the phenotype in models of neurodegenerative disorders such as HD, SCA3, PD, and AD (Rao et al., 2016; Diepenbroek et al., 2014; Haacke et al., 2007; Simoes et al., 2012; Gafni et al., 2004; Clemens et al., 2015). When generated as a transgenic model, CAST overexpression can start from the beginning of life and may counteract a potential disease-related elevation of early calpain activity (Wright and Vissel, 2016). Moreover, CAST is a very specific inhibitor, solely targeting calpains (Maki et al., 1987). However, pharmacologic calpain inhibition, despite lacking a very high specificity, offers a more translatable approach regarding treatment of patients and is already applied in phase I trials of AD (Wright and Vissel, 2016).

Here, both approaches were tested for their effectivity to reduce calpain activity and fragment formation of TBP in cell-based experiments with HEK 293T or PC12 cells.

4.6.1 Calpain inhibition via overexpression of the endogenous inhibitor calpastatin

Human CAST (hCAST) and a mock vector were cotransfected in HEK 293T cells with myc-hTBP-38Q and myc-hTBP-64Q and expressed over 48 h. Afterwards, cell homogenates were analysed via western blotting for calpain activation markers and TBP cleavage (Figure 26a).

Very significantly elevated CAST levels (Figure 26b) were confirmed for HEK293T cells co-expressing hTBP-38Q and CAST (M = 12.0204, n = 3, SD = 1.6180) compared to those with co-expression of the mock vector (M = 1.0, n = 3, SD = 0.1643), $t(2.041) = -11.737$, $^{**}p = .0067$ (unpaired t-test). Also for hTBP-64Q cells, CAST levels showed a highly significant increase when cells expressed CAST (M = 12.2743, n = 3, SD = 1.4861) compared to the mock

vector (*M* = 0.9511, *n* = 3, *SD* = 0.2748), *t*(4) = -12.977, ***p* = .0002 (unpaired *t*-test).

Despite a clear tendency was visible, for spectrin cleavage (Figure 26c) in HEK293T cells co-expressing hTBP-38Q and CAST (*M* = 0.6373, *n* = 3, *SD* = 0.0339) no significant difference in comparison to hTBP-38Q mock cells (*M* = 1.0, *n* = 3, *SD* = 0.2422) could be measured, *t*(4) = 2.569, *p* = .62 (unpaired *t*-test). In hTBP-64Q cells expressing polyQ-expanded TBP, spectrin cleavage neither showed significant results when CAST overexpression (*M* = 0.6042, *n* = 3, *SD* = 0.2208) was compared to those co-expressing the mock vector (*M* = 1.1952, *n* = 3, *SD* = 0.4423), *t*(4) = 2.070, *p* = .107 (unpaired *t*-test). These results may be due to low sample amount and high variance.

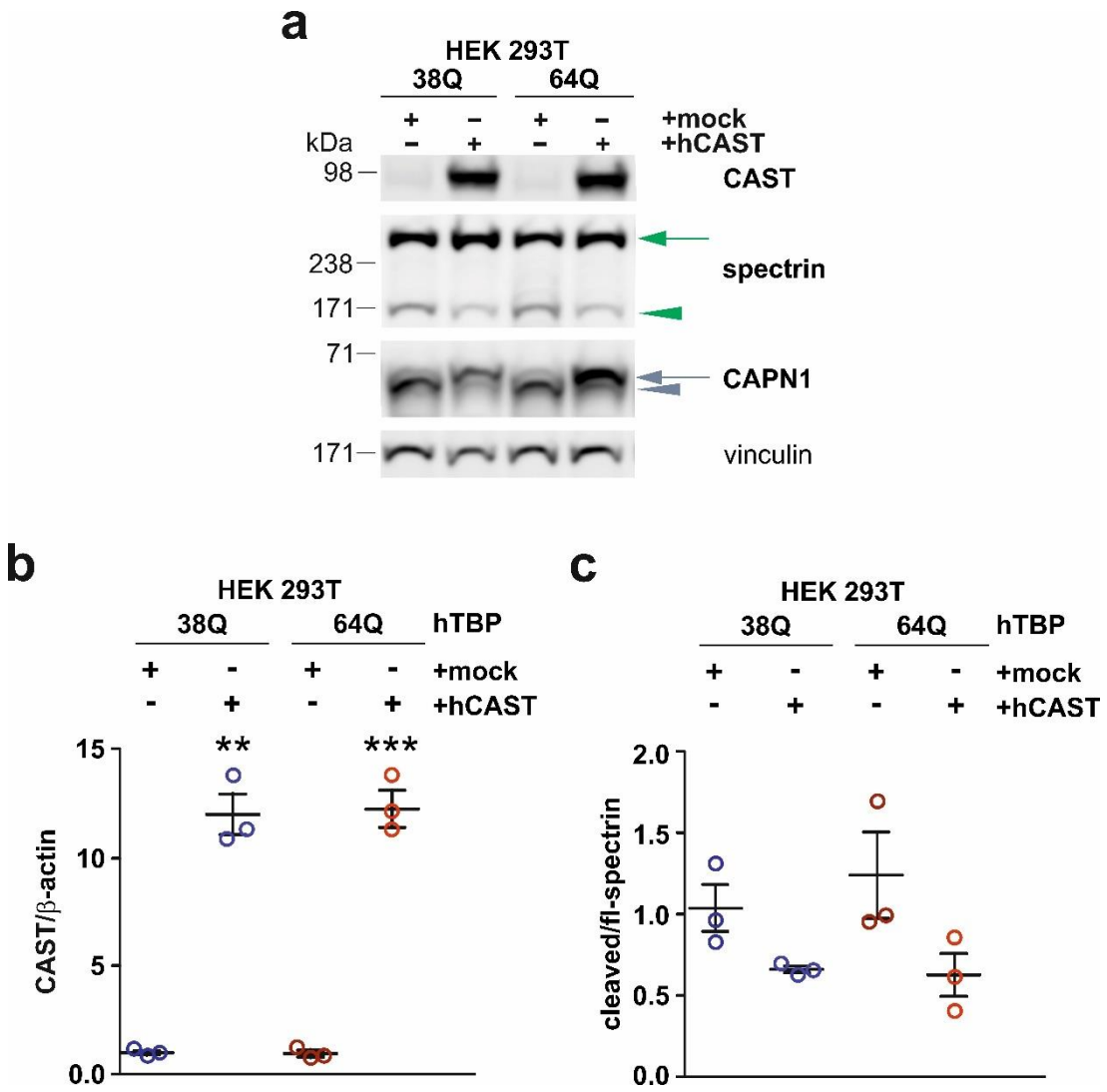

Figure 25. Immunodetection of calpain activity markers in CAST-overexpressing HEK 293T cells. HEK 293T cells were cotransfected for 48 h with myc-hTBP-38Q or -64Q together with a control vector (mock) or human CAST (hCAST). a) Immunoblotting of the cell lysates hints to successful CAST overexpression and resulting calpain activity suppression as detected by spectrin cleavage and CAPN1 autolysis. b) Densitometric and statistical analysis does display very to highly significantly increased CAST levels, while it does not display significance of spectrin cleavage (c). Full-length spectrin: green arrow. Cleaved spectrin: green arrowhead. Full-length CAPN1: grey arrow. Autolysed CAPN1: grey arrowhead. Vinculin served as loading control. *n* = 3. Bars represent mean ± SEM. **p ≤ .01; ***p ≤ .001; unpaired *t*-test.

Calpain-mediated TBP cleavage as represented by the two fragment bands could be reduced by CAST overexpression for both genotypes (Figure 26a). For hTBP-38Q cells expressing CAST (M = 0.5411, n = 3, SD = 0.5446) compared to expression of mock (M = 0.8069, n = 3, SD = 0.2892) TBP fragmentation was not significantly different, $t(4) = 1.564$, $p = .1928$ (unpaired t-test). In cells with co-expression of hTBP-64Q and CAST (M = 0.4846, n = 3, SD = 0.1046), there was

significantly reduced TBP fragmentation compared to control samples with expression of the mock vector (M = 1.0, n = 3, SD = 0.2775), $t(4) = 2.868$, $^*p = .0456$ (unpaired t-test) (Figure 26b).

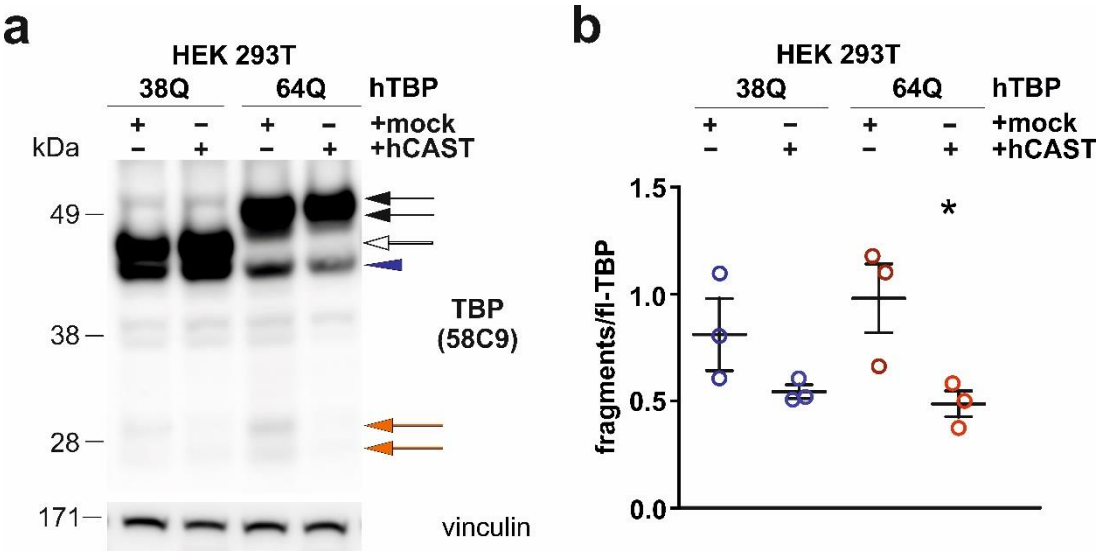

Figure 26. Immunodetection of TBP fragmentation in CAST-overexpressing HEK 293T cells. HEK 293T cells were cotransfected for 48 h with myc-hTBP-38Q or -64Q together with a control vector (mock) or human CAST (hCAST). a) Staining with anti-TBP 58C9 indicates a decreased TBP proteolysis by CAST overexpression. b) Reduced calpain-mediated cleavage by CAST overexpression can be measured for both genotypes Full-length hTBP-64Q: black arrow; full-length hTBP-38Q: white arrow; endogenous hTBP: dark blue arrowhead; TBP fragments: orange arrows. Vinculin served as loading control. n = 3. Bars represent mean ± SEM. *p ≤ .05; unpaired t-test.

4.6.2 Cell-based inhibition with calpain inhibitor III for 48 h

As mentioned earlier, CAST overexpression is an effective but impractical way to inhibit calpain-mediated effects regarding translational approaches, whereas pharmacological inhibition offers a therapeutical opportunity in an applicable form in contrast to genetic manipulations. Cell-based calpain activation assays (see 4.4) already showed that calpain inhibition with CI-III was able to reduce TBP fragmentation for a time range of 2.5 h of inhibition under activating conditions. As fragmentation and aggregation are cellular processes occurring over time, the effects of cell-based inhibition by incubation with 25 µM CI-III over 24 h and 48 h were investigated in PC12 cells expressing mTBP-13Q or mTBP-105Q. CI-III was

replenished after 24 h for the 48 h-inhibitor treatment condition to reach a constantly high-dosed inhibition effect.

Western blot analysis of CI-III treated cells showed that inhibitor treatment suppressed calpain activity markedly in comparison to DMSO-treated control, especially in those carrying expanded mTBP-105Q as substantiated by the increased levels of CAST (Figure 27a). Calpain inhibitor treatment had a significant effect on TBP fragmentation of mTBP-13Q-expressing PC12 cells, $F(2, 9) = 13.07$, $^{**}p = .0022$, $n = 12$ (one-way ANOVA). Dunnett's multiple comparisons test showed significantly reduced fragmentation after 24 h ($M = 0.5816$, $SD = 0.1378$, $^{**}p = .0012$, $n = 4$) and 48 h ($M = 0.7491$, $SD = 0.139$, $^{*}p = .0251$, $n = 4$) of calpain inhibitor treatment incubation (Figure 27c). In mTBP-105Q-expressing cells, CI-III treatment restored full-length TBP levels clearly (Figure 27b) with highly significant reduction of fragmentation of approximately 50%, $F(2, 15) = 19.65$, $^{****}p < .0001$, $n = 18$ (one-way ANOVA). Dunnett's multiple comparisons test confirmed highly significant decreases of fragment levels after 24 h ($M = 0.4807$, $^{***}p = .0003$, $n = 6$) and 48 h ($M = 0.4034$, $^{****}p < .0001$, $n = 6$) of CI-III treatment (Figure 27d). These results have been published by Weber et al. (2022).

On the one hand, these results give an idea of the extent of calpain-mediated cleavage of the full-length TBP within 48 h due to overactivation in glutamine expansion expressing cells at baseline, and on the other hand, they approve CI-III treatment as effective to avert this process also as long-term treatment of 24 h and 48 h.

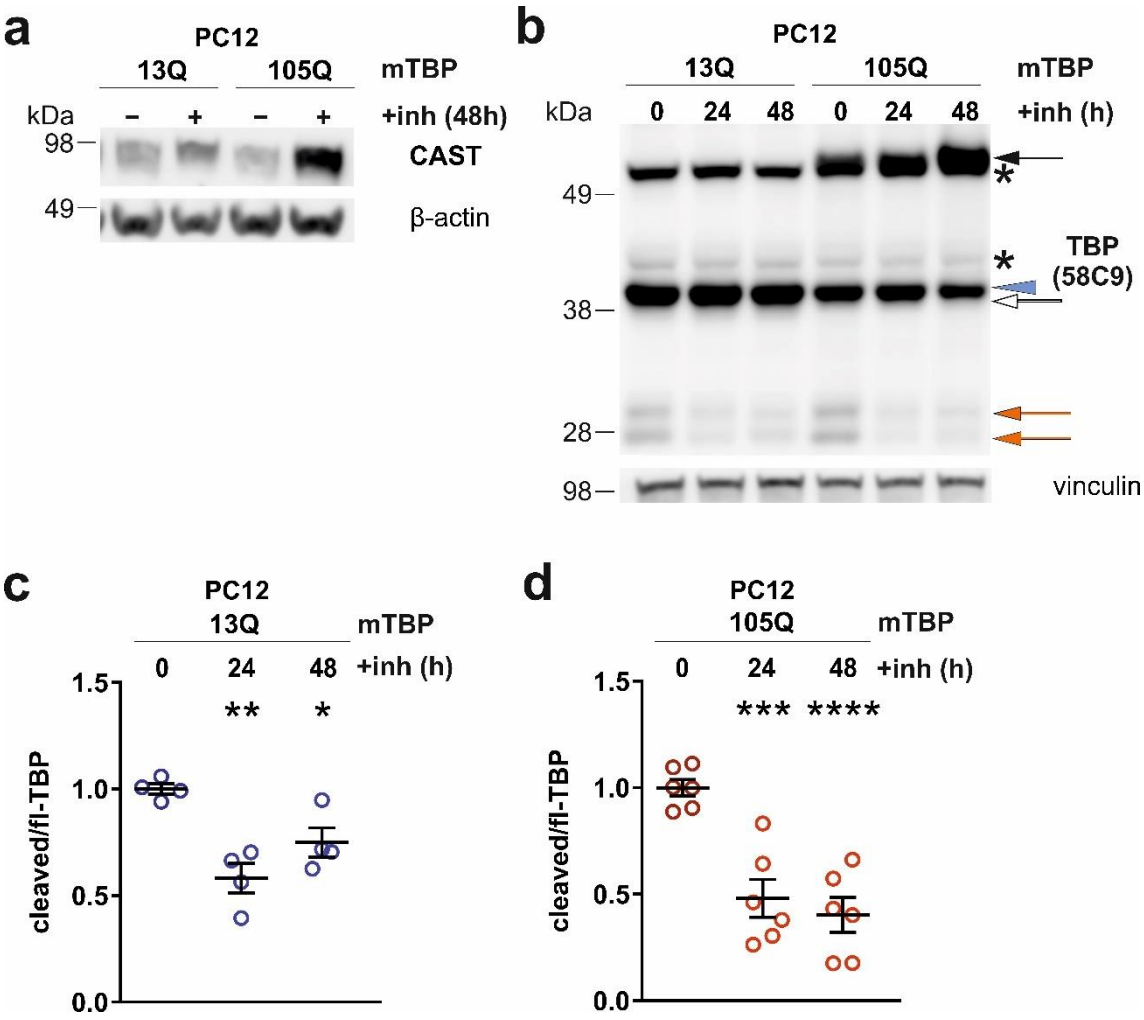

Figure 27. Immunodetection of calpain activity markers and TBP fragmentation in PC12 cells treated with CI-III for 24 h and 48 h. Incubation with CI-III for 24 h and 48 h was performed with PC12 cells expressing mTBP-13Q and mTBP-105Q and cells analysed via western blotting. a) Increased CAST levels confirm the effective calpain inhibition (inh) after 48 h treatment. b) Levels of TBP fragments are reduced for mTBP-13Q and -105Q cells after 24 h and 48 h of inhibitor incubation compared to the vehicle control treated with DMSO (0). Full-length protein levels were preserved by protection from proteolysis and accumulated in the case of mTBP-105Q in long-term inhibition. c, d) The fragment levels were reduced significantly by calpain inhibition for cells with non-expanded and expanded TBP. Full-length mTBP-105Q: black arrow. Endogenous rat TBP: light blue arrowhead. Full-length mTBP-13Q: white arrow. Unspecific band: asterisk. TBP fragments: orange arrows. *β*-actin and vinculin served as loading controls. *n*(13Q) = 4, *n*(105Q) = 6. Bars represent mean ± SEM. *: p ≤ .05; **p ≤ .01; ***p ≤ .001; ****p ≤ .0001; one-way ANOVA. Figure adapted from Weber et al. (2022).

4.7 Association between calpain inhibition and occurrence of SDS-insoluble aggregates

It was shown previously in this study that calpains are overactivated in our SCA17 cell and rat models, which was associated with significantly increased

polyQ-expanded TBP fragment levels *in vivo* (see 4.5). As mentioned earlier, aggregates in polyQ diseases were shown to consist of truncated forms of the disease proteins, together with according full-length proteins and other cellular components (Weber et al., 2014). The prevalence of fragments in polyQ aggregates is explained by a higher tendency of polyQ protein fragments to interact and aggregate with each other, which is facilitated by higher exposure of the polyQ tract when cleaved out of its sequential context (Lunkes et al., 1999; Scherzinger et al., 1997). Broadly speaking, this emphasizes the connection between proteolytic cleavage, appearance of fragments, and generation of aggregates. Friedman et al. found N-terminal fragments of polyQ-expanded TBP in nuclear inclusions of HEK 293T cells and SCA17 mouse brains Friedman et al. (2008). The more truncated protein was available the more aggregates were formed.

First, to confirm that polyQ-expanded TBP aggregation is present in SCA17 rat cerebellum and PC12 cells, SDS-containing sample buffer-based filter retardation assays were conducted, which trap SDS-insoluble protein aggregates on a nitrocellulose membrane. Trapped aggregates were then immunostained similarly to the procedure of western blotting.

The results of these experiments are presented in Figure 28 and show immunodetection signals using anti-TBP N-12 antibody in rat cerebellum of hTBP-64Q rats, whereas wild-type animals as well as brain regions without polyQ-expanded TBP expression show only a background staining (Figure 28a). Interestingly, aggregates were only clearly detectable using the antibodies anti-TBP N-12 and anti-polyQ 1C2, but not by the C-terminally-binding antibody anti-TBP 58C9, that was mainly used to detect fragments. This indicates that the C-terminal epitope of TBP could not be detected in the trapped aggregates due to its absence or its inaccessibility for the antibody (Figure 28b). According to rat cerebellum, PC12 cells expressing mTBP-105Q showed a strong occurrence of aggregates compared to cells expressing mTBP-13Q (Figure 28c).

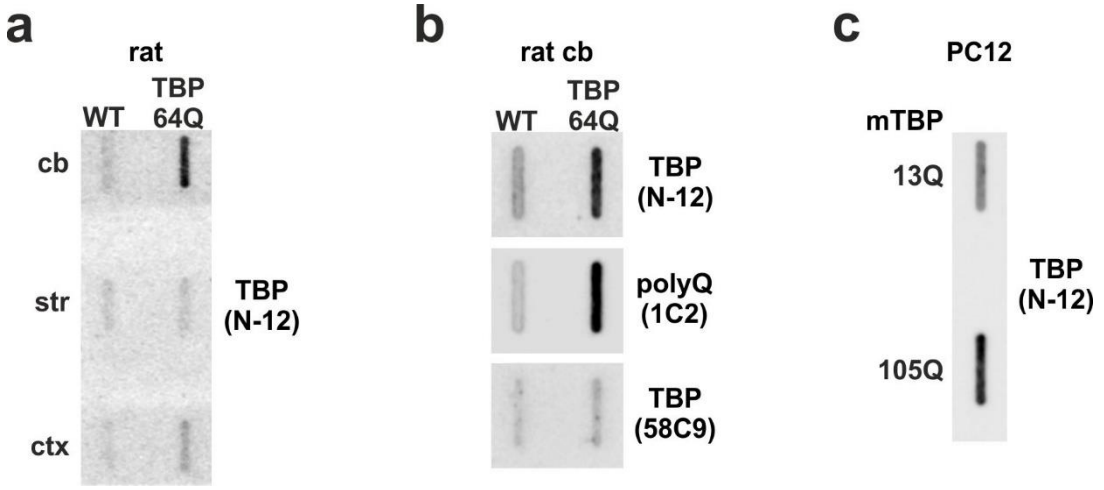

Figure 28. Filter retardation assays of rat brain and PC12 cells for detection of SDS-insoluble TBP aggregates. 25 µg of protein of rat brain tissue and PC12 cell homogenates were diluted in SDS-containing DPBS and filtered through a nitrocellulose membrane to retain SDS-insoluble aggregates. a) Immunostaining with anti-TBP N-12 shows TBP aggregates in rat cerebellum (cb) of hTBP-64Q rats, but neither in wild-type cerebellum, nor any of the other brain areas (str, ctx) lacking expression of the transgene. b) The antibodies anti-TBP N-12, binding to N-terminus of TBP, and anti-polyQ 1C2, which recognizes the polyQ stretch, but not the C-terminally-binding anti-TBP 58C9 antibody, detect aggregates in cerebellum of SCA17 rats, indicating that solely N-terminal parts containing a polyQ stretch of hTBP are present or detectable in the aggregates. c) Filter retardation assay of PC12 cells, show a higher load for SDS-insoluble TBP when expressing mTBP-105Q in comparison to cells expressing mTBP with 13 glutamine repeats.

The relevance of calpain-mediated cleavage in the axis of proteolysis, fragmentation, and aggregation as pathological hallmarks was contemplated by investigations of the influence of reduction of calpain activity on the aggregation process. Like the previous investigations on the effect of a long-term lowering of calpain activity by using a pharmacological inhibitor or calpastatin overexpression regarding TBP cleavage (see 4.6), repercussions on TBP aggregation were assessed by treating PC12 cells expressing mTBP-13Q or -105Q with CI-III for 24 h and 48 h.

Aggregate analysis based on filter retardation assays showed that CI-III incubation on mTBP-105Q-expressing PC12 cells (M = 0.7469, SD = 0.06199, n = 3) reached around 30% reduction of the aggregate load after 48 h, t(2) = 7.071, *p = .0194 (one-sample t-test) (Figure 29) (Weber et al., 2022). A higher-dosed application of CI-III or securing a constant bioavailability of the compound over the full treatment time might reach a greater potency, as the

aggregation process seems to occur in a slower and constant manner than TBP fragmentation.

These findings underline the relation of TBP fragment and aggregate formation and the crucial role of calpain-mediated proteolysis on both pathogenic components, highlighting calpains as a druggable therapeutic target in the treatment of SCA17.

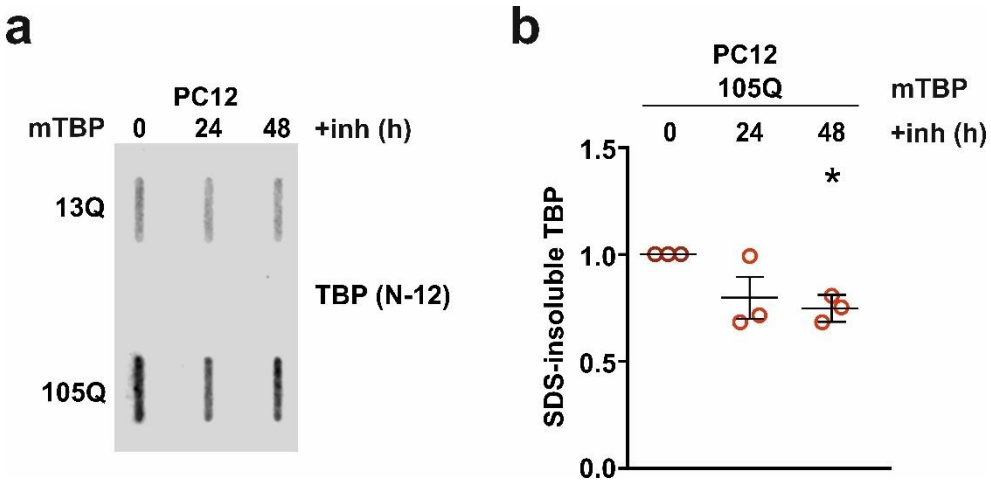

Figure 29. Effect of calpain inhibition by CI-III treatment on TBP aggregation. a) Filter retardation assay of CI-III-treated PC12 cells expressing mTBP with 13Q and 105Q show a reduction of N-terminally immunodetectable aggregates of mTBP-105Q after 24 h and 48 h of incubation. As shown in the previous experiments, PC12 cells expressing mTBP-13Q do not show a high signal for SDS-insoluble forms TBP. b) Quantification confirms the observations of (a) with significant reduction of the aggregate load by around 30% after 48 h of CI-III treatment, indicating successful alleviation of the aggregation process by calpain inhibition. *n* = 3. Bars represent mean ± SEM. *p ≤ .05; one sample *t*-test. Figure adapted from Weber et al. (2022).

5 Discussion

The group of polyQ disorders is characterized by a glutamine-coding trinucleotide repeat that is translated into a polyQ chain of the mutant protein. Spinocerebellar ataxia type 17, together with eight other diseases, belongs to this group and is characterized by a polyQ expansion in TBP. The pathogenetic principles include occurrence of cellular aggregates in neurons of affected brain areas and TBP-linked transcriptional dysregulations. Moreover, the formation of disease protein fragment seems to be an important factor, as specific polyQ stretch-containing TBP breakdown products can be found in these neuronal aggregates, which furthermore consist of other cellular components such as transcription factors and parts of the protein degradation systems (Koide et al., 1999; Friedman et al., 2008; Weber et al., 2014).

The aim of this study was to identify the role of a group of calcium-dependent proteases, the calpains, in the pathogenesis of SCA17 by analysing the potential association of fragment occurrence, aggregate formation, and calpain activity in relation to the polyQ mutation in TBP. The investigations comprised the evaluation of TBP as a substrate of calpains *in vivo, in vitro,* and *in cellulo* and of the calpain activation level in SCA17 cells and animals. For this, PC12 and HEK 293T cell lines and the TBPQ64 rat model, all expressing the polyQ-expanded TBP, were utilized. Furthermore, the potential of calpastatin overexpression and of pharmacological calpain inhibition by calpain inhibitor III (CI-III) was assessed as an experimental therapeutic approach to reduce calpain activity and the associated TBP fragmentation and aggregation in cell-based approaches.

5.1 Expanded TBP is highly expressed in cerebellum of SCA17 rat brains and reduces levels of endogenous TBP

While neuropathology in many ADCAs is restricted to cerebellar, spinal, olivopontocerebellar, and corticocerebellar atrophy, SCA17 can manifest neuropathologically with global atrophy (Stevanin and Brice, 2008; Manto, 2005). Reduction of total brain volume involves grey and white matter lesions, atrophy

of cerebellum as well as atrophy of thalamus, especially medial thalamic nuclei, and of frontal, parietal, and temporal cortex (Nakamura et al., 2001; Rolfs et al., 2003; Lasek et al., 2006; Bruni et al., 2004). Degeneration is additionally found prominently in the inferior olives, but also in the basal ganglia, most prominently in the caudate and nucleus accumbens, cerebral motor structures, limbic system, and hippocampus, whereas brainstem and pontine nuclei are mildly affected in comparison to other ADCAs (Zuhlke and Burk, 2007; Stevanin and Brice, 2008; Reetz et al., 2010). Despite this broad neuronal disease pattern, the cerebellum is considered the most affected brain area. Besides Purkinje cells as the cerebellar cell type showing the highest levels of degeneration, also stellate and basket cells are affected, resulting in Bergmann's gliosis and gliosis of dentate nucleus and the molecular layer (Stevanin and Brice, 2008). In accordance with results by Kelp et al. (2013), this analysis of the three brain areas cerebellum, cortex, and striatum of our SCA17 rat model confirmed high expression levels of hTBP-64Q in cerebellum, while both cortex and striatum had no detectable expression level of transgenic polyQ-expanded TBP. In contrast, Kelp et al. (2013) detected medium levels of hTBP-64Q in cortex and olfactory bulb, while low expression was shown in brain stem, hypothalamus, and striatum. Therefore, it was focused on investigations of rat cerebellum instead of other areas as being closest to neuropathological affection in human brains of SCA17 patients.

Expression of hTBP-64Q in rat cerebellum was further associated with significant reduction of endogenous TBP levels in this study (Weber et al., 2022). Mutant protein expression can lead to depletion of the wild-type protein in other polyQ diseases (Haacke et al., 2006; Gafni and Ellerby, 2002). As inclusions were already detected in our SCA17 rat model and wild-type TBP was shown to be sequestered into inclusion by polyQ proteins in other polyQ diseases and SCA17, overexpression of polyglutamine-containing full-length, and truncated TBP might recruit and thereby reduce endogenous, wild-type TBP (Kim et al., 2002; Kelp et al., 2013; Friedman et al., 2008; Rolfs et al., 2003). Another explanation could be the transcriptional reduction of endogenous TBP by overexpression of polyQ-expanded TBP. In addition to the altered expression patterns, the DNA

binding capacity of TBP itself was found to be decreased 15-fold in SCA17 (Hsu et al., 2014).

Furthermore, the assembly of TBP is an important rate-limiting step in transcription *in vivo,* which is why TBP levels need to be regulated sensitively. One way of autoregulation is the formation of inactive TBP dimers via a C-terminal dimerization domain. In case of overexpression, mass action drives dimerization leading to inactivation of transcription (Jackson-Fisher et al., 1999).

5.2 Fragments of TBP are detectable in rat brain samples and cell lines

Truncated TBP was found to be localized in inclusions of SCA17 patients and is thought to be more prone to form inclusions compared to the full-length counterpart (Friedman et al., 2008; Kim et al., 2002). Using antibodies binding TBP sequence C-terminal of the polyQ-stretch, two TBP fragment bands could be detected at baseline in rat cerebellum of SCA17 rats and HEK 293T cells overexpressing myc-hTBP-38Q and -64Q (Weber et al., 2022). Furthermore, full-length and fragment pattern for cells and brain tissue were comparable. As the two occurring fragments with an approximate size of 28 kDa and 30 kDa could neither be detected by the N-terminally binding anti-TBP N-12 nor by the polyQ binding antibody 1C2, and as both did not show a size shift between wild-type and expanded forms, the findings indicate the C-terminal origin of the breakdown product in the absence of the polyQ domain (Weber et al., 2022). The antigen of antibody anti-TBP 8515 at position Gln44 lies N-terminally of the polyQ stretch. A weak, polyQ-independent band is only seen for immunodetection of HEK cells, not for rat cerebellum samples. As this fragment of approximately 30 kDa corresponds to a size of more than 200 amino acids, it is excluded as a specific TBP fragment.

Conclusively, based on the estimated fragment length of about 240-280 amino acids and the lack of the polyQ stretch, the two potential cleavage sites must be located C-terminally of the polyQ domain. Moreover, no N-terminal fragments could be clearly detected by using our selection of antibodies. An alternative

origin of these fragments like an alternative splicing-related event could be excluded as the utilized TBP constructs are cDNA-based and do not comprise the natural structure of the gene, which would allow these processes to take place. In total contrast to these observations, Friedman et al. exclusively detected soluble N-terminal TBP fragments of approximately 30 kDa expressing a polyQ stretch but lacking the C-terminal domain of TBP in SCA17 mouse brains. Still, only N-terminal fragments of TBP were detected in nuclear inclusions of SCA17 mouse brains and PC12 cells (Friedman et al., 2008). This might explain the lack of evidence for N-terminal fragment counterparts in our SCA17 cells and rats, as these breakdown products may be readily recruited into inclusion bodies and therefore be unavailable to immunodetection.

We found truncated TBP not only in cells with overexpression of expanded hTBP-64Q, but also overexpressed non-expanded hTBP-38Q and for endogenous TBP, although endogenous fragments were detected at a comparably lower level due to weaker expression of the full-length protein. Hence, cleavage is not only happening in cells expressing expanded TBP, but it is apparently a product of normal TBP degradation, accumulating when overexpressed. Nevertheless, polyQ-containing truncated TBP in SCA17 brains was not only found to be more toxic than the expanded full-length form, but also more stable than non-expanded TBP fragments. Friedman et al. suggested that fragments lacking a polyQ expansion may be unstable *in vivo,* leading to their degradation without having the chance to form aggregates (Friedman et al., 2008). Although C-terminal fragments without a polyQ domain were also found *in vivo* and consequently need to be considered quite stable, a closer look needs to be taken on the aggregate formation of non-expanded TBP later, to be able to argument with the hypothesis by Friedman et al. On the other hand, even non-polyQ fragments of disease proteins have been associated with detrimental effects in studies on SCA3 and HD (Hubener et al., 2011; El-Daher et al., 2015).

Importantly, dose-dependent effects mediated by the quantity of TBP fragments needs to be considered, which may be even higher in relation to the substrate levels of the overexpressed polyQ-expanded TBP and by the overactivation of the proteases. These correlations were investigated in further experiments.

Nevertheless, studies of SCA1 and SCA2 disassociated the existent fragments from cytotoxicity in contrast to the other polyQ diseases, which must be kept in mind when transferring the toxic fragment hypothesis to SCA17. However, SCA17 might have a closer pathogenetic elation to HD and SCA3, which indicate a fragment-linked toxicity (Ng et al., 2007; Klement et al., 1998; Huynh et al., 2000; Weber et al., 2017).

5.3 Wild-type and polyQ-expanded TBP are calpain substrates *in vitro*

Calpains are calcium-dependent cysteine proteases that exert important physiological cellular functions which comprise cell signalling, cytoskeletal organization, motility, cell death including apoptosis and necrosis, synaptic plasticity, differentiation, and membrane repair (Noguchi et al., 1997; Pontremoli and Melloni, 1988; Wells et al., 2005; Glading et al., 2002; Squier et al., 1994; Yamashima, 2000; Baudry and Bi, 2013; Mingorance-Le Meur, 2009; Wang et al., 2013; Mellgren and Huang, 2007). Importantly, these proteases were partly demonstrated to cleave disease-causing proteins of polyQ diseases in a polyQ length dependent rate (Gafni and Ellerby, 2002; Hubener et al., 2013; Nixon et al., 1994; Wootz et al., 2006; Mouatt-Prigent et al., 1996; Goffredo et al., 2002; Haacke et al., 2007).

Regarding spinocerebellar ataxia type 17, TBP could not be shown to be cleaved by caspases (Wellington et al., 1998), which put TBP as a potential substrate of calpains in the focus of this study. Here, we based our investigations on the ubiquitously expressed and best characterized members of this class of proteases, CAPN1 and CAPN2, respectively. Both exogenous addition of CAPN1 and -2 and *in vitro* activation of endogenous calpains by calcium addition in our *in vitro* calpain cleavage assays (IVCCA) induced a time-dependent cleavage of both polyQ-expanded and non-expanded TBP in rat cerebellum and HEK 293T homogenates (Weber et al., 2022). Characteristically, TBP was cleaved into the same two C-terminal 28 kDa and 30 kDa large fragment species seen in the SCA17 rat model *in vivo* and in HEK cells at baseline. Therefore, it stands to reason that these baseline fragments derive from intrinsic calpain activity making

a general involvement of calpains in TBP fragmentation likely. Comparison of the detections of the core domain-binding anti-TBP 58C9 antibody and anti-TBP D5G7Y antibody, which binds around the amino acid Ala110, suggests that the cleavage sites lie within a range of a few amino acids around amino acid position 110. Alignment with results of the *in silico* cleavage site prediction using the GPS-CCD tool (Liu et al., 2011) make a cleavage in the area between amino acid at position A96 (alanine 96) and Q117 (glutamine 117) most likely for the generation of the two detected fragments (Weber et al., 2022). Interestingly, the time-dependent increase is mostly seen for a lower 28 kDa fragment, while the upper 30 kDa fragment does not react as distinct or almost vanishes over time of incubation. This could be explained by subsequent cleavage of the bigger fragment into smaller breakdown products such as the 28 kDa fragment and then further rendering it unavailable for detection. Studies of human HD brain suggested that bigger, caspase-mediated fragments of polyQ-expanded huntingtin are likewise further processed by calpains into smaller fragments, which are then able to transfer into the nucleus due to their short length (Gafni and Ellerby, 2002; Kim et al., 2001).

Interestingly, the TBP cleavage patterns by CAPN1 and CAPN2 were comparable (Weber et al., 2022). For SCA3, comparable results were found as calpain-1 and -2 were shown to cleave at similar sites of ataxin-3 (Weber et al., 2017). Those results lead to the assumption that these two isoforms may have resembling cleavage sites. In some functional systems, CAPN1 and CAPN2 were found to have opposing effects, e.g., in synaptic plasticity, learning and memory, and neurodegeneration, although they do not differ a lot in their substrates (Baudry and Bi, 2016).

As the degradation pattern was resembling for exogenous calpain addition and calcium addition, it is likely that alterations in calcium levels, as they were detected in early disease stages of other polyQ diseases and may be transferable to SCA17 pathogenesis, mostly lead to calpain-mediated proteolysis of TBP (Haacke et al., 2007; Gafni et al., 2004; Wellington et al., 2002; Kurbatskaya et al., 2016; Weber et al., 2016; Lin et al., 2000; Vig et al., 2000).

In vitro cleavage of TBP by recombinant calpains could be prevented by preincubation with CI-III, which inhibits both CAPN1 and CAPN2, and proved the specificity of the calpain-mediated TBP fragmentation (Weber et al., 2022). Furthermore, pharmacological treatment with calpain inhibitor offers a therapeutical approach to prevent TBP cleavage. In contrast to caspase inhibition, various approaches of calpain inhibition had ameliorating effects on proteolysis, aggregation, viability, and, in animal models, behavioural phenotypes in studies on SCA3 and HD (Gafni et al., 2004; Koch et al., 2011; Clemens et al., 2015; Wright and Vissel, 2016).

5.4 Endogenous calpains cleave wild-type and polyQ-expanded TBP *in cellulo*

To confirm if calpains cleave TBP in a vital cellular context, endogenous calpains were activated in HEK 293T and PC12 cells by addition of ionomycin and calcium. Ionomycin is a calcium-ionophore which allows calcium ions to pass the cellular membrane. This is facilitated by the ionophore's binding of the ion and its diffusing through the cell membrane, releasing calcium again on the intracellular side. The calcium increase is followed by activation of various calcium-dependent cellular systems including calpains. Time-dependent calpain activation was confirmed by the western blot-based detection of an increased cleavage of calpain substrate spectrin, the lowering of the endogenous calpain inhibitor CAST, and the autoproteolysis of CAPN1. Densitometric and statistical analysis confirmed a significantly elevated fragmentation for myc-hTBP-38Q- and -64Q-transfected HEK 293T cells after 1.5 h of ionomycin treatment (Weber et al., 2022). It is conceivable that the ionomycin treatment-associated TBP fragmentation could be due to another calcium-dependent cellular system. However, as the pattern of TBP cleavage perfectly resembles those induced after exogenous calpain addition, and the pre- and coincubation with CI-III readily prevented the formation of these fragments, the calpain-dependency of the observed TBP fragmentation could be validated. Application of ionomycin to activate calpain-dependent cleavage was so far done for cell-based cleavage of ataxin-3 as the disease-protein of SCA3 (Hubener et al., 2013; Weber et al., 2017), but also for MS

(Shields et al., 1999), PD and ALS (Vosler et al., 2008), and AD (Mahaman et al., 2019), all of which were shown to be associated with increased calpain activity.

As calpains are calcium-dependent proteases, it is not remarkable that endogenous calpains can be induced to cleave TBP by an intracellular increase of calcium. With 5 mM extracellular calcium concentration, it would exceed the required intracellular calcium concentrations needed for activation of CAPN1 (3-50 µM) and CAPN2 (0.4-0.8 mM) by far, while it is not known, to which levels levels ionomycin actually raises the intracellular calcium. However, the calpain activation pattern, represented by CAPN autoproteolysis, spectrin cleavage, CAST levels, and TBP cleavage pattern, resemble those seen in our baseline detections, indicating a representative calpain activation *in cellulo*.

It is worth mentioning that the CI-III treatments of TBP-overexpressing cells in these experiments led to an overcompensation of TBP fragmentation, undercutting the baseline calpain-mediated cleavage levels by a third. Taken together, these results, together with the *in vitro* data, corroborate TBP as a substrate of calpains. Moreover, calpain inhibition with CI-III appears promising in effectively lowering calpain activity and calpain-specific TBP fragmentation. Nevertheless, the known cross selectivity for CI-III for cathepsin has to be kept in mind, which could lead to confounded interpretations (Ennes-Vidal et al., 2017). Interestingly, there have been promising *in vitro* approaches to increase the selectivity of CI-III, which should be attempted in future investigations (Kim et al., 2011).

5.5 Fragmentation of TBP is associated with overactivation of calpains in SCA17 models in the presence of expanded TBP

Degenerative disorders which exhibit a raised calpain activity level comprise neurological and non-neurological diseases. These are AD (Nixon et al., 1994), ALS (Wootz et al., 2006), PD (Mouatt-Prigent et al., 1996), HD (Gafni and Ellerby, 2002; Goffredo et al., 2002), SCA3 (Haacke et al., 2007; Hubener et al., 2013), MS (Shields et al., 1999), and brain ischemia (Bartus et al., 1994), but also

muscular dystrophy, cataract, or cardiomyopathy (Ono and Sorimachi, 2012). This study showed that TBP fragment generation is a process happening *in vivo* at baseline, in a most likely calpain-dependent manner. As stated in 5.2, the occurrence of fragments is also found in wild-type rat brains. They may be disregarded for their toxic effects because of the missing properties of an expanded polyQ domain. An overactivation of the proteases in SCA17 models might result in a further increased fragment generation. It was therefore examined if there are alterations in basal calpain activity in association with expression of polyQ-expanded TBP.

PC12 cells expressing mTBP-13Q and -105Q as a neuronal-like cell model, as well as SCA17 rat cerebellum, were investigated regarding the calpain activity by assessing cleavage of the calpain substrate spectrin, levels of the endogenous inhibitor CAST, and calpain-1 proteolysis. Immunodetection of calpain-1 proteolysis was not quantified, as the bands of full-length and cleaved calpain overlap. Expression of polyQ-expanded mTBP-105Q in PC12 cells and the presence of TBP-64Q transgene in rat cerebellum were associated with a 50% increased calpain activation based on spectrin cleavage and CAST in comparison to their non-polyQ-expanded TBP expressing controls (Weber et al., 2022). Consistent with these results, rat cortex and striatum, which do not express expanded TBP, did not show differences in calpain activity between wild-type and SCA17 animals (Weber et al., 2022). This calpain overactivation in SCA17 rat cerebellum goes along with a 20% increase of TBP fragment levels when normalized to the full-length protein (Weber et al., 2022).

Consequently, it can be stated that there is polyQ-associated calpain overactivation in SCA17 cell lines and rats which is accompanied by an elevated calpain-mediated fragmentation of TBP (Weber et al., 2022). There is convincing evidence, that calcium disbalance early in disease progression is involved in polyQ-pathogenesis by induction of early calpain-mediated cleavage in affected neurons. In this study, investigations of one SCA17 cell line and 9-10 months old hTBP64Q rats represent rather the end-stage of the disease. Thus, assessment of calpain overactivation in brain samples of the same or another animal model at different ages could give a wider picture of this condition.

In SCA17 mouse brains, Chang et al. found downregulation of calbindin, a calcium-binding protein, and of the IP_3 receptor, an intracellular Ca^{2+} channel located in the smooth endoplasmic reticulum that is involved in neuronal signalling Chang et al. (2011). For HD, approximately twofold increased calcium levels were found in pyramidal neurons (Hodgson et al., 1999) and many of the altered expression levels comprise components involved in calcium signalling pathways, such as decreased IP_3 and ryanodine receptors, calcium channels, calcium binding proteins, and calmodulin (Luthi-Carter et al., 2000). Accordingly, early downregulation of calbindin and parvalbumin was found in SCA1 (Vig et al., 1996). Further mutual transcriptional changes in HD, DRPLA, SCA7, and SBMA include neuronal signal transduction such as NMDA receptors, signal proteins, e.g., protein kinase C, or neuropeptides such as enkephalin (Luthi-Carter et al., 2002). Gafni et al. considered the polyQ-expanded huntingtin itself to sensitize NMDA receptors and IP_3 receptors, that way facilitating the glutamate-dependent calcium influx into the cell and the calcium efflux out of the endoplasmic reticulum (Gafni et al., 2004). In AD, calpain-mediated cleavage of the NMDA receptor, induced by altered calcium homeostasis, is thought to contribute to excitotoxicity (Kurbatskaya et al., 2016). Furthermore, mitochondrial defects have been identified in HD, SCA1, and SCA3, phenotypically presenting as metabolic disbalance e.g., weight loss and altered metabolite concentrations (Cui et al., 2006; Weber et al., 2014; Clemens et al., 2015). Mitochondria maintain intracellular calcium levels or, if they cannot, induce cell death. These findings stress the involvement of polyQ-mediated calcium dysregulation and excitotoxicity in impaired neurons, that may result in overactivation of calcium-dependent proteases.

Furthermore, calpain activity is suggested an early event in pathogenesis of polyQ diseases. The conclusions of this study are drawn based on the investigations of one SCA17 cell line and 9-10 months old hTBP64Q rats with the latter representing rather the end-stage of the disease. Thus, assessment of calpain overactivation in brain samples of the same or another animal model at different ages as well as the investigation of human material could give a wider picture of this condition.

5.6 Calpastatin overexpression and inhibitor treatment effectively prevent calpain-mediated TBP cleavage

Calpastatin (CAST) is the highly specific, endogenous inhibitor of calpains (Maki et al., 1987). A surplus of CAST by overexpression in a physiologically overactivated calpain system, as observed in our SCA17 models, should therefore decrease calpain activity and thereby also polyQ-expanded TBP fragmentation.

For overexpression of hCAST, HEK 293T cells were cotransfected with myc-hTBP-38Q or -64Q and hCAST or a respective mock vector for 48 h. CAST overexpression could effectively, but not significantly, most likely due to low sample amount, lower calpain overactivation based on quantification of spectrin and TBP cleavage.

As a pharmacologic approach is more transferable to *in vivo* models and, eventually, to patients than an overexpression of CAST, experiments were performed using calpain inhibitor III (CI-III). Inhibitor administration to PC12 cells expressing mTBP-13Q or -105Q showed, analogously to the effects of CAST overexpression in HEK 293T cells, a lowering of calpain-mediated spectrin and TBP cleavage for treatment times of 24 h and 48 h (Weber et al., 2022). These time points were selected to test CI-III's long-term efficiency of preventing time-dependent basal cleavage and should resemble the effects of CAST overexpression. CI-III treatment showed a strongly significant reduction of TBP cleavage, with mTBP-105Q reaching around 50% lowering of fragment levels which was slightly more effective than for mTBP-13Q (Weber et al., 2022). After 48 h of treatment, fragment levels remained low in mTBP-105Q-expressing cells, whereas in mTBP-13Q-expressing cells fragments slightly increased for uncertain reasons. This observation might indicate a stronger efficacy of CI-III in cells, which exhibit a basal calpain overactivation as shown previously, which might be related to a higher mTBP-105Q cleavage. However, further experiments

must be performed to confirm this assertion. Additionally, the variance of these results is high and requires a greater sample number and perhaps a longer time range of inhibition to corroborate the apparent tendency of effect exponentiation.

Taken together, these results demonstrate both calpastatin overexpression and pharmacological calpain inhibition as comparable in their effects on downregulation of calpain activity, TBP cleavage prevention, and full-length TBP level restauration (Weber et al., 2022).

CAST overexpression showed resembling results for diseases known to be linked to calpain overactivation. The promising results comprise findings in SCA3 models, where CAST overexpression lead to reduction of inclusion formation containing the disease-protein and amelioration of neurodegeneration, whereas CAST knockout mice showed deteriorated phenotypical appearance, neurodegeneration, and increased aggregate formation of ataxin-3 (Simoes et al., 2012; Hubener et al., 2013). Accordingly, overexpression of CAST ameliorated axonal loss, delayed disease onset, and improved survival in a mouse model of ALS (Rao et al., 2016) and decreased truncation of the disease-protein and synaptic components in PD, while reduction of CAST levels resulted in enhanced aggregate formation (Diepenbroek et al., 2014). Likewise, reduced aggregate levels of mutant htt and alleviated phenotypical appearance followed CAST overexpression in HD (Weber et al., 2019).

Calpastatin overexpression might provide an appropriate experimental approach to investigate long term effects of calpain inhibition on our SCA17 rat model, as it can be genetically applied as a transgene by crossbreeding with a CAST-overexpressing line or on a selected time-point using a viral administration as shown previously for SCA3 mouse models (Simoes et al., 2012). Hence, ongoing attempts are made to make the CAST protein itself – due to its specificity - available for cellular import when applied externally (Donkor, 2015).

However, pharmacological treatment is better applicable as a potential therapeutic strategy compared to genetic approaches. Various pharmacological inhibitors using compounds that specifically target these proteases were already shown to reach beneficial effects in animal models: For SCA3, administration of

calpain inhibitors could reduce fragment formation, aggregation, and neurodegeneration, resulting in improved motor functions in SCA3 mice and zebrafish (Simões et al., 2014; Watchon et al., 2017). Calpain inhibitors restored hippocampal function and memory in an AD mouse model (Trinchese et al., 2008). Two different calpain inhibitors were able to lower synuclein deposition in PD mouse brains associated with reduced calpain activity (Hassen et al., 2018). Importantly, pharmacological calpain inhibition has even reached phase I trials in Alzheimer's disease (Wright and Vissel, 2016). Although over 52 calpain inhibitors have been developed in the last 5 years, the problem of specificity, particularly for the calpain isoforms, is still an obstacle for more phase I trials of calpain inhibitors for these diseases (Ennes-Vidal et al., 2017). An alternative, indirect approach of calpain inhibition was demonstrated by Clemens et al., who investigated the effect of olesoxime, a cholesterol derivate, which accumulates at the mitochondrial membrane. It resulted in mitochondrial stabilization, leading to restoration of proteins involved in calcium homeostasis, and thereby to a reduced calpain activation, which consequently ameliorated htt cleavage and aggregation as well as cognitive and psychiatric phenotypes in an HD rat model (Clemens et al., 2015). This strategy hints to a broad range of positive effects when influencing calpain activity by interrupting the vicious circle of calcium disbalance and mitochondrial dysfunction.

So far, only CAPN1, -2, -8, -9 are known to be inhibited by calpastatin. Regarding, that the isoforms CAPN8 and CAPN9 are expressed in the gastrointestinal tract and that also CI-III mainly inhibits CAPN1 and CAPN2, it is likely that those two forms are mostly responsible for our observed results (Ono and Sorimachi, 2012). Still, other calpain species must be considered to interact with TBP that might be not targeted by this calpain inhibition strategy. Furthermore, the involvement of CAPN1 and CAPN2 leave us humble towards potential effects of intervening in complex, ubiquitously involved systems such as the calpain system. While some studies show related substrate specificity for those two isoforms, regarding neurodegeneration, their role in individual systems is still unclear (Weber et al., 2017). It is even assumed, that CAPN1 inherits neuroprotective, CAPN2 in contrast, neurodegenerative functions. It was, for example, shown in

neurodegenerative conditions that activation of NMDA receptors by CAPN1 cleavage could have a neuroprotective effect, while CAPN2 cleavage of NMDAR resulted in additional neurotoxicity. Interestingly, a knockout model of CAPN1 resulted in cerebellar ataxia in human and mice. This would suggest that CAPN1 rather protects from cerebellar degeneration resulting in ataxia (Baudry and Bi, 2016; Wang et al., 2013; Wang et al., 2016). However, these investigations were obtained for an intact cellular system contrarily to the cellular and supracellular dyshomeostasis in polyQ disorders.

Assuming that calpains are mainly responsible for TBP fragmentation the proteolytic systems of the cells continue to be under constant interaction with each other. Inhibition of calpains might therefore induce compensation by another proteolytic system and thereby trigger a detrimental pathway. Furthermore, calpain inhibitor application is not yet highly selective and might inhibit other essential proteases (Pike et al., 1998; Chua et al., 2000; Lankiewicz et al., 2000). Therefore, additional investigations on affected pathways and the development of more specific inhibitors are crucial, and potential benefits of calpain inhibition by pharmacologic and genetic means on the SCA17 phenotype in different models must be evaluated in the future.

5.7 N-terminal TBP aggregates in SCA17 rats can be diminished by reduction of calpain activity

The occurrence of insoluble, fibrillar aggregates is a pathological hallmark that connects the polyQ diseases to other, non-polyQ, neurodegenerative diseases, such as AD, PD, or ALS. For polyQ diseases, including SCA17, insoluble inclusions consisting of the polyQ proteins of various subcellular localization could be detected in association with neurodegeneration (Weber et al., 2014; Havel et al., 2009). In many of these diseases, the truncated parts of the polyQ proteins were shown to be more prone to aggregate and rather found in these inclusions compared to the full-length protein (Davies et al., 1997; Igarashi et al., 1998; DiFiglia et al., 1997; Cemal et al., 2002). Although there is uncertainty about which aggregation species inherits the definite toxic characteristics, it is generally accepted that fragments provoke the aggregation and that insoluble

inclusion bodies both represent an aggregational process with toxic properties and a reliable marker for phenotypical appearance of the disease (Davies et al., 1997; Igarashi et al., 1998; Martindale et al., 1998; Hackam et al., 1998; Lunkes et al., 1998; Saudou et al., 1998; Klement et al., 1998; Slow et al., 2005; Hodgson et al., 1999; Arrasate and Finkbeiner, 2012; Sanchez et al., 2003; Taylor et al., 2003). Also for SCA17, N-terminal fragments of TBP were found in nuclear inclusions and in a cell model more intranuclear inclusion were formed by expression of the fragment than of the full-length mutant protein (Friedman et al., 2008). Therefore, the relevance of the aggregation species for the cytotoxicity and the development of the phenotype of SCA17 needs to be investigated further.

In this study, the occurrence of aggregates in association with expression of polyQ-expanded TBP in SCA17 rats was supported by detection of insoluble TBP in cerebellum, but not in striatum and cortex, which both did not express expanded protein. Only N-terminal, polyQ-containing epitopes of TBP could be detected in the aggregates using filter retardation assays (Weber et al., 2022). Based on the findings of western blotting, it can be hypothesized that the N-terminal counterparts of the C-terminal soluble fragments were not detectable due to a sequestration into these insoluble cellular compartments. However, neither soluble N-terminal fragments of non-polyQ-expanded TBP nor respective aggregates of the non-mutant protein could be detected. Referring to 5.2, non-polyQ-containing TBP fragments were though not to be stable enough to form aggregates due to a lacking polyQ expansion (Friedman et al., 2008). Thus, it is conceivable, that C-terminal fragments lacking the polyQ stretch are degraded further without assembly as aggregates, or that C-termini of TBP could not be detected in aggregates due to an inaccessibility of their epitopes. Nevertheless, the ascertained occurrence of TBP fragments and the detectability of aggregates with N-terminally binding antibodies in our SCA17 rats is in line with the findings by Friedman et al. for HEK cells and mouse brain (Friedman et al., 2008). However, our filter retardation assays just give an imagination of aggregation processes as they neither detect potentially existing SDS-soluble oligomers nor they give information on localisation, organisation, or size and number of

aggregates, which is why further aggregation analyses with immunofluorescence microscopy should be conducted.

As mentioned before, in previous studies, aggregate formation could be reduced by CAST overexpression and pharmacological calpain inhibition, indicating the role of calpains in aggregate formation in diseases like SCA3, HD, PD, and ALS (Diepenbroek et al., 2014; Rao et al., 2016; Hassen et al., 2018; Weber et al., 2019; Hubener et al., 2013). These approaches might be more beneficial than strategies targeting aggregates themselves as the intervention at the level of fragment formation prevents the formation of these inclusion bodies at an earlier stage, thereby avoiding the formation of potentially detrimental precursors of aggregates such as toxic fragments or oligomers.

In this study, cell-based calpain inhibition with CI-III over 48 h reduced aggregates significantly by around 30% in mTBP-105Q expressing PC12 cells (Weber et al., 2022). The parallel reduction of both TBP cleavage and aggregation suggests that the fragment species responsible for inclusion formation in the PC12 model of SCA17 derive most likely from calpain-mediated process.

Investigations of the protein clearance systems revealed that the occurrence of aggregates is not only attributed to the accumulation of the mutant fragment together with other cellular components, but also to a malfunction of two major cellular clearance mechanisms, the ubiquitin-proteasome system (UPS), and autophagy.

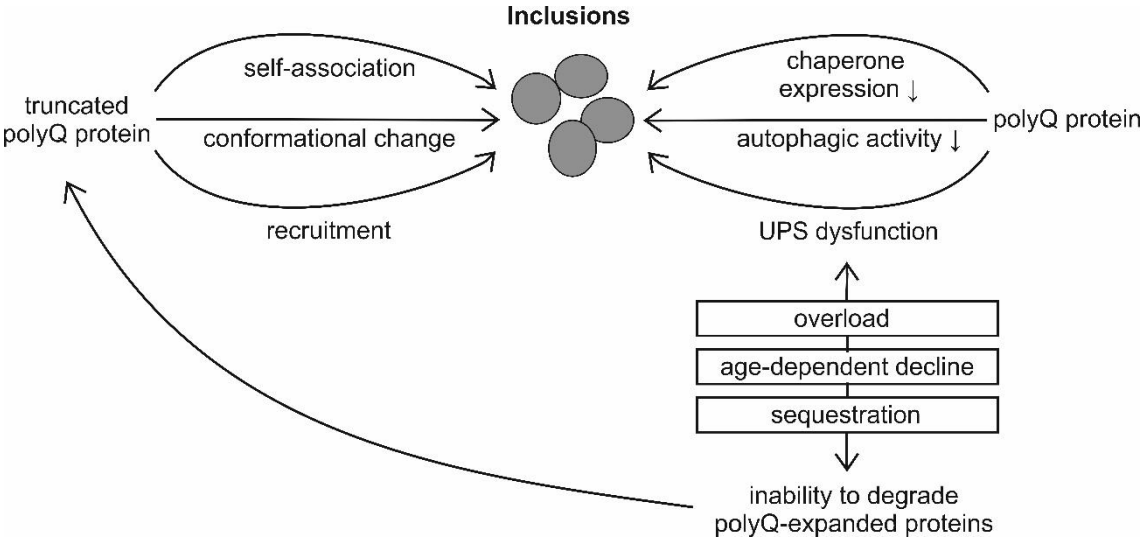

Figure 30. Contribution of protein degradation system failure and polyQ protein cleavage to inclusion body formation. PolyQ proteins do not only promote inclusion formation by being truncated by proteases, e.g., by calpains. They also interact and recruit other polyQ proteins and cellular components. Furthermore, polyQ proteins induce a dysfunction of the major protein degradation systems: chaperones, the ubiquitin-proteasome-system and autophagy.

Figure 30 shows the factors potentially contributing to inclusion body formation in polyQ diseases schematically. Reduction of autophagic activity, chaperone expression, and dysfunction of the ubiquitin proteasome system are thought to be associated with transcriptional disruption and recruitment of those components into cellular inclusions by polyQ proteins (Huang et al., 2011; Lee et al., 2014; Weber et al., 2014; Rolfs et al., 2003; Taylor et al., 2003). It is yet unclear, whether the sequestration of proteasomal components into aggregates is part of the cell's coping response because of a failing protein degradation system or if this recruitment is causative for the inactivation of these components (Taylor et al., 2003; Bence et al., 2001; Holmberg et al., 2004; Cowan et al., 2003; Breusing and Grune, 2008; Park et al., 2005). Interestingly, a connection between impaired autophagy and calpain activity was found, as calpains cleave components of the autophagic system (Cheng et al., 2018; Russo et al., 2011). Also, lysosomal permeability is modulated by calpains (Geronimo-Olvera et al., 2017). Therefore, it is conceivable that the beneficial effects of calpain inhibition on TBP aggregates in our SCA17 cell models do not exclusively relate to the reduction of TBP fragmentation but also to an improvement of a potentially impaired removal of aggregates. On that score, additional analysis in SCA17 is

necessary to understand whether calpain overactivation-mediated impairments of autophagy and lysosomal activity exist.

5.8 Technical limitations

Despite offering multiple robust conclusions based on reliable experimentation, this study had to fight with several technical limitations.

Analysis of TBP fragments in this study might be incomplete as fragments were suggested to be unstable and degraded into smaller breakdown products, making them undetectable in western blot analysis. A larger selection of antibodies with further epitopes within TBP and the use of substances inhibiting the further degradation of fragments, e.g., via proteasomal or autophagic pathways, might be a solution for this issue. To assess calpain activity, only immunodetection of a single substrate, spectrin, the calpain inhibitor CAST, and calpain-1 were conducted, omitting the fact that multiple calpains might be overactivated and involved in TBP cleavage. However, this was limited by the selection of available and reliable calpain antibodies and due to the lack of knowledge regarding the interpretation of detected protein bands. Moreover, *in vitro* cleavage assays could only be repeated in a limited number as the production of used rat rCAPN2 (208718) was terminated and the alternative human recombinant CAPNs of other vendors did not show proteolytic activity. Furthermore, analysis of calpain activation may also be compromised by the quality of the samples as these enzymes are involved in apoptosis and necrosis and may be induced by non-optimal sample handling, e.g., during cell treatment or animal dissection. Depending on the specific set-up, filter retardation experiments in general are rather able to detect bigger, SDS-insoluble aggregates, while this analysis gives no information about the proportion of misfolded monomers, oligomers, and fibrils. Moreover, the size and distribution of aggregates cannot be assessed with this methodology. To specify the number, size, and appearance as well as the cellular localization of aggregates that may come along with specific interferences and interactions, immunofluorescence microscopy would provide an appropriate tool for achieving this readout. Regarding quantitative investigation, only a low samples size was used which restricted the statistical validity of the analysis of

calpain overactivation as well as TBP expression and fragmentation levels in rat brain tissue. Likewise, filter retardation assays of PC12 cells were performed with a low sample number and both western blot analysis and filter trap assays alone might be insufficient as both represent semi-quantitative methods.

5.9 Conclusion

This study reveals wild-type and polyQ-expanded TBP as a substrate of calpains *in vitro* and *in vivo* and calpain overactivation as a hallmark in cell and animal models of SCA17. Thereby, it extends the involvement of these proteases and their associated pathogenetic principles of enhanced proteolytic disease protein fragmentation as a driver of aggregation to spinocerebellar ataxia type 17. The promising approach of calpain inhibition in diseases characterized by calpain overactivation was successfully transferred to our SCA17 cell models. Here, inhibition of calpains reduced both TBP fragmentation and aggregation *in vitro*, which thereby constitutes an important therapeutic candidate approach for treating SCA17.

Although targeting calpains alone does not fully compensate for the effects of the mutant polyQ domain in TBP, it might be beneficial in restoring multiple neuronal impairments which are connected to calpain overactivation by reducing the cytotoxicity caused by the TBP fragments and aggregates. These findings can provide another puzzle piece for deciphering pathomechanisms underlying SCA17 and related neurodegenerative diseases.

5.10 Outlook

The coherences found in this study provide the important and unique evidence that calpains are involved in the pathogenetic cleavage and subsequent aggregation of the SCA17 disease protein TBP *in vitro* and *in vivo* and may represent a potential therapeutic target in treating this disease. Yet, the relevance of the effects of calpain inhibition for cytotoxicity must be investigated in the future, considering the divergent impact of proteolytic cleavage in different SCAs. Calpains are enzymes with a broad range of functions, substrates, and

interactions, which is why calpain inhibition might produce unpredictable adverse side effects. Thus, one of the next steps would be testing different ways of calpain inhibition, e.g., by other calpain inhibitors or compounds such as olesoxime, and assess their effects on cell viability and the (molecular) phenotype *in vitro* and *in vivo.* Further projects could also address the identification of the precise calpain cleavage sites as a target for mutagenesis as a directed genetic approach of proteolysis inhibition instead of a rather undirected pharmacological treatment. Moreover, the effect of the polyQ expansion itself on TBP's cleavage propensity could be analysed to address a potential polyQ length-dependent susceptibility towards calpain cleavage. This study focussed mainly on the two best-characterized calpain isoforms, CAPN1 and CAPN2, indicating a resembling substrate specificity in TBP cleavage, whereas in other context, they may inherit opposite effects. This emphasizes, how little is known about the role and the regulation of calpains. Additionally, the cleavage propensity of TBP towards other calpain isoforms, with a focus on which isoforms cleaves TBP the best, could be addressed in follow-up studies opening the possibility of an isoform-targeted inhibitory approach. As the activation pathway of calpains is not known for SCA17 but only assumed to be caused by calcium disbalance, the influence of the polyQ-expanded TBP on calcium homeostasis should be further investigated. In respect of the underlying pathogenetic principles, targeted studies should be conducted on transcriptional disruption, autophagy, UPS, calcium homeostasis, glutamate transmission, and mitochondrial function in the context of calpain inhibition.

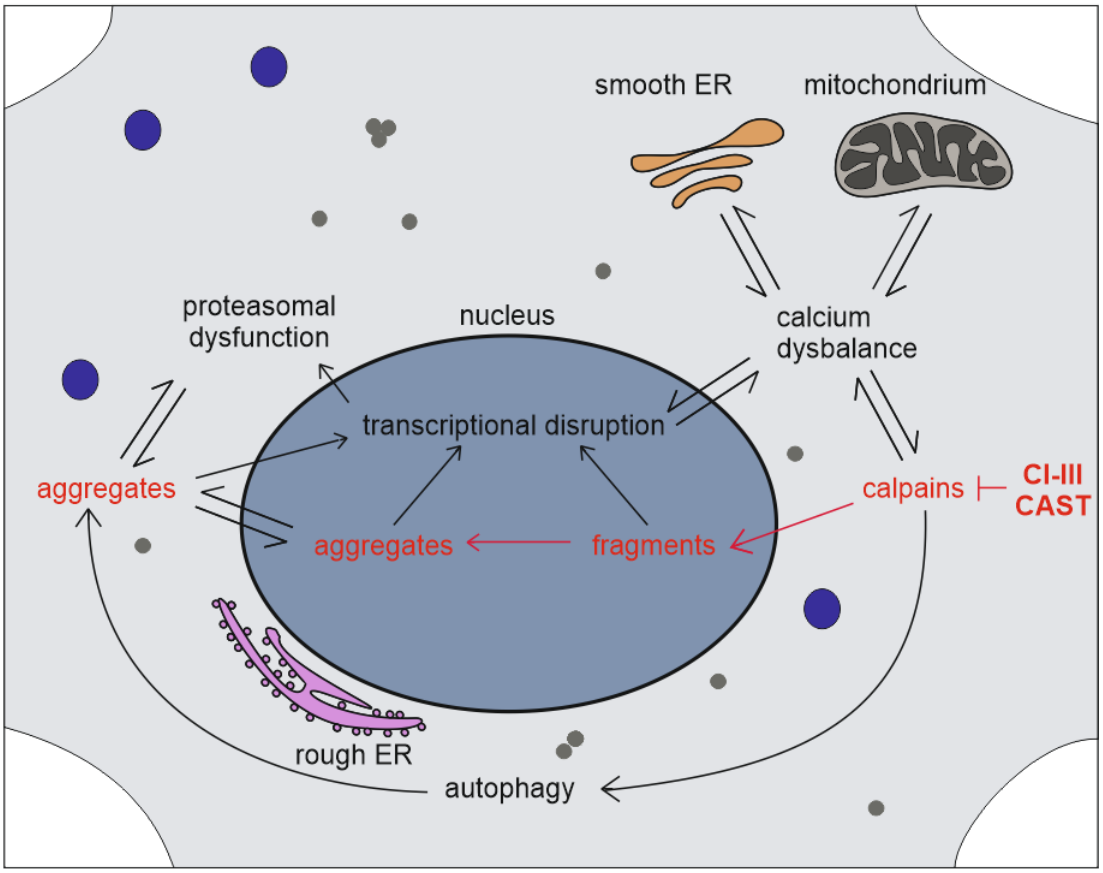

Figure 31. Potential model of pathogenetic findings and interactions in SCA17. The summary of the mechanisms found in SCA17 neuronal cells and cell models in this study (highlighted in red) is illustrated together with potential cellular relations as a putative pathogenetic model. It is characterized as a vicious circle with mutual interferences. The results of this study speak for calpain activity being a central mechanism. Disruption of the subsequent mechanisms of fragmentation and aggregation of TBP (red arrows) could be reached by CI-III or CAST dependent calpain inhibition *in vitro*. Still, the influence of calpain inhibition or the importance of other pathological components need to be clarified in the future. ER: endoplasmic reticulum.

With respect to the important findings of this study and the suggested further investigations, the research on the interaction of TBP with calpains in the molecular pathogenesis of SCA17 is still in its early stages (as summarized in Figure 31). Further studies are needed to approach the complexity of the linked neurodegenerative mechanisms and thereby develop a potential therapeutic strategy for SCA17.

6 Summary

Spinocerebellar ataxia type 17 (SCA17) is an autosomal-dominantly inherited neurodegenerative disease predominantly characterized with ataxia, dysarthria, chorea, dystonia, pyramidal disorders, dementia, psychiatric disorders, and seizures. These symptoms are consequence of neuronal failure and death that appears most prominently in the cerebellum, but also in many other parts of the central nervous system. So far, no causal treatment for this disease is available. The underlying genetic cause is a trinucleotide repeat expansion of the base triplets CAG and CAA in the gene of TATA box-binding protein (TBP), which is translated into an expanded polyglutamine (polyQ) stretch. This characteristic allocates it to the group of polyQ disorders, together with SCA3 and Huntington disease. Cellular effects of the polyQ expansion in TBP that are suspected to drive the molecular pathology comprise the occurrence of dysfunctional fragments of the mutant protein, the formation of TBP-positive neuronal aggregates containing protein fragments, and functional depletion of TBP in the affected neurons. So far, proteases that are responsible for the generation of TBP fragments inheriting cytotoxic properties were not yet identified.

In this dissertation, the role of calcium-dependent calpains in the cleavage of TBP and the related aggregation were investigated focusing on the ubiquitously expressed isoforms calpain-1 and calpain-2. Moreover, it was tested whether a targeted inhibition of these proteases may lead to a reduction of the pathological hallmarks. Cleavage assays were conducted *in vitro* upon addition of exogenous calpain-1 and calpain-2 to protein extracts derived from cerebellum tissue of a SCA17 rat model and from respective cell models, as well as cell-based by activation of endogenous calpains by cellular calcium increase. The evoked TBP fragmentation pattern corresponded to breakdown products found at physiological *in vivo* conditions in SCA17 rat cerebellum. The comparison of the immunodetection with different TBP-specific antibodies, the fragment length, and *in silico* cleavage site prediction suggest amino acids at positions between alanine 96 and glutamine 117 as potential calpain cleavage sites within TBP. Western blot analysis of the baseline calpain activation revealed an enhanced

calpain activity in association with increased occurrence of TBP fragments both in cell and animal models of SCA17. Calpain inhibition via calpain inhibitor III or overexpression of the endogenous calpain inhibitor calpastatin reduced the levels of TBP fragments in cell culture experiments. Furthermore, filter trap-based analysis of SDS-insoluble TBP consisting predominantly of N-terminal TBP fragments showed diminished load of aggregates upon calpain inhibition.

Taken together, for the first time, this study identified TBP as a substrate of calpain-1 and calpain-2 and confirms calpain-mediated cleavage of TBP and calpain overactivation in cell and animal models of SCA17, which may contribute to pathogenesis. Inhibition of calpains ameliorated specific molecular disease hallmarks significantly, namely TBP fragmentation and aggregation. These results provide a starting point for further testing of pharmacological calpain-inhibiting substances *in vitro* and *in vivo*, which may represent a promising therapeutic strategy for SCA17 and the related neurodegenerative diseases.

7 Zusammenfassung

Die Spinozerebelläre Ataxie Typ 17 (SCA17) ist eine autosomal-dominant vererbte neurodegenerative Erkrankung. Sie manifestiert sich durch zerebelläre Symptome wie Ataxie und Dysarthrie, sowie extrapyramidale Symptome wie Chorea und Dystonien. Darüber hinaus können sich epileptische Krampfanfälle, sowie psychiatrische und kognitive Einschränkungen präsentieren. Neuropathologisches Korrelat dieser Symptome ist der neuronale Zelluntergang insbesondere im Zerebellum, aber auch in anderen Teilen des zentralen Nervensystems. Bis zum heutigen Zeitpunkt ist keine kausale Therapie bekannt. Durch eine ursächliche Expansion eines Wiederholungsbereichs der Basentripletts CAG und CAA im Gen des ubiquitär vorkommenden Transkriptionsfaktors TATA-box bindendes Protein (TBP), welche für die abnorme Verlängerung einer Glutaminkette im TBP kodiert, zählt die SCA17, wie auch SCA3 und Chorea Huntington, zur Gruppe der Polyglutamin-Erkrankungen. Molekularpathologisch konnten neben dem Funktionsverlust von TBP als Transkriptionsfaktor das Auftreten von dysfunktionalen Fragmenten des TBP, sowie neuronalen Einschlüsse, in denen das Protein und dessen Fragmente enthalten sind, identifiziert werden. Welche Proteasen ursächlich zur Spaltung und damit der Entstehung von Fragmenten des TBP beitragen, konnte für die SCA17 bisher nicht geklärt werden.

In dieser Dissertation wurde die Rolle der Calcium-abhängigen Calpaine, hier der ubiquitär vorkommenden Isoformen Calpain-1 und Calpain-2, bei der Spaltung von TBP und der damit einhergehenden Bildung von Aggregaten untersucht. Des Weiteren wurde getestet, ob die Inhibition der Calpainaktivität diese pathogenen Merkmale reduzieren konnte. Proteolyse-Assays wurden *in vitro* durch exogene Zugabe von Calpain-1 und Calpain-2 zu Proteinextrakten von Kleinhirngewebe eines SCA17-Rattenmodells und repräsentativen Zellmodellen, sowie durch Aktivierung endogener Calpaine in zellkulturbasierten Ansätzen durchgeführt. Nach Calpainaktivierung zeigten sich Fragmente, die auch unter physiologischen *in vivo* Bedingungen im Zerebellum der SCA17 Ratten durch Western Blot Analysen detektiert werden konnten. Der Vergleich der Immundetektion mit

verschiedenen TBP-spezifischen Antikörpern, der Fragmentlänge und der *In-silico*-Spaltstellenprädiktion ergab einen Bereich innerhalb TBP zwischen den Aminosäuren Alanin 96 und Glutamin 117 als potenzielle Spaltstelle von Calpainen. Western Blot Analysen präsentierten eine mit dem Auftreten von TBP-Fragmenten assoziierte Grundaktivität von Calpainen sowohl in den Zellmodellen als auch in dem verwendeten Rattenmodell. Die Hemmung der Calpainaktivität durch den spezifischen Calpain-Inhibitor III oder durch die Überexpression des endogenen Calpain-Inhibitors Calpastatin reduzierte im Zellmodell das Auftreten von TBP Fragmenten. Darüber hinaus konnte mittels Filter-Trap-Experimenten gezeigt werden, dass durch diese Inhibition auch die Aggregation von TBP, insbesondere der N-terminalen Fragmente, vermindert werden konnte.

Zum ersten Mal wurde TBP somit als Substrat von Calpain-1 und Calpain-2 identifiziert. Die Calpain-vermittelte Spaltung von TBP und eine Überaktivierung der Calpaine konnten in Zell- und Tiermodellen der SCA17 nachgewiesen werden. Zudem führte die Inhibierung der Calpainaktivität zur signifikanten Reduktion sowohl der Fragmentierung als auch der Aggregation von TBP. Diese Ergebnisse unterstreichen die Relevanz der Calpain-vermittelten Spaltung von TBP für die Pathogenese der Spinozerebellären Ataxie Typ 17. Sie liefern einen Ansatz zur weiteren Testung pharmakologischer, Calpain-hemmender Substanzen *in vitro* und *in vivo*, welcher eine therapeutische Strategie für die SCA17 und verwandte neurodegenerative Erkrankungen darstellen könnte.

8 References

Alibardi, A., Squitieri, F., Fattapposta, F., Missori, P., Pierelli, F., Trompetto, C. & Curra, A. 2014. Psychiatric onset and late chorea in a patient with 41 CAG repeats in the TATA-binding protein gene. *Parkinsonism Relat Disord,* 20**,** 678-9.

Arrasate, M. & Finkbeiner, S. 2012. Protein aggregates in Huntington's disease. *Exp Neurol,* 238**,** 1-11.

Baig, S. S., Strong, M. & Quarrell, O. W. 2016. The global prevalence of Huntington's disease: a systematic review and discussion. *Neurodegener Dis Manag,* 6**,** 331-43.

Bañez-Coronel, M., Ayhan, F., Tarabochia, A. D., Zu, T., Perez, B. A., Tusi, S. K., Pletnikova, O., Borchelt, D. R., Ross, C. A., Margolis, R. L., Yachnis, A. T., Troncoso, J. C. & Ranum, L. P. 2015. RAN Translation in Huntington Disease. *Neuron,* 88**,** 667-77.

Bartus, R. T., Baker, K. L., Heiser, A. D., Sawyer, S. D., Dean, R. L., Elliott, P. J. & Straub, J. A. 1994. Postischemic administration of AK275, a calpain inhibitor, provides substantial protection against focal ischemic brain damage. *J Cereb Blood Flow Metab,* 14**,** 537-44.

Baudry, M. & Bi, X. 2013. Learning and memory: an emergent property of cell motility. *Neurobiol Learn Mem,* 104**,** 64-72.

Baudry, M. & Bi, X. 2016. Calpain-1 and Calpain-2: The Yin and Yang of Synaptic Plasticity and Neurodegeneration. *Trends Neurosci,* 39**,** 235-245.

Bauer, P., Laccone, F., Rolfs, A., Wullner, U., Bosch, S., Peters, H., Liebscher, S., Scheible, M., Epplen, J. T., Weber, B. H., Holinski-Feder, E., Weirich-Schwaiger, H., Morris-Rosendahl, D. J., Andrich, J. & Riess, O. 2004. Trinucleotide repeat expansion in SCA17/TBP in white patients with Huntington's disease-like phenotype. *J Med Genet,* 41**,** 230-2.

Bence, N. F., Sampat, R. M. & Kopito, R. R. 2001. Impairment of the ubiquitin-proteasome system by protein aggregation. *Science,* 292**,** 1552-5.

Bogomazova, A. N., Eremeev, A. V., Pozmogova, G. E. & Lagarkova, M. A. 2019. [The Role of Mutant RNA in the Pathogenesis of Huntington's Disease and Other Polyglutamine Diseases]. *Mol Biol (Mosk),* 53**,** 954-967.

Boonkongchuen, P., Pongpakdee, S., Jindahra, P., Papsing, C., Peerapatmongkol, P., Wetchaphanphesat, S., Paiboonpol, S., Dejthevaporn, C., Tanprawate, S., Nudsasarn, A., Jariengprasert, C., Muntham, D., Ingsathit, A. & Pulkes, T. 2014. Clinical analysis of adult-onset spinocerebellar ataxias in Thailand. *BMC Neurol,* 14**,** 75.

Boutell, J. M., Thomas, P., Neal, J. W., Weston, V. J., Duce, J., Harper, P. S. & Jones, A. L. 1999. Aberrant interactions of transcriptional repressor proteins with the Huntington's disease gene product, huntingtin. *Hum Mol Genet,* 8**,** 1647-55.

Breusing, N. & Grune, T. 2008. Regulation of proteasome-mediated protein degradation during oxidative stress and aging. *Biol Chem,* 389**,** 203-9.

Briz, V. & Baudry, M. 2017. Calpains: Master Regulators of Synaptic Plasticity. *Neuroscientist,* 23**,** 221-231.

Briz, V., Hsu, Y. T., Li, Y., Lee, E., Bi, X. & Baudry, M. 2013. Calpain-2-mediated PTEN degradation contributes to BDNF-induced stimulation of dendritic protein synthesis. *J Neurosci,* 33**,** 4317-28.

Bruni, A. C., Takahashi-Fujigasaki, J., Maltecca, F., Foncin, J. F., Servadio, A., Casari, G., D'adamo, P., Maletta, R., Curcio, S. A., De Michele, G., Filla, A., El Hachimi, K. H. & Duyckaerts, C. 2004. Behavioral disorder, dementia, ataxia, and rigidity in a large family with TATA box-binding protein mutation. *Arch Neurol,* 61**,** 1314-20.

Brusco, A., Gellera, C., Cagnoli, C., Saluto, A., Castucci, A., Michielotto, C., Fetoni, V., Mariotti, C., Migone, N., Di Donato, S. & Taroni, F. 2004. Molecular genetics of hereditary spinocerebellar ataxia: mutation analysis of spinocerebellar ataxia genes and CAG/CTG repeat expansion detection in 225 Italian families. *Arch Neurol,* 61**,** 727-33.

Camins, A., Verdaguer, E., Folch, J. & Pallas, M. 2006. Involvement of calpain activation in neurodegenerative processes. *CNS Drug Rev,* 12**,** 135-48.

Carafoli, E. & Molinari, M. 1998. Calpain: a protease in search of a function? *Biochem Biophys Res Commun,* 247**,** 193-203.

Carragher, N. O. 2006. Calpain inhibition: a therapeutic strategy targeting multiple disease states. *Curr Pharm Des,* 12**,** 615-38.

Cemal, C. K., Carroll, C. J., Lawrence, L., Lowrie, M. B., Ruddle, P., Al-Mahdawi, S., King, R. H., Pook, M. A., Huxley, C. & Chamberlain, S. 2002. YAC transgenic mice carrying pathological alleles of the MJD1 locus exhibit a mild and slowly progressive cerebellar deficit. *Hum Mol Genet,* 11**,** 1075-94.

Chang, Y. C., Lin, C. Y., Hsu, C. M., Lin, H. C., Chen, Y. H., Lee-Chen, G. J., Su, M. T., Ro, L. S., Chen, C. M. & Hsieh-Li, H. M. 2011. Neuroprotective effects of granulocyte-colony stimulating factor in a novel transgenic mouse model of SCA17. *J Neurochem,* 118**,** 288-303.

Cheng, S. Y., Wang, S. C., Lei, M., Wang, Z. & Xiong, K. 2018. Regulatory role of calpain in neuronal death. *Neural Regen Res,* 13**,** 556-562.

Choubtum, L., Witoonpanich, P., Hanchaiphiboolkul, S., Bhidayasiri, R., Jitkritsadakul, O., Pongpakdee, S., Wetchaphanphesat, S., Boonkongchuen, P. & Pulkes, T. 2015. Analysis of SCA8, SCA10, SCA12, SCA17 and SCA19 in patients with unknown spinocerebellar ataxia: a Thai multicentre study. *BMC Neurol,* 15**,** 166.

Chua, B. T., Guo, K. & Li, P. 2000. Direct cleavage by the calcium-activated protease calpain can lead to inactivation of caspases. *J Biol Chem,* 275**,** 5131-5.

Cleary, J. D. & Ranum, L. P. 2013. Repeat-associated non-ATG (RAN) translation in neurological disease. *Hum Mol Genet,* 22**,** R45-51.

Clemens, L. E., Weber, J. J., Wlodkowski, T. T., Yu-Taeger, L., Michaud, M., Calaminus, C., Eckert, S. H., Gaca, J., Weiss, A., Magg, J. C., Jansson, E. K., Eckert, G. P., Pichler, B. J., Bordet, T., Pruss, R. M., Riess, O. & Nguyen, H. P. 2015. Olesoxime suppresses calpain activation and mutant huntingtin fragmentation in the BACHD rat. *Brain,* 138**,** 3632-53.

Cowan, K. J., Diamond, M. I. & Welch, W. J. 2003. Polyglutamine protein aggregation and toxicity are linked to the cellular stress response. *Hum Mol Genet,* 12**,** 1377-91.

Craig, K., Keers, S. M., Walls, T. J., Curtis, A. & Chinnery, P. F. 2005. Minimum prevalence of spinocerebellar ataxia 17 in the north east of England. *J Neurol Sci,* 239**,** 105-9.

Cui, L., Jeong, H., Borovecki, F., Parkhurst, C. N., Tanese, N. & Krainc, D. 2006. Transcriptional repression of PGC-1alpha by mutant huntingtin leads to mitochondrial dysfunction and neurodegeneration. *Cell,* 127**,** 59-69.

Curcio, M., Salazar, I. L., Mele, M., Canzoniero, L. M. & Duarte, C. B. 2016. Calpains and neuronal damage in the ischemic brain: The swiss knife in synaptic injury. *Prog Neurobiol,* 143**,** 1-35.

Davies, S. W., Turmaine, M., Cozens, B. A., Difiglia, M., Sharp, A. H., Ross, C. A., Scherzinger, E., Wanker, E. E., Mangiarini, L. & Bates, G. P. 1997. Formation of neuronal intranuclear inclusions underlies the neurological dysfunction in mice transgenic for the HD mutation. *Cell,* 90**,** 537-48.

De Michele, G., Maltecca, F., Carella, M., Volpe, G., Orio, M., De Falco, A., Gombia, S., Servadio, A., Casari, G., Filla, A. & Bruni, A. 2003. Dementia, ataxia, extrapyramidal features, and epilepsy: phenotype spectrum in two Italian families with spinocerebellar ataxia type 17. *Neurol Sci,* 24**,** 166-7.

Diepenbroek, M., Casadei, N., Esmer, H., Saido, T. C., Takano, J., Kahle, P. J., Nixon, R. A., Rao, M. V., Melki, R., Pieri, L., Helling, S., Marcus, K., Krueger, R., Masliah, E., Riess, O. & Nuber, S. 2014. Overexpression of the calpain-specific inhibitor calpastatin reduces human alpha-Synuclein processing, aggregation and synaptic impairment in [A30P]alphaSyn transgenic mice. *Hum Mol Genet,* 23**,** 3975-89.

Difiglia, M., Sapp, E., Chase, K. O., Davies, S. W., Bates, G. P., Vonsattel, J. P. & Aronin, N. 1997. Aggregation of huntingtin in neuronal intranuclear inclusions and dystrophic neurites in brain. *Science,* 277**,** 1990-3.

Doherty, K. M., Warner, T. T. & Lees, A. J. 2014. Late onset ataxia: MSA-C or SCA 17? A gene penetrance dilemma. *Mov Disord,* 29**,** 36-8.

Donkor, I. O. 2015. An updated patent review of calpain inhibitors (2012 - 2014). *Expert Opin Ther Pat,* 25**,** 17-31.

Dunah, A. W., Jeong, H., Griffin, A., Kim, Y. M., Standaert, D. G., Hersch, S. M., Mouradian, M. M., Young, A. B., Tanese, N. & Krainc, D. 2002. Sp1 and TAFII130 transcriptional activity disrupted in early Huntington's disease. *Science,* 296**,** 2238-43.

Durr, A. 2010. Autosomal dominant cerebellar ataxias: polyglutamine expansions and beyond. *Lancet Neurol,* 9**,** 885-94.

Duyao, M. P., Auerbach, A. B., Ryan, A., Persichetti, F., Barnes, G. T., Mcneil, S. M., Ge, P., Vonsattel, J. P., Gusella, J. F., Joyner, A. L. & Et Al. 1995. Inactivation of the mouse Huntington's disease gene homolog Hdh. *Science,* 269**,** 407-10.

El-Daher, M. T., Hangen, E., Bruyère, J., Poizat, G., Al-Ramahi, I., Pardo, R., Bourg, N., Souquere, S., Mayet, C., Pierron, G., Lévêque-Fort, S., Botas, J., Humbert, S. & Saudou, F. 2015. Huntingtin proteolysis releases non-polyQ fragments that cause toxicity through dynamin 1 dysregulation. *EMBO J,* 34**,** 2255-71.

Ellerby, L. M., Hackam, A. S., Propp, S. S., Ellerby, H. M., Rabizadeh, S., Cashman, N. R., Trifiro, M. A., Pinsky, L., Wellington, C. L., Salvesen, G. S., Hayden, M. R. & Bredesen, D. E. 1999. Kennedy's disease: caspase cleavage of the androgen receptor is a crucial event in cytotoxicity. *J Neurochem,* 72**,** 185-95.

Ennes-Vidal, V., Menna-Barreto, R. F., Branquinha, M. H., Dos Santos, A. L. & D'avila-Levy, C. M. 2017. Why calpain inhibitors are interesting leading compounds to search for new therapeutic options to treat leishmaniasis? *Parasitology,* 144**,** 117-123.

Friedman, M. J., Shah, A. G., Fang, Z. H., Ward, E. G., Warren, S. T., Li, S. & Li, X. J. 2007. Polyglutamine domain modulates the TBP-TFIIB interaction: implications for its normal function and neurodegeneration. *Nat Neurosci,* 10**,** 1519-28.

Friedman, M. J., Wang, C. E., Li, X. J. & Li, S. 2008. Polyglutamine expansion reduces the association of TATA-binding protein with DNA and induces DNA binding-independent neurotoxicity. *J Biol Chem,* 283**,** 8283-90.

Fujigasaki, H., Martin, J. J., De Deyn, P. P., Camuzat, A., Deffond, D., Stevanin, G., Dermaut, B., Van Broeckhoven, C., Durr, A. & Brice, A. 2001. CAG repeat expansion in the TATA box-binding protein gene causes autosomal dominant cerebellar ataxia. *Brain,* 124**,** 1939-47.

Gafni, J. & Ellerby, L. M. 2002. Calpain activation in Huntington's disease. *J Neurosci,* 22**,** 4842-9.

Gafni, J., Hermel, E., Young, J. E., Wellington, C. L., Hayden, M. R. & Ellerby, L. M. 2004. Inhibition of calpain cleavage of huntingtin reduces toxicity: accumulation of calpain/caspase fragments in the nucleus. *J Biol Chem,* 279**,** 20211-20.

Gan-Or, Z., Bouslam, N., Birouk, N., Lissouba, A., Chambers, D. B., Vérièpe, J., Androschuk, A., Laurent, S. B., Rochefort, D., Spiegelman, D., Dionne-Laporte, A., Szuto, A., Liao, M., Figlewicz, D. A., Bouhouche, A., Benomar, A., Yahyaoui, M., Ouazzani, R., Yoon, G., Dupré, N., Suchowersky, O., Bolduc, F. V., Parker, J. A., Dion, P. A., Drapeau, P., Rouleau, G. A. & Ouled Amar Bencheikh, B. 2016. Mutations in CAPN1 Cause Autosomal-Recessive Hereditary Spastic Paraplegia. *Am J Hum Genet,* 98**,** 1038-1046.

Garden, G. A., Libby, R. T., Fu, Y. H., Kinoshita, Y., Huang, J., Possin, D. E., Smith, A. C., Martinez, R. A., Fine, G. C., Grote, S. K., Ware, C. B., Einum, D. D., Morrison, R. S., Ptacek, L. J., Sopher, B. L. & La Spada, A. R. 2002. Polyglutamine-expanded ataxin-7 promotes non-cell-autonomous purkinje cell degeneration and displays proteolytic cleavage in ataxic transgenic mice. *J Neurosci,* 22**,** 4897-905.

Gatchel, J. R. & Zoghbi, H. Y. 2005. Diseases of unstable repeat expansion: mechanisms and common principles. *Nat Rev Genet,* 6**,** 743-55.

Geronimo-Olvera, C., Montiel, T., Rincon-Heredia, R., Castro-Obregon, S. & Massieu, L. 2017. Autophagy fails to prevent glucose deprivation/glucose reintroduction-induced neuronal death due to calpain-mediated lysosomal dysfunction in cortical neurons. *Cell Death Dis,* 8**,** e2911.

Glading, A., Lauffenburger, D. A. & Wells, A. 2002. Cutting to the chase: calpain proteases in cell motility. *Trends Cell Biol,* 12**,** 46-54.

Goffredo, D., Rigamonti, D., Tartari, M., De Micheli, A., Verderio, C., Matteoli, M., Zuccato, C. & Cattaneo, E. 2002. Calcium-dependent cleavage of endogenous wild-type huntingtin in primary cortical neurons. *J Biol Chem,* 277**,** 39594-8.

Goll, D. E., Thompson, V. F., Taylor, R. G. & Zalewska, T. 1992. Is calpain activity regulated by membranes and autolysis or by calcium and calpastatin? *Bioessays,* 14**,** 549-56.

Gostout, B., Liu, Q. & Sommer, S. S. 1993. "Cryptic" repeating triplets of purines and pyrimidines (cRRY(i)) are frequent and polymorphic: analysis of coding cRRY(i) in the proopiomelanocortin (POMC) and TATA-binding protein (TBP) genes. *Am J Hum Genet,* 52**,** 1182-90.

Gunther, P., Storch, A., Schwarz, J., Sabri, O., Steinbach, P., Wagner, A. & Hesse, S. 2004. Basal ganglia involvement of a patient with SCA 17--a new form of autosomal dominant spinocerebellar ataxia. *J Neurol,* 251**,** 896-7.

Gutekunst, C. A., Li, S. H., Yi, H., Mulroy, J. S., Kuemmerle, S., Jones, R., Rye, D., Ferrante, R. J., Hersch, S. M. & Li, X. J. 1999. Nuclear and neuropil aggregates in Huntington's disease: relationship to neuropathology. *J Neurosci,* 19**,** 2522-34.

Haacke, A., Broadley, S. A., Boteva, R., Tzvetkov, N., Hartl, F. U. & Breuer, P. 2006. Proteolytic cleavage of polyglutamine-expanded ataxin-3 is critical for aggregation and sequestration of non-expanded ataxin-3. *Hum Mol Genet,* 15**,** 555-68.

Haacke, A., Hartl, F. U. & Breuer, P. 2007. Calpain inhibition is sufficient to suppress aggregation of polyglutamine-expanded ataxin-3. *J Biol Chem,* 282**,** 18851-6.

Hackam, A. S., Singaraja, R., Wellington, C. L., Metzler, M., Mccutcheon, K., Zhang, T., Kalchman, M. & Hayden, M. R. 1998. The influence of huntingtin protein size on nuclear localization and cellular toxicity. *J Cell Biol,* 141**,** 1097-105.

Hagenah, J. M., Zuhlke, C., Hellenbroich, Y., Heide, W. & Klein, C. 2004. Focal dystonia as a presenting sign of spinocerebellar ataxia 17. *Mov Disord,* 19**,** 217-20.

Hanna, R. A., Garcia-Diaz, B. E. & Davies, P. L. 2007. Calpastatin simultaneously binds four calpains with different kinetic constants. *FEBS Lett,* 581**,** 2894-8.

Hassen, G. W., Kesner, L., Stracher, A., Shulman, A., Rockenstein, E., Mante, M., Adame, A., Overk, C., Rissman, R. A. & Masliah, E. 2018. Effects of Novel Calpain Inhibitors in Transgenic Animal Model of Parkinson's disease/dementia with Lewy bodies. *Sci Rep,* 8**,** 18083.

Havel, L. S., Li, S. & Li, X. J. 2009. Nuclear accumulation of polyglutamine disease proteins and neuropathology. *Mol Brain,* 2**,** 21.

Hernandez, N. 1993. TBP, a universal eukaryotic transcription factor? *Genes Dev,* 7**,** 1291-308.

Herrema, H., Mikkelsen, T., Robin, A., Lewitt, P. & Sidiropoulos, C. 2014. SCA 17 phenotype with intermediate triplet repeat number. *J Neurol Sci,* 345**,** 269-70.

Higuchi, M., Iwata, N., Matsuba, Y., Takano, J., Suemoto, T., Maeda, J., Ji, B., Ono, M., Staufenbiel, M., Suhara, T. & Saido, T. C. 2012. Mechanistic involvement of the calpain-calpastatin system in Alzheimer neuropathology. *FASEB J,* 26**,** 1204-17.

Hodgson, J. G., Agopyan, N., Gutekunst, C. A., Leavitt, B. R., Lepiane, F., Singaraja, R., Smith, D. J., Bissada, N., Mccutcheon, K., Nasir, J., Jamot, L., Li, X. J., Stevens, M. E., Rosemond, E., Roder, J. C., Phillips, A. G., Rubin, E. M., Hersch, S. M. & Hayden, M. R. 1999. A YAC mouse model for Huntington's disease with full-length mutant huntingtin, cytoplasmic toxicity, and selective striatal neurodegeneration. *Neuron,* 23**,** 181-92.

Hoffman, A., Sinn, E., Yamamoto, T., Wang, J., Roy, A., Horikoshi, M. & Roeder, R. G. 1990. Highly conserved core domain and unique N terminus with presumptive regulatory motifs in a human TATA factor (TFIID). *Nature,* 346**,** 387-90.

Holmberg, C. I., Staniszewski, K. E., Mensah, K. N., Matouschek, A. & Morimoto, R. I. 2004. Inefficient degradation of truncated polyglutamine proteins by the proteasome. *EMBO J,* 23**,** 4307-18.

Hoshino, M., Tagawa, K., Okuda, T. & Okazawa, H. 2004. General transcriptional repression by polyglutamine disease proteins is not directly linked to the presence of inclusion bodies. *Biochem Biophys Res Commun,* 313**,** 110-6.

Hosseini, M., Najmabadi, H. & Kahrizi, K. 2018. Calpains: Diverse Functions but Enigmatic. *Arch Iran Med,* 21**,** 170-179.

Hsu, T. C., Wang, C. K., Yang, C. Y., Lee, L. C., Hsieh-Li, H. M., Ro, L. S., Chen, C. M., Lee-Chen, G. J. & Su, M. T. 2014. Deactivation of TBP contributes to SCA17 pathogenesis. *Hum Mol Genet,* 23**,** 6878-93.

Huang, S., Ling, J. J., Yang, S., Li, X. J. & Li, S. 2011. Neuronal expression of TATA box-binding protein containing expanded polyglutamine in knock-in mice reduces chaperone protein response by impairing the function of nuclear factor-Y transcription factor. *Brain,* 134**,** 1943-58.

Huang, S., Yang, S., Guo, J., Yan, S., Gaertig, M. A., Li, S. & Li, X. J. 2015. Large Polyglutamine Repeats Cause Muscle Degeneration in SCA17 Mice. *Cell Rep,* 13**,** 196-208.

Hubener, J., Vauti, F., Funke, C., Wolburg, H., Ye, Y., Schmidt, T., Wolburg-Buchholz, K., Schmitt, I., Gardyan, A., Driessen, S., Arnold, H. H., Nguyen, H. P. & Riess, O. 2011. N-terminal ataxin-3 causes neurological symptoms with inclusions, endoplasmic reticulum stress and ribosomal dislocation. *Brain,* 134**,** 1925-42.

Hubener, J., Weber, J. J., Richter, C., Honold, L., Weiss, A., Murad, F., Breuer, P., Wullner, U., Bellstedt, P., Paquet-Durand, F., Takano, J., Saido, T. C., Riess, O. & Nguyen, H. P. 2013. Calpain-mediated ataxin-3 cleavage in the molecular pathogenesis of spinocerebellar ataxia type 3 (SCA3). *Hum Mol Genet,* 22**,** 508-18.

Huynh, D. P., Figueroa, K., Hoang, N. & Pulst, S. M. 2000. Nuclear localization or inclusion body formation of ataxin-2 are not necessary for SCA2 pathogenesis in mouse or human. *Nat Genet,* 26**,** 44-50.

Igarashi, S., Koide, R., Shimohata, T., Yamada, M., Hayashi, Y., Takano, H., Date, H., Oyake, M., Sato, T., Sato, A., Egawa, S., Ikeuchi, T., Tanaka, H.,

Nakano, R., Tanaka, K., Hozumi, I., Inuzuka, T., Takahashi, H. & Tsuji, S. 1998. Suppression of aggregate formation and apoptosis by transglutaminase inhibitors in cells expressing truncated DRPLA protein with an expanded polyglutamine stretch. *Nat Genet,* 18**,** 111-7.

Ikeda, H., Yamaguchi, M., Sugai, S., Aze, Y., Narumiya, S. & Kakizuka, A. 1996. Expanded polyglutamine in the Machado-Joseph disease protein induces cell death in vitro and in vivo. *Nat Genet,* 13**,** 196-202.

Imbert, G., Trottier, Y., Beckmann, J. & Mandel, J. L. 1994. The gene for the TATA binding protein (TBP) that contains a highly polymorphic protein coding CAG repeat maps to 6q27. *Genomics,* 21**,** 667-8.

Ishihara, K., Yamagishi, N., Saito, Y., Adachi, H., Kobayashi, Y., Sobue, G., Ohtsuka, K. & Hatayama, T. 2003. Hsp105alpha suppresses the aggregation of truncated androgen receptor with expanded CAG repeats and cell toxicity. *J Biol Chem,* 278**,** 25143-50.

Jackson-Fisher, A. J., Chitikila, C., Mitra, M. & Pugh, B. F. 1999. A role for TBP dimerization in preventing unregulated gene expression. *Mol Cell,* 3**,** 717-27.

Kazantsev, A., Walker, H. A., Slepko, N., Bear, J. E., Preisinger, E., Steffan, J. S., Zhu, Y. Z., Gertler, F. B., Housman, D. E., Marsh, J. L. & Thompson, L. M. 2002. A bivalent Huntingtin binding peptide suppresses polyglutamine aggregation and pathogenesis in Drosophila. *Nat Genet,* 30**,** 367-76.

Kelp, A., Koeppen, A. H., Petrasch-Parwez, E., Calaminus, C., Bauer, C., Portal, E., Yu-Taeger, L., Pichler, B., Bauer, P., Riess, O. & Nguyen, H. P. 2013. A novel transgenic rat model for spinocerebellar ataxia type 17 recapitulates neuropathological changes and supplies in vivo imaging biomarkers. *J Neurosci,* 33**,** 9068-81.

Kim, J. Y., Kim, S. Y., Kim, J. M., Kim, Y. K., Yoon, K. Y., Kim, J. Y., Lee, B. C., Kim, J. S., Paek, S. H., Park, S. S., Kim, S. E. & Jeon, B. S. 2009. Spinocerebellar ataxia type 17 mutation as a causative and susceptibility gene in parkinsonism. *Neurology,* 72**,** 1385-9.

Kim, S., Nollen, E. A., Kitagawa, K., Bindokas, V. P. & Morimoto, R. I. 2002. Polyglutamine protein aggregates are dynamic. *Nat Cell Biol,* 4**,** 826-31.

Kim, S. H., Lee, Y. H., Jung, S. Y., Kim, H. J., Jin, C. & Lee, Y. S. 2011. Synthesis of chromone carboxamide derivatives with antioxidative and calpain inhibitory properties. *Eur J Med Chem,* 46**,** 1721-8.

Kim, Y. J., Yi, Y., Sapp, E., Wang, Y., Cuiffo, B., Kegel, K. B., Qin, Z. H., Aronin, N. & Difiglia, M. 2001. Caspase 3-cleaved N-terminal fragments of wild-type and mutant huntingtin are present in normal and Huntington's disease brains, associate with membranes, and undergo calpain-dependent proteolysis. *Proc Natl Acad Sci U S A,* 98**,** 12784-9.

Klement, I. A., Skinner, P. J., Kaytor, M. D., Yi, H., Hersch, S. M., Clark, H. B., Zoghbi, H. Y. & Orr, H. T. 1998. Ataxin-1 nuclear localization and aggregation: role in polyglutamine-induced disease in SCA1 transgenic mice. *Cell,* 95**,** 41-53.

Koch, P., Breuer, P., Peitz, M., Jungverdorben, J., Kesavan, J., Poppe, D., Doerr, J., Ladewig, J., Mertens, J., Tuting, T., Hoffmann, P., Klockgether, T., Evert, B. O., Wullner, U. & Brustle, O. 2011. Excitation-induced ataxin-3

aggregation in neurons from patients with Machado-Joseph disease. *Nature,* 480**,** 543-6.

Koide, R., Kobayashi, S., Shimohata, T., Ikeuchi, T., Maruyama, M., Saito, M., Yamada, M., Takahashi, H. & Tsuji, S. 1999. A neurological disease caused by an expanded CAG trinucleotide repeat in the TATA-binding protein gene: a new polyglutamine disease? *Hum Mol Genet,* 8**,** 2047-53.

Kurbatskaya, K., Phillips, E. C., Croft, C. L., Dentoni, G., Hughes, M. M., Wade, M. A., Al-Sarraj, S., Troakes, C., O'neill, M. J., Perez-Nievas, B. G., Hanger, D. P. & Noble, W. 2016. Upregulation of calpain activity precedes tau phosphorylation and loss of synaptic proteins in Alzheimer's disease brain. *Acta Neuropathol Commun,* 4**,** 34.

Laemmli, U. K. 1970. Cleavage of structural proteins during the assembly of the head of bacteriophage T4. *Nature,* 227**,** 680-5.

Lankiewicz, S., Marc Luetjens, C., Truc Bui, N., Krohn, A. J., Poppe, M., Cole, G. M., Saido, T. C. & Prehn, J. H. 2000. Activation of calpain I converts excitotoxic neuron death into a caspase-independent cell death. *J Biol Chem,* 275**,** 17064-71.

Lasek, K., Lencer, R., Gaser, C., Hagenah, J., Walter, U., Wolters, A., Kock, N., Steinlechner, S., Nagel, M., Zuhlke, C., Nitschke, M. F., Brockmann, K., Klein, C., Rolfs, A. & Binkofski, F. 2006. Morphological basis for the spectrum of clinical deficits in spinocerebellar ataxia 17 (SCA17). *Brain,* 129**,** 2341-52.

Lee, D., Lee, Y.-I., Lee, Y.-S. & Lee, S. B. 2020. The Mechanisms of Nuclear Proteotoxicity in Polyglutamine Spinocerebellar Ataxias. *Frontiers in Neuroscience,* 14.

Lee, L. C., Chen, C. M., Wang, P. R., Su, M. T., Lee-Chen, G. J. & Chang, C. Y. 2014. Role of high mobility group box 1 (HMGB1) in SCA17 pathogenesis. *PLoS One,* 9**,** e115809.

Lieberman, A. P., Shakkottai, V. G. & Albin, R. L. 2019. Polyglutamine Repeats in Neurodegenerative Diseases. *Annu Rev Pathol,* 14**,** 1-27.

Lin, X., Antalffy, B., Kang, D., Orr, H. T. & Zoghbi, H. Y. 2000. Polyglutamine expansion down-regulates specific neuronal genes before pathologic changes in SCA1. *Nat Neurosci,* 3**,** 157-63.

Liu, Z., Cao, J., Gao, X., Ma, Q., Ren, J. & Xue, Y. 2011. GPS-CCD: a novel computational program for the prediction of calpain cleavage sites. *PLoS One,* 6**,** e19001.

Lunkes, A., Trottier, Y., Fagart, J., Schultz, P., Zeder-Lutz, G., Moras, D. & Mandel, J. L. 1999. Properties of polyglutamine expansion in vitro and in a cellular model for Huntington's disease. *Philos Trans R Soc Lond B Biol Sci,* 354**,** 1013-9.

Lunkes, A., Trottier, Y. & Mandel, J. L. 1998. Pathological mechanisms in Huntington's disease and other polyglutamine expansion diseases. *Essays Biochem,* 33**,** 149-63.

Luthi-Carter, R., Strand, A., Peters, N. L., Solano, S. M., Hollingsworth, Z. R., Menon, A. S., Frey, A. S., Spektor, B. S., Penney, E. B., Schilling, G., Ross, C. A., Borchelt, D. R., Tapscott, S. J., Young, A. B., Cha, J. H. & Olson, J. M. 2000. Decreased expression of striatal signaling genes in a mouse model of Huntington's disease. *Hum Mol Genet,* 9**,** 1259-71.

Luthi-Carter, R., Strand, A. D., Hanson, S. A., Kooperberg, C., Schilling, G., La Spada, A. R., Merry, D. E., Young, A. B., Ross, C. A., Borchelt, D. R. & Olson, J. M. 2002. Polyglutamine and transcription: gene expression changes shared by DRPLA and Huntington's disease mouse models reveal context-independent effects. *Hum Mol Genet,* 11**,** 1927-37.

Mahajan, V. B., Skeie, J. M., Bassuk, A. G., Fingert, J. H., Braun, T. A., Daggett, H. T., Folk, J. C., Sheffield, V. C. & Stone, E. M. 2012. Calpain-5 mutations cause autoimmune uveitis, retinal neovascularization, and photoreceptor degeneration. *PLoS Genet,* 8**,** e1003001.

Mahaman, Y. a. R., Huang, F., Kessete Afewerky, H., Maibouge, T. M. S., Ghose, B. & Wang, X. 2019. Involvement of calpain in the neuropathogenesis of Alzheimer's disease. *Med Res Rev,* 39**,** 608-630.

Maki, M., Takano, E., Mori, H., Sato, A., Murachi, T. & Hatanaka, M. 1987. All four internally repetitive domains of pig calpastatin possess inhibitory activities against calpains I and II. *FEBS Lett,* 223**,** 174-80.

Maltecca, F., Filla, A., Castaldo, I., Coppola, G., Fragassi, N. A., Carella, M., Bruni, A., Cocozza, S., Casari, G., Servadio, A. & De Michele, G. 2003. Intergenerational instability and marked anticipation in SCA-17. *Neurology,* 61**,** 1441-3.

Mangiarini, L., Sathasivam, K., Seller, M., Cozens, B., Harper, A., Hetherington, C., Lawton, M., Trottier, Y., Lehrach, H., Davies, S. W. & Bates, G. P. 1996. Exon 1 of the HD gene with an expanded CAG repeat is sufficient to cause a progressive neurological phenotype in transgenic mice. *Cell,* 87**,** 493-506.

Manto, M. U. 2005. The wide spectrum of spinocerebellar ataxias (SCAs). *Cerebellum,* 4**,** 2-6.

Martianov, I., Viville, S. & Davidson, I. 2002. RNA polymerase II transcription in murine cells lacking the TATA binding protein. *Science,* 298**,** 1036-9.

Martindale, D., Hackam, A., Wieczorek, A., Ellerby, L., Wellington, C., Mccutcheon, K., Singaraja, R., Kazemi-Esfarjani, P., Devon, R., Kim, S. U., Bredesen, D. E., Tufaro, F. & Hayden, M. R. 1998. Length of huntingtin and its polyglutamine tract influences localization and frequency of intracellular aggregates. *Nat Genet,* 18**,** 150-4.

Maruyama, H., Izumi, Y., Morino, H., Oda, M., Toji, H., Nakamura, S. & Kawakami, H. 2002. Difference in disease-free survival curve and regional distribution according to subtype of spinocerebellar ataxia: a study of 1,286 Japanese patients. *Am J Med Genet,* 114**,** 578-83.

Matilla, A., Roberson, E. D., Banfi, S., Morales, J., Armstrong, D. L., Burright, E. N., Orr, H. T., Sweatt, J. D., Zoghbi, H. Y. & Matzuk, M. M. 1998. Mice lacking ataxin-1 display learning deficits and decreased hippocampal paired-pulse facilitation. *J Neurosci,* 18**,** 5508-16.

Mellgren, R. L. & Huang, X. 2007. Fetuin A stabilizes m-calpain and facilitates plasma membrane repair. *J Biol Chem,* 282**,** 35868-77.

Mingorance-Le Meur, A. 2009. Internal regulation of neurite plasticity: A general model. *Commun Integr Biol,* 2**,** 318-20.

Mouatt-Prigent, A., Karlsson, J. O., Agid, Y. & Hirsch, E. C. 1996. Increased M-calpain expression in the mesencephalon of patients with Parkinson's

disease but not in other neurodegenerative disorders involving the mesencephalon: a role in nerve cell death? *Neuroscience,* 73**,** 979-87.

Muddapu, V. R., Dharshini, S. a. P., Chakravarthy, V. S. & Gromiha, M. M. 2020. Neurodegenerative Diseases - Is Metabolic Deficiency the Root Cause? *Front Neurosci,* 14**,** 213.

Mykowska, A., Sobczak, K., Wojciechowska, M., Kozlowski, P. & Krzyzosiak, W. J. 2011. CAG repeats mimic CUG repeats in the misregulation of alternative splicing. *Nucleic Acids Res,* 39**,** 8938-51.

Nakamura, K., Jeong, S. Y., Uchihara, T., Anno, M., Nagashima, K., Nagashima, T., Ikeda, S., Tsuji, S. & Kanazawa, I. 2001. SCA17, a novel autosomal dominant cerebellar ataxia caused by an expanded polyglutamine in TATA-binding protein. *Hum Mol Genet,* 10**,** 1441-8.

Nanda, A., Jackson, S. A., Schwankhaus, J. D. & Metzer, W. S. 2007. Case of spinocerebellar ataxia type 17 (SCA17) associated with only 41 repeats of the TATA-binding protein (TBP) gene. *Mov Disord,* 22**,** 436.

Ng, H., Pulst, S. M. & Huynh, D. P. 2007. Ataxin-2 mediated cell death is dependent on domains downstream of the polyQ repeat. *Exp Neurol,* 208**,** 207-15.

Nixon, R. A., Saito, K. I., Grynspan, F., Griffin, W. R., Katayama, S., Honda, T., Mohan, P. S., Shea, T. B. & Beermann, M. 1994. Calcium-activated neutral proteinase (calpain) system in aging and Alzheimer's disease. *Ann N Y Acad Sci,* 747**,** 77-91.

Noguchi, M., Sarin, A., Aman, M. J., Nakajima, H., Shores, E. W., Henkart, P. A. & Leonard, W. J. 1997. Functional cleavage of the common cytokine receptor gamma chain (gammac) by calpain. *Proc Natl Acad Sci U S A,* 94**,** 11534-9.

Nolte, D., Sobanski, E., Wissen, A., Regula, J. U., Lichy, C. & Muller, U. 2010. Spinocerebellar ataxia type 17 associated with an expansion of 42 glutamine residues in TATA-box binding protein gene. *J Neurol Neurosurg Psychiatry,* 81**,** 1396-9.

Nucifora, F. C., Jr., Sasaki, M., Peters, M. F., Huang, H., Cooper, J. K., Yamada, M., Takahashi, H., Tsuji, S., Troncoso, J., Dawson, V. L., Dawson, T. M. & Ross, C. A. 2001. Interference by huntingtin and atrophin-1 with cbp-mediated transcription leading to cellular toxicity. *Science,* 291**,** 2423-8.

Oda, M., Maruyama, H., Komure, O., Morino, H., Terasawa, H., Izumi, Y., Imamura, T., Yasuda, M., Ichikawa, K., Ogawa, M., Matsumoto, M. & Kawakami, H. 2004. Possible reduced penetrance of expansion of 44 to 47 CAG/CAA repeats in the TATA-binding protein gene in spinocerebellar ataxia type 17. *Arch Neurol,* 61**,** 209-12.

Ono, Y. & Sorimachi, H. 2012. Calpains: an elaborate proteolytic system. *Biochim Biophys Acta,* 1824**,** 224-36.

Orr, H. T. & Zoghbi, H. Y. 2007. Trinucleotide repeat disorders. *Annu Rev Neurosci,* 30**,** 575-621.

Park, H., Jeon, B. S., Shin, J. H. & Park, S. H. 2016. A patient with 41 CAG repeats in SCA17 presenting with parkinsonism and chorea. *Parkinsonism Relat Disord,* 22**,** 106-7.

Park, Y., Hong, S., Kim, S. J. & Kang, S. 2005. Proteasome function is inhibited by polyglutamine-expanded ataxin-1, the SCA1 gene product. *Mol Cells,* 19**,** 23-30.

Patel, A. B., Louder, R. K., Greber, B. J., Grünberg, S., Luo, J., Fang, J., Liu, Y., Ranish, J., Hahn, S. & Nogales, E. 2018. Structure of human TFIID and mechanism of TBP loading onto promoter DNA. *Science,* 362.

Paulson, H. L., Perez, M. K., Trottier, Y., Trojanowski, J. Q., Subramony, S. H., Das, S. S., Vig, P., Mandel, J. L., Fischbeck, K. H. & Pittman, R. N. 1997. Intranuclear inclusions of expanded polyglutamine protein in spinocerebellar ataxia type 3. *Neuron,* 19**,** 333-44.

Perez, M. K., Paulson, H. L., Pendse, S. J., Saionz, S. J., Bonini, N. M. & Pittman, R. N. 1998. Recruitment and the role of nuclear localization in polyglutamine-mediated aggregation. *J Cell Biol,* 143**,** 1457-70.

Perutz, M. F., Johnson, T., Suzuki, M. & Finch, J. T. 1994. Glutamine repeats as polar zippers: their possible role in inherited neurodegenerative diseases. *Proc Natl Acad Sci U S A,* 91**,** 5355-8.

Pike, B. R., Zhao, X., Newcomb, J. K., Posmantur, R. M., Wang, K. K. & Hayes, R. L. 1998. Regional calpain and caspase-3 proteolysis of alpha-spectrin after traumatic brain injury. *Neuroreport,* 9**,** 2437-42.

Pontremoli, S. & Melloni, E. 1988. The role of calpain and protein kinase C in activation of human neutrophils. *Prog Clin Biol Res,* 282**,** 195-208.

Pringsheim, T., Wiltshire, K., Day, L., Dykeman, J., Steeves, T. & Jette, N. 2012. The incidence and prevalence of Huntington's disease: a systematic review and meta-analysis. *Mov Disord,* 27**,** 1083-91.

Rao, M. V., Campbell, J., Palaniappan, A., Kumar, A. & Nixon, R. A. 2016. Calpastatin inhibits motor neuron death and increases survival of hSOD1(G93A) mice. *J Neurochem,* 137**,** 253-65.

Rao, M. V., Mohan, P. S., Peterhoff, C. M., Yang, D. S., Schmidt, S. D., Stavrides, P. H., Campbell, J., Chen, Y., Jiang, Y., Paskevich, P. A., Cataldo, A. M., Haroutunian, V. & Nixon, R. A. 2008. Marked calpastatin (CAST) depletion in Alzheimer's disease accelerates cytoskeleton disruption and neurodegeneration: neuroprotection by CAST overexpression. *J Neurosci,* 28**,** 12241-54.

Rawlins, M. D., Wexler, N. S., Wexler, A. R., Tabrizi, S. J., Douglas, I., Evans, S. J. & Smeeth, L. 2016. The Prevalence of Huntington's Disease. *Neuroepidemiology,* 46**,** 144-53.

Reetz, K., Lencer, R., Hagenah, J. M., Gaser, C., Tadic, V., Walter, U., Wolters, A., Steinlechner, S., Zuhlke, C., Brockmann, K., Klein, C., Rolfs, A. & Binkofski, F. 2010. Structural changes associated with progression of motor deficits in spinocerebellar ataxia 17. *Cerebellum,* 9**,** 210-7.

Reid, S. J., Rees, M. I., Van Roon-Mom, W. M., Jones, A. L., Macdonald, M. E., Sutherland, G., During, M. J., Faull, R. L., Owen, M. J., Dragunow, M. & Snell, R. G. 2003. Molecular investigation of TBP allele length: a SCA17 cellular model and population study. *Neurobiol Dis,* 13**,** 37-45.

Ren, J., Jegga, A. G., Zhang, M., Deng, J., Liu, J., Gordon, C. B., Aronow, B. J., Lu, L. J., Zhang, B. & Ma, J. 2011. A Drosophila model of the neurodegenerative disease SCA17 reveals a role of RBP-J/Su(H) in modulating the pathological outcome. *Hum Mol Genet,* 20**,** 3424-36.

Rolfs, A., Koeppen, A. H., Bauer, I., Bauer, P., Buhlmann, S., Topka, H., Schols, L. & Riess, O. 2003. Clinical features and neuropathology of autosomal dominant spinocerebellar ataxia (SCA17). *Ann Neurol,* 54**,** 367-75.

Russo, R., Berliocchi, L., Adornetto, A., Varano, G. P., Cavaliere, F., Nucci, C., Rotiroti, D., Morrone, L. A., Bagetta, G. & Corasaniti, M. T. 2011. Calpain-mediated cleavage of Beclin-1 and autophagy deregulation following retinal ischemic injury in vivo. *Cell Death Dis,* 2**,** e144.

Sanchez, I., Mahlke, C. & Yuan, J. 2003. Pivotal role of oligomerization in expanded polyglutamine neurodegenerative disorders. *Nature,* 421**,** 373-9.

Sathasivam, K., Neueder, A., Gipson, T. A., Landles, C., Benjamin, A. C., Bondulich, M. K., Smith, D. L., Faull, R. L., Roos, R. A., Howland, D., Detloff, P. J., Housman, D. E. & Bates, G. P. 2013. Aberrant splicing of HTT generates the pathogenic exon 1 protein in Huntington disease. *Proc Natl Acad Sci U S A,* 110**,** 2366-70.

Saudou, F., Finkbeiner, S., Devys, D. & Greenberg, M. E. 1998. Huntingtin acts in the nucleus to induce apoptosis but death does not correlate with the formation of intranuclear inclusions. *Cell,* 95**,** 55-66.

Savinkova, L. K., Ponomarenko, M. P., Ponomarenko, P. M., Drachkova, I. A., Lysova, M. V., Arshinova, T. V. & Kolchanov, N. A. 2009. TATA box polymorphisms in human gene promoters and associated hereditary pathologies. *Biochemistry (Mosc),* 74**,** 117-29.

Schaefer, M. H., Wanker, E. E. & Andrade-Navarro, M. A. 2012. Evolution and function of CAG/polyglutamine repeats in protein-protein interaction networks. *Nucleic Acids Res,* 40**,** 4273-87.

Schaffar, G., Breuer, P., Boteva, R., Behrends, C., Tzvetkov, N., Strippel, N., Sakahira, H., Siegers, K., Hayer-Hartl, M. & Hartl, F. U. 2004. Cellular toxicity of polyglutamine expansion proteins: mechanism of transcription factor deactivation. *Mol Cell,* 15**,** 95-105.

Scherzinger, E., Lurz, R., Turmaine, M., Mangiarini, L., Hollenbach, B., Hasenbank, R., Bates, G. P., Davies, S. W., Lehrach, H. & Wanker, E. E. 1997. Huntingtin-encoded polyglutamine expansions form amyloid-like protein aggregates in vitro and in vivo. *Cell,* 90**,** 549-58.

Schols, L., Bauer, P., Schmidt, T., Schulte, T. & Riess, O. 2004. Autosomal dominant cerebellar ataxias: clinical features, genetics, and pathogenesis. *Lancet Neurol,* 3**,** 291-304.

Shah, A. G., Friedman, M. J., Huang, S., Roberts, M., Li, X. J. & Li, S. 2009. Transcriptional dysregulation of TrkA associates with neurodegeneration in spinocerebellar ataxia type 17. *Hum Mol Genet,* 18**,** 4141-52.

Shao, J. & Diamond, M. I. 2007. Polyglutamine diseases: emerging concepts in pathogenesis and therapy. *Hum Mol Genet,* 16 Spec No. 2**,** R115-23.

Shields, D. C., Schaecher, K. E., Saido, T. C. & Banik, N. L. 1999. A putative mechanism of demyelination in multiple sclerosis by a proteolytic enzyme, calpain. *Proc Natl Acad Sci U S A,* 96**,** 11486-91.

Shimohata, T., Nakajima, T., Yamada, M., Uchida, C., Onodera, O., Naruse, S., Kimura, T., Koide, R., Nozaki, K., Sano, Y., Ishiguro, H., Sakoe, K., Ooshima, T., Sato, A., Ikeuchi, T., Oyake, M., Sato, T., Aoyagi, Y., Hozumi, I., Nagatsu, T., Takiyama, Y., Nishizawa, M., Goto, J., Kanazawa, I.,

Davidson, I., Tanese, N., Takahashi, H. & Tsuji, S. 2000. Expanded polyglutamine stretches interact with TAFII130, interfering with CREB-dependent transcription. *Nat Genet,* 26**,** 29-36.

Simoes, A. T., Goncalves, N., Koeppen, A., Deglon, N., Kugler, S., Duarte, C. B. & Pereira De Almeida, L. 2012. Calpastatin-mediated inhibition of calpains in the mouse brain prevents mutant ataxin 3 proteolysis, nuclear localization and aggregation, relieving Machado-Joseph disease. *Brain,* 135**,** 2428-39.

Simões, A. T., Gonçalves, N., Nobre, R. J., Duarte, C. B. & Pereira De Almeida, L. 2014. Calpain inhibition reduces ataxin-3 cleavage alleviating neuropathology and motor impairments in mouse models of Machado-Joseph disease. *Hum Mol Genet,* 23**,** 4932-44.

Slow, E. J., Graham, R. K., Osmand, A. P., Devon, R. S., Lu, G., Deng, Y., Pearson, J., Vaid, K., Bissada, N., Wetzel, R., Leavitt, B. R. & Hayden, M. R. 2005. Absence of behavioral abnormalities and neurodegeneration in vivo despite widespread neuronal huntingtin inclusions. *Proc Natl Acad Sci U S A,* 102**,** 11402-7.

Sorimachi, H., Hata, S. & Ono, Y. 2011. Calpain chronicle--an enzyme family under multidisciplinary characterization. *Proc Jpn Acad Ser B Phys Biol Sci,* 87**,** 287-327.

Squier, M. K., Miller, A. C., Malkinson, A. M. & Cohen, J. J. 1994. Calpain activation in apoptosis. *J Cell Physiol,* 159**,** 229-37.

Steffan, J. S., Kazantsev, A., Spasic-Boskovic, O., Greenwald, M., Zhu, Y. Z., Gohler, H., Wanker, E. E., Bates, G. P., Housman, D. E. & Thompson, L. M. 2000. The Huntington's disease protein interacts with p53 and CREB-binding protein and represses transcription. *Proc Natl Acad Sci U S A,* 97**,** 6763-8.

Stevanin, G. & Brice, A. 2008. Spinocerebellar ataxia 17 (SCA17) and Huntington's disease-like 4 (HDL4). *Cerebellum,* 7**,** 170-8.

Stevanin, G., Fujigasaki, H., Lebre, A. S., Camuzat, A., Jeannequin, C., Dode, C., Takahashi, J., San, C., Bellance, R., Brice, A. & Durr, A. 2003. Huntington's disease-like phenotype due to trinucleotide repeat expansions in the TBP and JPH3 genes. *Brain,* 126**,** 1599-603.

Szebenyi, G., Morfini, G. A., Babcock, A., Gould, M., Selkoe, K., Stenoien, D. L., Young, M., Faber, P. W., Macdonald, M. E., Mcphaul, M. J. & Brady, S. T. 2003. Neuropathogenic forms of huntingtin and androgen receptor inhibit fast axonal transport. *Neuron,* 40**,** 41-52.

Takano, J., Tomioka, M., Tsubuki, S., Higuchi, M., Iwata, N., Itohara, S., Maki, M. & Saido, T. C. 2005. Calpain mediates excitotoxic DNA fragmentation via mitochondrial pathways in adult brains: evidence from calpastatin mutant mice. *J Biol Chem,* 280**,** 16175-84.

Takeuchi, T. & Nagai, Y. 2017. Protein Misfolding and Aggregation as a Therapeutic Target for Polyglutamine Diseases. *Brain Sci,* 7.

Takiyama, Y., Igarashi, S., Rogaeva, E. A., Endo, K., Rogaev, E. I., Tanaka, H., Sherrington, R., Sanpei, K., Liang, Y., Saito, M. & Et Al. 1995. Evidence for inter-generational instability in the CAG repeat in the MJD1 gene and for conserved haplotypes at flanking markers amongst Japanese and

Caucasian subjects with Machado-Joseph disease. *Hum Mol Genet,* 4**,** 1137-46.

Tang, P. H., Chemudupati, T., Wert, K. J., Folk, J. C., Mahajan, M., Tsang, S. H., Bassuk, A. G. & Mahajan, V. B. 2020. Phenotypic variance in Calpain-5 retinal degeneration. *Am J Ophthalmol Case Rep,* 18**,** 100627.

Taylor, J. P., Tanaka, F., Robitschek, J., Sandoval, C. M., Taye, A., Markovic-Plese, S. & Fischbeck, K. H. 2003. Aggresomes protect cells by enhancing the degradation of toxic polyglutamine-containing protein. *Hum Mol Genet,* 12**,** 749-57.

Thomas, M. C. & Chiang, C. M. 2006. The general transcription machinery and general cofactors. *Crit Rev Biochem Mol Biol,* 41**,** 105-78.

Toyoshima, Y. & Takahashi, H. 2018. Spinocerebellar Ataxia Type 17 (SCA17). *Adv Exp Med Biol,* 1049**,** 219-231.

Toyoshima, Y., Yamada, M., Onodera, O., Shimohata, M., Inenaga, C., Fujita, N., Morita, M., Tsuji, S. & Takahashi, H. 2004. SCA17 homozygote showing Huntington's disease-like phenotype. *Ann Neurol,* 55**,** 281-6.

Trinchese, F., Fa, M., Liu, S., Zhang, H., Hidalgo, A., Schmidt, S. D., Yamaguchi, H., Yoshii, N., Mathews, P. M., Nixon, R. A. & Arancio, O. 2008. Inhibition of calpains improves memory and synaptic transmission in a mouse model of Alzheimer disease. *J Clin Invest,* 118**,** 2796-807.

Van Roon-Mom, W. M., Reid, S. J., Jones, A. L., Macdonald, M. E., Faull, R. L. & Snell, R. G. 2002. Insoluble TATA-binding protein accumulation in Huntington's disease cortex. *Brain Res Mol Brain Res,* 109**,** 1-10.

Vig, P. J., Fratkin, J. D., Desaiah, D., Currier, R. D. & Subramony, S. H. 1996. Decreased parvalbumin immunoreactivity in surviving Purkinje cells of patients with spinocerebellar ataxia-1. *Neurology,* 47**,** 249-53.

Vig, P. J., Subramony, S. H., Qin, Z., Mcdaniel, D. O. & Fratkin, J. D. 2000. Relationship between ataxin-1 nuclear inclusions and Purkinje cell specific proteins in SCA-1 transgenic mice. *J Neurol Sci,* 174**,** 100-10.

Vosler, P. S., Brennan, C. S. & Chen, J. 2008. Calpain-mediated signaling mechanisms in neuronal injury and neurodegeneration. *Mol Neurobiol,* 38**,** 78-100.

Wang, Y., Briz, V., Chishti, A., Bi, X. & Baudry, M. 2013. Distinct roles for mu-calpain and m-calpain in synaptic NMDAR-mediated neuroprotection and extrasynaptic NMDAR-mediated neurodegeneration. *J Neurosci,* 33**,** 18880-92.

Wang, Y., Hersheson, J., Lopez, D., Hammer, M., Liu, Y., Lee, K. H., Pinto, V., Seinfeld, J., Wiethoff, S., Sun, J., Amouri, R., Hentati, F., Baudry, N., Tran, J., Singleton, A. B., Coutelier, M., Brice, A., Stevanin, G., Durr, A., Bi, X., Houlden, H. & Baudry, M. 2016. Defects in the CAPN1 Gene Result in Alterations in Cerebellar Development and Cerebellar Ataxia in Mice and Humans. *Cell Rep,* 16**,** 79-91.

Wanker, E. E. 2000. Protein aggregation and pathogenesis of Huntington's disease: mechanisms and correlations. *Biol Chem,* 381**,** 937-42.

Watchon, M., Yuan, K. C., Mackovski, N., Svahn, A. J., Cole, N. J., Goldsbury, C., Rinkwitz, S., Becker, T. S., Nicholson, G. A. & Laird, A. S. 2017. Calpain Inhibition Is Protective in Machado-Joseph Disease Zebrafish Due to Induction of Autophagy. *J Neurosci,* 37**,** 7782-7794.

Weber, J. J., Anger, S. C., Pereira Sena, P., Incebacak Eltemur, R. D., Huridou, C., Fath, F., Gross, C., Casadei, N., Riess, O., & Nguyen, H. P. (2022). Calpains as novel players in the molecular pathogenesis of spinocerebellar ataxia type 17. *Cellular and molecular life sciences : CMLS*, *79*(5), 262.

Weber, J. J., Golla, M., Guaitoli, G., Wanichawan, P., Hayer, S. N., Hauser, S., Krahl, A. C., Nagel, M., Samer, S., Aronica, E., Carlson, C. R., Schols, L., Riess, O., Gloeckner, C. J., Nguyen, H. P. & Hubener-Schmid, J. 2017. A combinatorial approach to identify calpain cleavage sites in the Machado-Joseph disease protein ataxin-3. *Brain,* 140**,** 1280-1299.

Weber, J. J., Kloock, S. J., Nagel, M., Ortiz-Rios, M. M., Hofmann, J., Riess, O. & Nguyen, H. P. 2018. Calpastatin ablation aggravates the molecular phenotype in cell and animal models of Huntington disease. *Neuropharmacology,* 133**,** 94-106.

Weber, J. J., Ortiz Rios, M. M., Riess, O., Clemens, L. E. & Nguyen, H. P. 2016. The calpain-suppressing effects of olesoxime in Huntington's disease. *Rare Dis,* 4**,** e1153778.

Weber, J. J., Pereira Sena, P., Singer, E. & Nguyen, H. P. 2019. Killing Two Angry Birds with One Stone: Autophagy Activation by Inhibiting Calpains in Neurodegenerative Diseases and Beyond. *Biomed Res Int,* 2019**,** 4741252.

Weber, J. J., Sowa, A. S., Binder, T. & Hubener, J. 2014. From pathways to targets: understanding the mechanisms behind polyglutamine disease. *Biomed Res Int,* 2014**,** 701758.

Wellington, C. L., Ellerby, L. M., Gutekunst, C. A., Rogers, D., Warby, S., Graham, R. K., Loubser, O., Van Raamsdonk, J., Singaraja, R., Yang, Y. Z., Gafni, J., Bredesen, D., Hersch, S. M., Leavitt, B. R., Roy, S., Nicholson, D. W. & Hayden, M. R. 2002. Caspase cleavage of mutant huntingtin precedes neurodegeneration in Huntington's disease. *J Neurosci,* 22**,** 7862-72.

Wellington, C. L., Ellerby, L. M., Hackam, A. S., Margolis, R. L., Trifiro, M. A., Singaraja, R., Mccutcheon, K., Salvesen, G. S., Propp, S. S., Bromm, M., Rowland, K. J., Zhang, T., Rasper, D., Roy, S., Thornberry, N., Pinsky, L., Kakizuka, A., Ross, C. A., Nicholson, D. W., Bredesen, D. E. & Hayden, M. R. 1998. Caspase cleavage of gene products associated with triplet expansion disorders generates truncated fragments containing the polyglutamine tract. *J Biol Chem,* 273**,** 9158-67.

Wellington, C. L. & Hayden, M. R. 1997. Of molecular interactions, mice and mechanisms: new insights into Huntington's disease. *Curr Opin Neurol,* 10**,** 291-8.

Wells, A., Huttenlocher, A. & Lauffenburger, D. A. 2005. Calpain proteases in cell adhesion and motility. *Int Rev Cytol,* 245**,** 1-16.

Wendt, A., Thompson, V. F. & Goll, D. E. 2004. Interaction of calpastatin with calpain: a review. *Biol Chem,* 385**,** 465-72.

Wexler, N. S., Young, A. B., Tanzi, R. E., Travers, H., Starosta-Rubinstein, S., Penney, J. B., Snodgrass, S. R., Shoulson, I., Gomez, F., Ramos Arroyo, M. A. & Et Al. 1987. Homozygotes for Huntington's disease. *Nature,* 326**,** 194-7.

Whaley, N. R., Fujioka, S. & Wszolek, Z. K. 2011. Autosomal dominant cerebellar ataxia type I: a review of the phenotypic and genotypic characteristics. *Orphanet J Rare Dis,* 6**,** 33.

Wojciechowska, M. & Krzyzosiak, W. J. 2011. Cellular toxicity of expanded RNA repeats: focus on RNA foci. *Hum Mol Genet,* 20**,** 3811-21.

Wong, J. M. & Bateman, E. 1994. TBP-DNA interactions in the minor groove discriminate between A:T and T:A base pairs. *Nucleic Acids Res,* 22**,** 1890-6.

Wootz, H., Hansson, I., Korhonen, L. & Lindholm, D. 2006. XIAP decreases caspase-12 cleavage and calpain activity in spinal cord of ALS transgenic mice. *Exp Cell Res,* 312**,** 1890-8.

Wright, A. L. & Vissel, B. 2016. CAST your vote: is calpain inhibition the answer to ALS? *J Neurochem,* 137**,** 140-1.

Wu, Y. R., Lin, H. Y., Chen, C. M., Gwinn-Hardy, K., Ro, L. S., Wang, Y. C., Li, S. H., Hwang, J. C., Fang, K., Hsieh-Li, H. M., Li, M. L., Tung, L. C., Su, M. T., Lu, K. T. & Lee-Chen, G. J. 2004. Genetic testing in spinocerebellar ataxia in Taiwan: expansions of trinucleotide repeats in SCA8 and SCA17 are associated with typical Parkinson's disease. *Clin Genet,* 65**,** 209-14.

Yamada, M., Hayashi, S., Tsuji, S. & Takahashi, H. 2001. Involvement of the cerebral cortex and autonomic ganglia in Machado-Joseph disease. *Acta Neuropathol,* 101**,** 140-4.

Yamashima, T. 2000. Implication of cysteine proteases calpain, cathepsin and caspase in ischemic neuronal death of primates. *Prog Neurobiol,* 62**,** 273-95.

Yang, S., Huang, S., Gaertig, M. A., Li, X. J. & Li, S. 2014. Age-dependent decrease in chaperone activity impairs MANF expression, leading to Purkinje cell degeneration in inducible SCA17 mice. *Neuron,* 81**,** 349-65.

Yang, S., Li, X. J. & Li, S. 2016. Molecular mechanisms underlying Spinocerebellar Ataxia 17 (SCA17) pathogenesis. *Rare Dis,* 4**,** e1223580.

Yang, S., Yang, H., Huang, L., Chen, L., Qin, Z., Li, S. & Li, X. J. 2020. Lack of RAN-mediated toxicity in Huntington's disease knock-in mice. *Proc Natl Acad Sci U S A,* 117**,** 4411-4417.

Yella, V. R. & Bansal, M. 2017. DNA structural features of eukaryotic TATA-containing and TATA-less promoters. *FEBS Open Bio,* 7**,** 324-334.

Yvert, G., Lindenberg, K. S., Picaud, S., Landwehrmeyer, G. B., Sahel, J. A. & Mandel, J. L. 2000. Expanded polyglutamines induce neurodegeneration and trans-neuronal alterations in cerebellum and retina of SCA7 transgenic mice. *Hum Mol Genet,* 9**,** 2491-506.

Zadran, S., Qin, Q., Bi, X., Zadran, H., Kim, Y., Foy, M. R., Thompson, R. & Baudry, M. 2009. 17-Beta-estradiol increases neuronal excitability through MAP kinase-induced calpain activation. *Proc Natl Acad Sci U S A,* 106**,** 21936-41.

Zeitlin, S., Liu, J. P., Chapman, D. L., Papaioannou, V. E. & Efstratiadis, A. 1995. Increased apoptosis and early embryonic lethality in mice nullizygous for the Huntington's disease gene homologue. *Nat Genet,* 11**,** 155-63.

Zuhlke, C. & Burk, K. 2007. Spinocerebellar ataxia type 17 is caused by mutations in the TATA-box binding protein. *Cerebellum,* 6**,** 300-7.

Zuhlke, C., Hellenbroich, Y., Dalski, A., Kononowa, N., Hagenah, J., Vieregge, P., Riess, O., Klein, C. & Schwinger, E. 2001. Different types of repeat expansion in the TATA-binding protein gene are associated with a new form of inherited ataxia. *Eur J Hum Genet,* 9**,** 160-4.

9 Declaration of Authorship

I hereby declare that this thesis and the work presented is my own and has been generated as the result of my own original research except where otherwise indicated. All experiments were carried out under the auspices of the Institute of Medical Genetics and Applied Genomics of the Eberhard Karls University of Tübingen under supervision by Prof. Dr. med. Olaf Riess and followed the guidelines of good clinical practice. I have not used any sources other than those listed and identified as references. I further declare that I have not submitted this thesis at any other institution in order to obtain a degree.

Hiermit erkläre ich, dass ich diese Arbeit selbst verfasst habe und das Ergebnis meiner eigenen Forschung ist, sofern nicht anders angegeben. Die Arbeit wurde am Institut für Medizinische Genetik und Angewandte Genomik der Eberhard Karls Universität Tübingen unter der Betreuung von Prof. Dr. med. Olaf Rieß und nach den Leitlinien guter wissenschaftlicher Praxis durchgeführt. Ich versichere, keine weiteren als die von mir angegebenen Quellen verwendet zu haben und diese Arbeit an keiner anderen Institution zur Erlangung eines akademischen Grades eingereicht zu haben.

_____

10 Publications

Parts of the dissertation have been published in:

Anger, S.C., Weber, J.J., Nguyen, H.P. 2016. The HD-like type 4/SCA17 disease protein TBP is cleaved by calpains in vitro and in vivo. *Journal of Neurology, Neurosurgery & Psychiatry* ; 87:A25. (Poster).

Weber, J. J., Anger, S. C., Pereira Sena, P., Incebacak Eltemur, R. D., Huridou, C., Fath, F., Gross, C., Casadei, N., Riess, O., & Nguyen, H. P. (2022). Calpains as novel players in the molecular pathogenesis of spinocerebellar ataxia type 17. *Cellular and molecular life sciences : CMLS*, *79*(5), 262. https://doi.org/10.1007/s00018-022-04274-6. This work is licensed under a CC BY 4.0.

Acknowledgements

I would like to express my gratitude firstly towards my laboratory supervisor Dr. rer. nat. Jonasz Jeremiasz Weber. Without his expertise, guidance, and ongoing patience this dissertation would not have been possible. As a role-model for our laboratory he demonstrated that ambition, enthusiasm, and dedication is equally essential for successful research as support and empathy towards others.

Then, I would like to thank the head of my research group HD, Prof. Dr. med. Hoa Huu Phuc Nguyen, for a professional advice, an open ear, and supporting words at any time. His effort helped me overcome the organisational and subject-specific obstacles along the way. I am grateful to my doctorate supervisor Prof. Dr. med. Olaf Rieß for providing me with the topic of my dissertation and the opportunity to accomplish it at the Institute of Medical Genetics and Applied Genomics. I thank my colleagues Daniel Weishäupl and Priscila Sena for the conduction and providence of supporting statistical analyses and allocated advice. I thank the IZKF Promotionskolleg for offering the organisational framework and financial support to acquire the skills of good scientific practice and presentation. I acknowledge the Institute of Medical Genetics and Applied Genomics with all the contributors for a motivating and kind working atmosphere.

Last, I want to thank my family and friends for accompanying me throughout my work with a balancing emotional support, counsel and, simultaneously, with the right dose of distraction. Without them I would not have managed this professional and personal process.